LASER RAMAN SPECTROSCOPIC AND DIELECTRIC STUDIES OF SOME MOLECULES OF BIOLOGICAL SIGNIFICANCE

ABSTRACT

By

RADHENDU DAS

DEPARTMENT OF PHYSICS

SCHOOL OF PHYSICAL SCIENCES

A THESIS

SUBMITTED

IN

FULFILMENT OF THE REQUIREMENT FOR THE DEGREE OF

DOCTOR OF PHILOSOPHY

To

THE NORTH-EASTERN HILL UNIVERSITY

SHILLONG - 793 001

INDIA

JULY, 1991

PL-F

DAS;1

LASER RAMAN SPECTROSCOPIC AND DIELECTRIC STUDIES OF SOME MOLECULES OF BIOLOGICAL SIGNIFICANCE

RADHENDU DAS

Synopsis of the dissertation for *Ph.D* degree of the North-Eastern Hill University, Shillong.

Thesis Supervisor : Dr. Kamal Kumar
Reader in Physics.

Forwarded

K. Kumar 12/7/91

D. Kumar Kamal
Reader in Physics
North Eastern Hill University
Shillong-793003

S Y N O P S I S

SYNOPSIS

This thesis deals with the Laser Raman spectroscopic and dielectric studies of substituted aromatic Schiff bases. The structural and behavioural properties of aromatic Schiff bases make them unique model system to investigate a wide variety of biological phenomena. Our knowledge of these systems may be applied towards better understanding of bilogical processes involving membranes and visual systems. The visual pigments, rhodopsin is composed of the chromophore 11-cis-retinal linked by a Schiff base[1] to the membrane glycoprotein opsin. The absorption bands of the resulting pigment are considerably red-shifted from those of the free chromophore and from protonated and unprotonated Schiff bases formed with retinal in organic solvents. An understanding of the retinal-opsin interactions responsible for the colour of the visual pigments requires information about the retinal-opsin complex. The photoreceptors respond to electrical stimulation in a similar fashion as liquid crystals and are sensitive to changes in the environment. The understanding of the changes due to the variation in environment, thus, becomes important in interpreting biological structures at the molecular level. The understanding of the structural chemistry operating at the biological sites such as the C=N linkage may come through the application of physical and chemical structure probes. Vibrational studies of the protonated and

unprotonated Schiff bases reveal that the C=N linkage plays a significant role in controlling biological processes. In several such molecular systems, vibrational spectroscopic studies of the C=N stretching mode was attempted by earlier workers.[2-4] Many Schiff bases are known to behave as liquid crystals[5-8], the present spectroscopic studies may provide basic spectral data for the liquid crystal studies. In addition, it has been proposed by some research workers[9,10] that the Schiff base linkage may be playing role in charge-transfer interactions with a neighbouring peptide unit by creating mobile holes within protein valence bands. The monitoring of the C=N linkage is therefore important for such studies as well. In an attempt to provide more structural information and spectroscopic data on molecules containing the C=N linkage, we have investigated the aromatic Schiff bases having substituent groups of varying chemical character. The molecules studied in the present investigation, essentially contain benzylidene and aniline moiety on either side of the Schiff base linkage. Raman spectroscopic studies assisted by the infrared and electronic absorption spectroscopic techniques have been used to provide information about the conformation of the aromatic Schiff bases and the extent of conjugation in these complex molecules. The benzylidene and the aniline rings of aromatic Schiff bases have been substituted by groups of varying electron donating and accepting properties. The dimethylamino ($-NMe_2$), hydroxy (-OH) and methoxy ($-OCH_3$) groups have been chosen as electron donors whereas the nitro ($-NO_2$)group

is used as an acceptor group. By correlating the spectral changes in the electronic absorption band as well as in the relevent Raman bands it has been inferred that the aniline moiety of the aromatic Schiff bases is playing the central role. The benzylidene ring seems to have comparatively less contribution in *controlling the position and intensity of the electronic* absorption bands in these molecules. These results suggest non-coplanar configuration for the aniline and the benzylidene rings in the aromatic Schiff base molecules.

The normal Raman spectrum is obtained by excitation in a transparent region of the electronic absorption spectrum and in such a case, the Raman-allowed vibrational modes of the scatterers appear, with variable intensity. When the exciting wavelength approaches an electronic absorption band of the sample, intensity of the specific bands may be enhanced. This is pre-resonance Raman effect. The specific site of a complex molecular system can be detected with the needed sensitivity and selectivity via the pre-resonance Raman effect[11-13], provided that the site gives rise to an electronic absorption band whose wavelength can be approached by available excitation sources. Although the potential of the pre-resonance technique is easy to appreciate in general terms, the particular manifestation of the pre-resonance Raman effect varies from one kind of chromophore to another. The intensity variation of the structurally sensitive Raman bands as a function of the exciting wavelength in pre-

resonance region can reveal geometric changes and vibronic couplings of the excited molecular states. The significant terms which contribute to the polarizability tensor under pre-resonance conditions are the terms which involve the change in the internuclear distance during electronic transition (F_A^2-term) and the vibronic coupling between two electronic excited states (F_B^2-term). Raman intensity enhancement through F_A^2-term contains contribution from the Franck-Condon factor which depends on the extent to which the excited electronic state potential is displaced along the normal co-ordinate. On the other hand, the contribution of the F_B^2-term towards the pre-resonance Raman intensity, depends on the magnitude of the vibronic coupling. The pre-resonance Raman studies on several conjugated molecular systems reveal that the enhancement in Raman intensity is better determined by the F_B^2-term rather than the F_A^2-term.[11-16] In aromatic Schiff bases, due to the non-coplanar conformation of the benzylidene and the aniline rings, the extent of conjugation is not expected to be high. The vibrational modes involved in the coupling of the electronic states gain intensity as the exciting wavelength progressively approaches the wavelength corresponding to the excited electronic states. The Raman excitation profiles of the selected three bands [ν_{8a}, ν_{8b} (Wilson's notation)[17] and $\nu_{C=N}$ mode] in four Schiff bases namely Benzylidene-p-nitroaniline (BPNA), p-dimethylaminobenzylidene-p'-methoxyaniline (DABPMA), p-dimethylaminobenzylideneaniline (DABA) and Benzylidene-O-hydroxyaniline (BOHA) reveal that the C-C

stretching vibrational modes of benzenoid moiety ν_{8a} and ν_{8b} are dominant in coupling the excited electronic states. The observed low intensity of the Raman band corresponding to the C=N stretching mode indicates weak conjugation in these systems. For all the three modes, theoretical calculations for the intensity variations were done using Albrecht and Hutley's[15] approach. It is observed that in all the four molecules intensity enhancement of the three bands corresponding to ν_{8a}, ν_{8b} and $\nu_{C=N}$ modes is better determined by the B-term compared to A-term. Therefore, it can be inferred that the vibronic coupling plays a major role in controlling the pre-resonance Raman intensity of bands corresponding to ν_{8a}, ν_{8b} and $\nu_{C=N}$ vibrations. The vibrational modes in the aniline moiety seem to be dominant in coupling the charge-transfer and $\pi - \pi^*$ electronic transitions. The Franck-Condon factors, on the other hand, appear to be less important in the pre-resonance region of these systems.

The dielectric behaviour of complex biological molecules in living organism is substantially influenced by the effects associated with dissolved ionic contents and other chemicals whose concentration varies in a wide range. Frequency-dependent polarization and dielectric losses in complex molecular systems embedded in ionic matrix are capable of providing information needed for the understanding of the behaviour of these complex molecules when surrounded by charges. In an attempt to get deeper insight into the dielectric behaviour of molecules

which have biological significance, we have studied the frequency-dependent dielectric behaviour of four aromatic Schiff bases namely Benzylidene-p-nitroaniline (BPNA), Benzylidene-m-hydroxyaniline (BMHA), p-dimethylaminobenzylidene-p'-hydroxyaniline (DABPHA) and p-methoxybenzylidene-p'-nitroaniline (PMBPNA), dispersed in KBr-matrix. The solid phase studies were preferred for the present investigation to avoid possible complications of liquid state.

This thesis consists of seven Chapters. Chapter I introduces the problem and also outlines the interpretations and limitations by earlier workers working on relevent and related systems.

Chapter II presents the basic theoretical background of the Raman spectroscopic and dielectric relaxation techniques. The theoretical aspects of these studies have been presented in two parts. The first part of this Chapter deals with the Raman theories with special emphasis on the intensity variation of structurally sensitive vibrational bands as a function of the exciting wavelength under the pre-resonance conditions. The treatment, is based on Albrecht and Hutley's theoretical approach[15] for the calculation of Raman intensity under pre-resonance conditions. The second part of this Chapter is concerned mainly with the theoretical aspects of dielectric relaxation and related physical processes. Brief theoretical treatments of interactions

such as charge-dipole and dipole-dipole interactions are also presented in this part of Chapter II.

A short description of the instrumentation and experimental techniques used in the present work is presented in Chapter III. Among the instruments, the Raman spectrometer and the laser sources have been dealt with in detail. In addition, this chapter also contains a brief introduction to the instrumentation for recording the electronic absorption spectra and the IR spectra of the samples. Some of the important specifications of these instruments are presented in tabular form at the end of this chapter. The salient features of the instrument used for dielectric measurements are also presented in this chapter.

The aromatic Schiff bases with which the present investigation is concerned, were synthesized in our laboratory. The purification of the synthesized compounds is of utmost importance in spectroscopic and dielectric studies. The procedure followed for the synthesis and purification of the aromatic Schiff bases, used in present studies, has been outlined in Chapter IV. The H'NMR spectral data were used for confirming the formation of the compounds. The microanalytical technique was applied for estimating the extent of purity in the synthesized samples.

Vibrational assignments are necessary for providing information regarding structural features and are also needed for carrying out systematic vibrational studies. Assignment of the vibrational bands associated with the Schiff base linkage is of special value in the sense that the site containing the Schiff base linkage is of biological importance since the linkage is found to be present in biological systems. The assignment of the C=N stretching vibration of some biological systems like rhodopsin are reported in literature[3,4]. The vibrational assignments for the substituted aromatic Schiff bases containing donor and acceptor groups may throw light on the environmental effects on Raman bands as the substituted aromatic Schiff bases could be treated as model systems for complex biological sites. The details of the band assignments for the four aromatic Schiff bases, are presented in Chapter V.

Chapter VI contains the theoretically calculated Raman intensity factors F_A^2 and F_B^2 of Albrecht and Hutley's theory, for three well-resolved Raman bands corresponding to ν_{8a}, ν_{8b} and $\nu_{C=N}$ modes of vibration. The experimentally measured values of relative Raman intensities of the bands corresponding to the above mentioned vibrational modes are also presented at various exciting wavelegths. Both the theoretically calculated values and the experimentally measured values of the intensity factors are normalized with respect to the exciting wavelength λ_o = 4880 Å and the normalized Raman ointensity factors R_A, R_B and R_I

corresponding to the F_A^2, F_B^2 terms and the experimentally observed values are compared in Tables VI-1-4. In addition, the electronic absorption spectra of these molecules are presented in this chapter as they are required for plotting the intensity variation as a function of wavelength which is known as excitation profile. The interpretation of the electronic absorption spectra has also been given in order to identify electronic transitions which are likely to be mixed. The Raman spectra in conjunction with electronic absorption spectra indicate that in these four aromatic Schiff bases the benzylidene and the aniline rings do not have coplanar configurations. X-ray crystallographic analysis shows that trans-azobenzene and trans-stilbene molecules which are iso-π-electronic with the aromatic Schiff bases have a planar or nearly planar structure.[18,19] Comparative study with these molecules clearly indicates that the Schiff base molecules are not highly conjugated systems and suggests that the molecule is twisted around the C=N bond thus leading to a non-coplanar conformation. The non-coplanarity of the benzylidene and the aniline rings, therefore, divides the molecule into two weakly interacting conjugated fragments. One of the π-systems is probably localized at the aniline moiety containing the nitrogen lone pair whereas the other π-system is localized at the benzylidene moiety. It has been observed that the substitution in the aniline ring by hydroxyl group in the ortho-position enhances the relative Raman intensity of the band corresponding to the C=N stretching mode whereas substitution in

the para-position appears to be less effective, in enhancing such conjugation in the aromatic Schiff base molecules. The non-coplanarity in the aromatic Schiff base molecules is also found to be in agreement with the X-ray and electron-diffraction studies.[20,21]

Chapter VII presents the experimental dielectric data of four Schiff bases i.e. BPNA, BMHA, DABPHA and PMBPNA in solid phase, dispersed in the strong ionic matrix of Potassium Bromide (KBr). All the four Schiff bases are observed to exhibit dielectric relaxation at frequencies below 5KHz. The frequency-dependent data of these molecular systems, reveal, that mainly two physical processes are prominent in governing the dielectric behaviour in these complex molecules. This behaviour is, however, a function of the molecular structure and the relaxation frequency varies from molecule to molecule. The relaxation frequencies are observed around 1KHz and 4KHz for BMHA and DABPHA respectively. However, for BPNA and PMBPNA, the relaxation frequency is around 100Hz. The variation of the dissipation factor as a function of frequency reveals that in all the four systems the frequency region below the relaxation frequency is dominated by the electronic type of nomadic polarization which arises mainly due to the long range delocalization of the π-electrons in these systems. In the frequency-region above the observed relaxation frequency the time allowed is not sufficient for delocalization of π-electrons and hence, the nomadic

polarization ceases to respond to the applied electric field. In this frequency region, the motion of molecular fragments seems to play role towards the dielectric properties of these dispersed systems. Due to the randomly distributed ionic environment around the Schiff base molecules, the applied electric field suffers spatial non-uniformity leading to the electrostatic strain in sensitive molecular fragments. The motion of these molecular fragments with respect to the applied electric field seems to be important in controlling the high frequency dielectric behaviour. The chemical nature and the position of the substituent-groups in these molecules appeared to contribute significantly towards the dielectric properties in the higher frequency region, presently investigated.

References

1. A.R. Oseroff and R.H. Callender *Biochemistry* 13, No 20, 4243 (1974) and references therein.
2. A.G. Doukas, B. Aton, R.H. Callender and B. Honig *Chem. Phys. Lett.* 56, 248 (1978) and references therein.
3. R. Mendelson, A.L. Verma, H.J. Bernstein and M. Kates *Can. J. Biochem.* 52, 774 (1974).
4. A. Lewis, J. Spoonhower, R.A. Bogomolni, R.H. Lozier and W. Stoeckenius *Proc. Nat. Acad. Sci.* 11, 4462 (1974).
5. I. Teucher, C.M. Paleos and M.M. Labes *Mol. Cryst. Liquid Cryst.* 11, 187 (1970).
6. R.A. Champa *Mol. Cryst. Liquid Cryst.* 16, 175 (1972). *"Liquid Crystals and Ordered Fluids"* J.F. Johnson and R.S. Porter, Eds., vol 2, p.507, Plenum Press, New York (1974).
7. C.S. Oh *Mol. Cryst. Liquid Cryst.* 19, 95 (1972).
8. S. Jen, N.A. Clark and P.S. Pershan *Phys. Rev. Letts.* 31, No 26 p.1552 (1973).
9. R. Pethig and A. Szent-Gyorgyi *Proc. Nat. Acad. Sci., USA* 74, 226 (1977).
10. S. Bone, T.J. Lewis, R. Pethig and A. Szent-Gyorgyi *Proc. Nat. Acad. Sci., USA* 75, 315 (1978).
11. K. Kumar and P.R. Carey *Can. J. Chem.* 55, 1443 (1977).
12. V.R. Salares, R. Mendelsohn, P.R. Carey and H.J. Bernstein *J. Phys. Chem.* 80, 1137 (1976).
13. P. Gaber, V. Miskowski and T.G. Spiro *J. Am. Chem. Soc.* 96, 6868 (1974).

14. K. Kumar and P.R. Carey *J. Chem. Phys.* 63, 3697 (1975).

15. A.C. Albrecht and M.C. Hutley *J. Chem. Phys.* 55, 4438 (1971).

16. M. Ito and I. Suzuka *Chem. Phys. Lett.* 31, 367 (1975).

17. *"Molecular Vibrations"* E.B. Wilson, J.C. Decius and P.C. Cross, McGraw-Hill, London (1955).

18. J.M. Robertson *J. Chem. Soc.* 232 (1939).

19. J.M. Robertson and I. Woodward *Proc. Roy. Soc. (London)* A162, 568 (1937).

20. H.B. Burgi and J.D. Dunitz *Chem. Com.* 472 (1969).

21. H. Nakai, M. Shiro, K. Ezumi, S. Sakata and T. Kubota *Acta Cryst.* B32, 1827 (1976).

LASER RAMAN SPECTROSCOPIC AND DIELECTRIC STUDIES OF SOME MOLECULES OF BIOLOGICAL SIGNIFICANCE

By

RADHENDU DAS

DEPARTMENT OF PHYSICS

SCHOOL OF PHYSICAL SCIENCES

A THESIS

SUBMITTED

IN

FULFILMENT OF THE REQUIREMENT FOR THE DEGREE OF

DOCTOR OF PHILOSOPHY

To

THE NORTH-EASTERN HILL UNIVERSITY

SHILLONG - 793 001

INDIA

JULY, 1991

DS
539.12
DAS

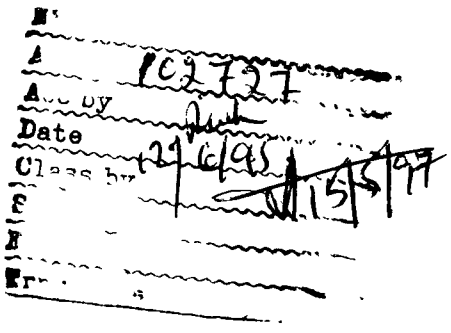

DEDICATED

In

MEMORY

Of My

LOVING FATHER

DR. KAMAL KUMAR
Department of Physics

North-Eastern Hill University
SHILLONG 793003

CERTIFICATE

I certify that the thesis entitled "Laser Raman Spectroscopic and dielectric studies of some molecules of Biological Significance" submitted by Shri Radhendu Das for the Degree of Doctor of Philosophy of the North-Eastern Hill University, Shillong, embodies the record of original investigation carried out by him under my supervision. He has been duly registered and the thesis presented is worthy of being considered for the Award of Ph.D. Degree. This work has not been submitted for any Degree of any other University.

K. Kumar 12.7.91

Dated: 12 July, 1991
Shillong.

(DR. KAMAL KUMAR)
Supervisor

Phone :
Grams : NEHU

North - Eastern Hill University

Bijni Complex
Bhagyakul, Shillong - 793003 (Meghalaya)

Department of.....
Physics

10 July 1991

CERTIFICATE

This is to certify that Shri Radhendu Das has cleared the following four Pre-Ph.D. Courses obtaining 'A' grade in all of them.

Course	Grade
1. The Theory and Techniques on Magnetic Resonance	A
2. Advanced Nuclear Physics	A
3. Many body Theory	A
4. French Language	A

Prabodh Shukla

(Dr. P. SHUKLA)
Professor and Head,
Department of Physics

ACKNOWLEDGEMENTS

It is with great pleasure that I wish to express my deepest sense of gratitude to Dr. Kamal Kumar for his supervision and guidance on this work. I am grateful for his constant encouragement, advice and help without which this work would not have been possible.

I take this opportunity to thank Prof. A.L. Verma for his help and encouragement during the course of this work.

This column remains incomplete if I forget to acknowledge all the members of my family for their keen interest and encouragement. I thank Dr. Anusree Ghose, Mr. G.S.S. Saini and other friends for their cooperation and encouragement throughout the course of this work.

I acknowledge my sincere thanks to Mr. A.K. Rathore for his adept typing of this thesis.

Finally, I am grateful to the Department of Atomic Energy, Bombay for providing the financial support.

Radhendu Das

(RADHENDU DAS)

Shillong,

12 July, 1991.

C O N T E N T S

S Y N O P S I S

SYNOPSIS

This thesis deals with the Laser Raman spectroscopic and dielectric studies of substituted aromatic Schiff bases. The structural and behavioural properties of aromatic Schiff bases make them unique model system to investigate a wide variety of biological phenomena. Our knowledge of these systems may be applied towards better understanding of bilogical processes involving membranes and visual systems. The visual pigments, rhodopsin is composed of the chromophore 11-cis-retinal linked by a Schiff base[1] to the membrane glycoprotein opsin. The absorption bands of the resulting pigment are considerably red-shifted from those of the free chromophore and from protonated and unprotonated Schiff bases formed with retinal in organic solvents. An understanding of the retinal-opsin interactions responsible for the colour of the visual pigments requires information about the retinal-opsin complex. The photoreceptors respond to electrical stimulation in a similar fashion as liquid crystals and are sensitive to changes in the environment. The understanding of the changes due to the variation in environment, thus, becomes important in interpreting biological structures at the molecular level. The understanding of the structural chemistry operating at the biological sites such as the C=N linkage may come through the application of physical and chemical structure probes. Vibrational studies of the protonated and

unprotonated Schiff bases reveal that the C=N linkage plays a significant role in controlling biological processes. In several such molecular systems, vibrational spectroscopic studies of the C=N stretching mode was attempted by earlier workers.[2-4] Many Schiff bases are known to behave as liquid crystals[5-8], the present spectroscopic studies may provide basic spectral data for the liquid crystal studies. In addition, it has been proposed by some research workers[9,10] that the Schiff base linkage may be playing role in charge-transfer interactions with a neighbouring peptide unit by creating mobile holes within protein valence bands. The monitoring of the C=N linkage is therefore important for such studies as well. In an attempt to provide more structural information and spectroscopic data on molecules containing the C=N linkage, we have investigated the aromatic Schiff bases having substituent groups of varying chemical character. The molecules studied in the present investigation, essentially contain benzylidene and aniline moiety on either side of the Schiff base linkage. Raman spectroscopic studies assisted by the infrared and electronic absorption spectroscopic techniques have been used to provide information about the conformation of the aromatic Schiff bases and the extent of conjugation in these complex molecules. The benzylidene and the aniline rings of aromatic Schiff bases have been substituted by groups of varying electron donating and accepting properties. The dimethylamino ($-NMe_2$), hydroxy (-OH) and methoxy ($-OCH_3$) groups have been chosen as electron donors whereas the nitro ($-NO_2$)group

is used as an acceptor group. By correlating the spectral changes in the electronic absorption band as well as in the relevent Raman bands it has been inferred that the aniline moiety of the aromatic Schiff bases is playing the central role. The benzylidene ring seems to have comparatively less contribution in controlling the position and intensity of the electronic absorption bands in these molecules. These results suggest non-coplanar configuration for the aniline and the benzylidene rings in the aromatic Schiff base molecules.

The normal Raman spectrum is obtained by excitation in a transparent region of the electronic absorption spectrum and in such a case, the Raman-allowed vibrational modes of the scatterers appear, with variable intensity. When the exciting wavelength approaches an electronic absorption band of the sample, intensity of the specific bands may be enhanced. This is pre-resonance Raman effect. The specific site of a complex molecular system can be detected with the needed sensitivity and selectivity via the pre-resonance Raman effect[11-13], provided that the site gives rise to an electronic absorption band whose wavelength can be approached by available excitation sources. Although the potential of the pre-resonance technique is easy to appreciate in general terms, the particular manifestation of the pre-resonance Raman effect varies from one kind of chromophore to another. The intensity variation of the structurally sensitive Raman bands as a function of the exciting wavelength in pre-

resonance region can reveal geometric changes and vibronic couplings of the excited molecular states. The significant terms which contribute to the polarizability tensor under pre-resonance conditions are the terms which involve the change in the internuclear distance during electronic transition (F_A^2-term) and the vibronic coupling between two electronic excited states (F_B^2-term). Raman intensity enhancement through F_A^2-term contains contribution from the Franck-Condon factor which depends on the extent to which the excited electronic state potential is displaced along the normal co-ordinate. On the other hand, the contribution of the F_B^2-term towards the pre-resonance Raman intensity, depends on the magnitude of the vibronic coupling. The pre-resonance Raman studies on several conjugated molecular systems reveal that the enhancement in Raman intensity is better determined by the F_B^2-term rather than the F_A^2-term.[11-16] In aromatic Schiff bases, due to the non-coplanar conformation of the benzylidene and the aniline rings, the extent of conjugation is not expected to be high. The vibrational modes involved in the coupling of the electronic states gain intensity as the exciting wavelength progressively approaches the wavelength corresponding to the excited electronic states. The Raman excitation profiles of the selected three bands [ν_{8a}, ν_{8b} (Wilson's notation)[17] and $\nu_{C=N}$ mode] in four Schiff bases namely Benzylidene-p-nitroaniline (BPNA), p-dimethylaminobenzylidene-p'-methoxyaniline (DABPMA), p-dimethylaminobenzylideneaniline (DABA) and Benzylidene-O-hydroxyaniline (BOHA) reveal that the C-C

stretching vibrational modes of benzenoid moiety ν_{8a} and ν_{8b} are dominant in coupling the excited electronic states. The observed low intensity of the Raman band corresponding to the C=N stretching mode indicates weak conjugation in these systems. For all the three modes, theoretical calculations for the intensity variations were done using Albrecht and Hutley's[15] approach. It is observed that in all the four molecules intensity enhancement of the three bands corresponding to ν_{8a}, ν_{8b} and $\nu_{C=N}$ modes is better determined by the B-term compared to A-term. Therefore, it can be inferred that the vibronic coupling plays a major role in controlling the pre-resonance Raman intensity of bands corresponding to ν_{8a}, ν_{8b} and $\nu_{C=N}$ vibrations. The vibrational modes in the aniline moiety seem to be dominant in coupling the charge-transfer and $n - \pi^*$ electronic transitions. The Franck-Condon factors, on the other hand, appear to be less important in the pre-resonance region of these systems.

The dielectric behaviour of complex biological molecules in living organism is substantially influenced by the effects associated with dissolved ionic contents and other chemicals whose concentration varies in a wide range. Frequency-dependent polarization and dielectric losses in complex molecular systems embedded in ionic matrix are capable of providing information needed for the understanding of the behaviour of these complex molecules when surrounded by charges. In an attempt to get deeper insight into the dielectric behaviour of molecules

which have biological significance, we have studied the frequency-dependent dielectric behaviour of four aromatic Schiff bases namely Benzylidene-p-nitroaniline (BPNA), Benzylidene-m-hydroxyaniline (BMHA), p-dimethylaminobenzylidene-p'-hydroxyaniline (DABPHA) and p-methoxybenzylidene-p'-nitroaniline (PMBPNA), dispersed in KBr-matrix. The solid phase studies were preferred for the present investigation to avoid possible complications of liquid state.

This thesis consists of seven Chapters. Chapter I introduces the problem and also outlines the interpretations and limitations by earlier workers working on relevent and related systems.

Chapter II presents the basic theoretical background of the Raman spectroscopic and dielectric relaxation techniques. The theoretical aspects of these studies have been presented in two parts. The first part of this Chapter deals with the Raman theories with special emphasis on the intensity variation of structurally sensitive vibrational bands as a function of the exciting wavelength under the pre-resonance conditions. The treatment, is based on Albrecht and Hutley's[15] theoretical approach for the calculation of Raman intensity under pre-resonance conditions. The second part of this Chapter is concerned mainly with the theoretical aspects of dielectric relaxation and related physical processes. Brief theoretical treatments of interactions

such as charge-dipole and dipole-dipole interactions are also presented in this part of Chapter II.

A short description of the instrumentation and experimental techniques used in the present work is presented in Chapter III. Among the instruments, the Raman spectrometer and the laser sources have been dealt with in detail. In addition, this chapter also contains a brief introduction to the instrumentation for recording the electronic absorption spectra and the IR spectra of the samples. Some of the important specifications of these instruments are presented in tabular form at the end of this chapter. The salient features of the instrument used for dielectric measurements are also presented in this chapter.

The aromatic Schiff bases with which the present investigation is concerned, were synthesized in our laboratory. The purification of the synthesized compounds is of utmost importance in spectroscopic and dielectric studies. The procedure followed for the synthesis and purification of the aromatic Schiff bases, used in present studies, has been outlined in Chapter IV. The H'NMR spectral data were used for confirming the formation of the compounds. The microanalytical technique was applied for estimating the extent of purity in the synthesized samples.

Vibrational assignments are necessary for providing information regarding structural features and are also needed for carrying out systematic vibrational studies. Assignment of the vibrational bands associated with the Schiff base linkage is of special value in the sense that the site containing the Schiff base linkage is of biological importance since the linkage is found to be present in biological systems. The assignment of the C=N stretching vibration of some biological systems like rhodopsin are reported in literature[3,4]. The vibrational assignments for the substituted aromatic Schiff bases containing donor and acceptor groups may throw light on the environmental effects on Raman bands as the substituted aromatic Schiff bases could be treated as model systems for complex biological sites. The details of the band assignments for the four aromatic Schiff bases, are presented in Chapter V.

Chapter VI contains the theoretically calculated Raman intensity factors F_A^2 and F_B^2 of Albrecht and Hutley's theory, for three well-resolved Raman bands corresponding to ν_{8a}, ν_{8b} and $\nu_{C=N}$ modes of vibration. The experimentally measured values of relative Raman intensities of the bands corresponding to the above mentioned vibrational modes are also presented at various exciting wavelegths. Both the theoretically calculated values and the experimentally measured values of the intensity factors are normalized with respect to the exciting wavelength λ_o = 4880 Å and the normalized Raman intensity factors R_A, R_B and R_I

corresponding to the F_A^2, F_B^2 terms and the experimentally observed values are compared in Tables VI-1-4. In addition, the electronic absorption spectra of these molecules are presented in this chapter as they are required for plotting the intensity variation as a function of wavelength which is known as excitation profile. The interpretation of the electronic absorption spectra has also been given in order to identify electronic transitions which are likely to be mixed. The Raman spectra in conjunction with electronic absorption spectra indicate that in these four aromatic Schiff bases the benzylidene and the aniline rings do not have coplanar configurations. X-ray crystallographic analysis shows that trans-azobenzene and trans-stilbene molecules which are iso-π-electronic with the aromatic Schiff bases have a planar or nearly planar structure.[18,19] Comparative study with these molecules clearly indicates that the Schiff base molecules are not highly conjugated systems and suggests that the molecule is twisted around the C=N bond thus leading to a non-coplanar conformation. The non-coplanarity of the benzylidene and the aniline rings, therefore, divides the molecule into two weakly interacting conjugated fragments. One of the π-systems is probably localized at the aniline moiety containing the nitrogen lone pair whereas the other π-system is localized at the benzylidene moiety. It has been observed that the substitution in the aniline ring by hydroxyl group in the ortho-position enhances the relative Raman intensity of the band corresponding to the C=N stretching mode whereas substitution in

the para-position appears to be less effective, in enhancing such conjugation in the aromatic Schiff base molecules. The non-coplanarity in the aromatic Schiff base molecules is also found to be in agreement with the X-ray and electron-diffraction studies.[20,21]

Chapter VII presents the experimental dielectric data of four Schiff bases i.e. BPNA, BMHA, DABPHA and PMBPNA in solid phase, dispersed in the strong ionic matrix of Potassium Bromide (KBr). All the four Schiff bases are observed to exhibit dielectric relaxation at frequencies below 5KHz. The frequency-dependent data of these molecular systems, reveal that mainly two physical processes are prominent in governing the dielectric behaviour in these complex molecules. This behaviour is, however, a function of the molecular structure and the relaxation frequency varies from molecule to molecule. The relaxation frequencies are observed around 1KHz and 4KHz for BMHA and DABPHA respectively. However, for BPNA and PMBPNA, the relaxation frequency is around 100Hz. The variation of the dissipation factor as a function of frequency reveals that in all the four systems the frequency region below the relaxation frequency is dominated by the electronic type of nomadic polarization which arises mainly due to the long range delocalization of the π - electrons in these systems. In the frequency-region above the observed relaxation frequency the time allowed is not sufficient for delocalization of π-electrons and hence, the nomadic

polarization ceases to respond to the applied electric field. In this frequency region, the motion of molecular fragments seems to play role towards the dielectric properties of these dispersed systems. Due to the randomly distributed ionic environment around the Schiff base molecules, the applied electric field suffers spatial non-uniformity leading to the electrostatic strain in sensitive molecular fragments. The motion of these molecular fragments with respect to the applied electric field seems to be important in controlling the high frequency dielectric behaviour. The chemical nature and the position of the substituent-groups in these molecules appear to contribute significantly towards the dielectric properties in the higher frequency region, presently investigated.

References

1. A.R. Oseroff and R.H. Callender *Biochemistry* 13, No 20,4243 (1974) and references therein.
2. A.G. Doukas, B. Aton, R.H. Callender and B. Honig *Chem. Phys. Lett.* 56, 248 (1978) and references therein.
3. R. Mendelson, A.L. Verma, H.J. Bernstein and M. Kates *Can. J. Biochem.* 52, 774 (1974).
4. A. Lewis, J. Spoonhower, R.A. Bogomolni, R.H. Lozier and W. Stoeckenius *Proc. Nat. Acad. Sci.* 11, 4462 (1974).
5. I. Teucher, C.M. Paleos and M.M. Labes *Mol. Cryst. Liquid Cryst.* 11, 187 (1970).
6. R.A. Champa *Mol. Cryst. Liquid Cryst.* 16, 175 (1972). *"Liquid Crystals and Ordered Fluids"* J.F. Johnson and R.S. Porter, Eds., vol 2, p.507, Plenum Press, New York (1974).
7. C.S. Oh *Mol. Cryst. Liquid Cryst.* 19, 95 (1972).
8. S. Jen, N.A. Clark and P.S. Pershan *Phys. Rev. Letts.* 31, No 26 p.1552 (1973).
9. R. Pethig and A. Szent-Györgyi *Proc. Nat. Acad. Sci., USA* 74, 226 (1977).
10. S. Bone, T.J. Lewis, R. Pethig and A. Szent-Györgyi *Proc. Nat. Acad. Sci., USA* 75, 315 (1978).
11. K. Kumar and P.R. Carey *Can. J. Chem.* 55, 1443 (1977).
12. V.R. Salares, R. Mendelsohn, P.R. Carey and H.J. Bernstein *J. Phys. Chem.* 80, 1137 (1976).
13. P. Gaber, V. Miskowski and T.G. Spiro *J. Am. Chem. Soc.* 96, 6868 (1974).

14. K. Kumar and P.R. Carey *J. Chem. Phys.* 63, 3697 (1975).

15. A.C. Albrecht and M.C. Hutley *J. Chem. Phys.* 55, 4438 (1971).

16. M. Ito and I. Suzuka *Chem. Phys. Lett.* 31, 367 (1975).

17. *"Molecular Vibrations"* E.B. Wilson, J.C. Decius and P.C. Cross, McGraw-Hill, London (1955).

18. J.M. Robertson *J. Chem. Soc.* 232 (1939).

19. J.M. Robertson and I. Woodward *Proc. Roy. Soc. (London)* A162, 568 (1937).

20. H.B. Burgi and J.D. Dunitz *Chem. Com.* 472 (1969).

21. H. Nakai, M. Shiro, K. Ezumi, S. Sakata and T. Kubota *Acta Cryst.* B32, 1827 (1976).

CHAPTER – I

INTRODUCTION

Introduction

The work presented in this thesis is concerned with the Laser Raman spectroscopic and dielectric studies of aromatic Schiff base molecules. This class of molecules is of considerable importance in many spheres of studies. The biological significance and the liquid crystalline behaviour of these molecules deserve special mention in this context. The protonated Schiff bases are found to play central role in controlling the retinal mechanism. One of the significant contribution of Raman studies of the retinal mechanism is the proof[1-3] that opsin and retinal are joined by a protonated Schiff base linkage as

$$\text{(retinal)} - CH = \underset{H}{N^{+}} - (CH_2)_4 - \text{(opsin)}$$

Vibrational studies on protonated Schiff bases such as rhodopsin, bathorhodopsin provided evidence[4-6] that absorption of light by these systems does not change the state of protonation. Evidence in favour of existence of an unprotonated Schiff base linkage was found[6] in metarhodopsin II. For a wide variety of such molecular systems, the assignment of the C=N stretching mode was attempted.[4,7-11] The vibrational studies on these molecules reveal that the site containing the C=N linkage plays a

significant role in governing the processes involved in retinal mechanism. For deeper insight into these mechanism, a detailed spectroscopic study seems to be of significance which may provide information about excited states and the vibronic coupling of vibrational modes. Application of Laser Raman technique is expected to be useful under pre-resonance conditions for such studies. Besides the Schiff base linkage, the interactions at the other sites is also of importance. Therefore, the study of a large number of molecules having substituents of various chemical nature may be of significance in understanding the various processes involving molecules containing the Schiff base linkage. In an attempt to proceed with such investigations, we have selected aromatic Schiff base as the molecular system for Laser Raman spectroscopic studies. We have investigated four aromatic Schiff bases containing substituent groups of varying chemical characters. The spectroscopic studies of these systems are mostly based on Raman data. However, Raman spectroscopic study is assisted by the electronic absorption spectra which are even otherwise required for pre-resonance Raman spectroscopic investigations. The infrared data have also been used to support the band assignments which are required to identify the band due to Schiff base linkage.

The Raman studies, coupled with the electronic absorption studies are of utmost importance in providing information regarding the geometry of the ground as well as

excited electronic states of complex organic molecules. The Raman intensity of the specific bands in pre-resonance region is capable of providing detailed information about the nature of the lowest excited electronic states. An electronic transition between two states is accompanied by simultaneous changes in the vibrational states, so that the absorption due to the electronic transition, in principle, consists of a large number of lines. The rotational fine structures are usually unresolvable in liquids as rotational states are usually not well-defined. The shape of an absorption band due to a single electronic transition may, therefore, be considered to be determined by the spacing of the vibrational subbands and by the distribution of the total intensity of the electronic transition among the vibrational subbands. The intensity distribution among the vibrational subbands is determined by the *Franck-Condon* principle which states that the most probable vibrational component of an electronic transition is one which involves no change in the nuclear configuration.

In condensed phases, molecules generally can not rotate freely and as such the rotational energy levels lose their meaning. It is, therefore, not possible to seperate rotational lines in the spectra of liquids, solutions and solids. In liquids and solutions, the vibrational levels are broadened because of varying interactions of molecules with their neighbours. This broadening is often quite sufficient to obscure most or all the

vibrational structure of bands. Although in some cases, the equilibrium geometry of a molecule in an excited electronic state can be inferred from theoretical considerations of the electronic structure of the state, it is, in general, difficult to determine experimentally the geometry of a molecule in an excited electronic state. Since the life time of excited states is usually quite short, it is not possible to obtain the requisite quantities of molecules in the excited state for the time needed. Thus, customary experimental techniques used for the determination of the geometry of a molecule in its ground state are not applicable in an excited state. We have attempted to utilize the pre-resonance Raman techniques to get some information. The Raman excitation profiles of some specific bands in the pre-resonance region could be used for providing information about the excited electronic states. Such studies are essentially based on the fact that the most prominen t vibrational progression, if present in an absorption band may provide information about the geometry of the molecule in the corresponding excited state.

Substitution at different positions on the rings of the aromatic Schiff base molecules brings about changes in the electron cloud of the benzenoid moiety and as such may perturb the coupling between the sensitive vibrational mode(s) and the electronic states. The extent to which coupling phenomena are perturbed depends upon the chemical nature as well as the

position of the substituent groups in the benzene rings. A systematic study of the Raman excitation profile in the pre-resonance region for a particular band corresponding to a mode of vibration, appears to be informative. The choice of chemical groups with high degree of electron donating or accepting ability is therefore expected to be of significant value in such a context. Such substitution-dependent studies are expected to monitor the active moiety of the Schiff base molecules which are mainly responsible for the coupling of vibrational modes to the electronic states. The aromatic Schiff bases in the present study consist of the benzylidene and the aniline rings linked by the -C=N- linkage. Depending on the geometry of the molecules which may be non-planar due to steric considerations, only a part of the molecule in expected to provide major contribution towards the coupling phenomena. The electron absorption spectrum useful for pre-resonance work may arise due to a segment of the molecule. A comparative study of the Raman spectra of Schiff bases with different substituent-characters assisted by the pre-resonance excitation profile may provide important clues in this direction. Such studies will also be useful in sorting out the vibrational mode which are strongly coupled to the electronic states in these molecules.

Raman scattering can reveal information about the vibronic coupling of excited molecular states through the intensity variation of the scattered Raman radiation as the

frequency of the incident laser light changes. According to *Albrecht and Hutley's*[12] theory, under pre-resonance conditions, the significant terms contributing to the polarizability tensor are determined by two terms known as A and B terms. The intensity factors are represented by F_A^2 and F_B^2 terms. The F_A^2 term contains contribution from the single state and depends on the extent of displacement of the excited electronic state potential along the normal co-ordinate. Since for non-totally symmetric modes, the origin shift upon electronic excitation is zero, only the totally-symmetric modes gain intensity via the A-term. The intensity enhancement through F_B^2-term, on the other hand, depends on the coupling where two or more energetically nearby electronic excited states are involved. In several conjugated molecular systems, the pre-resonance Raman intensity was found to be better determined by the F_B^2-term rather than the F_A^2-term. In the molecular systems of aromatic Schiff bases, the extent of conjugation is not expected to be high due to non-coplanarity of the benzylidene and aniline rings of the Schiff bases due to possible steric hindrance. In the pre-resonance region, due to mixing of the electronic transitions, some of the sensitive vibrational bands coupling the excited states are expected to gain intensity. It may, therefore, be interesting to investigate which of the two terms determine the pre-resonance Raman intensity for this class of molecules. A comparative study of the theoretically calculated values of the intensity factors with the experimentally observed values may provide information about the

coupling. It may also lead to better understanding of the excited states in complex molecular systems.

Some of the aromatic Schiff bases are also important for their liquid crystalline behaviour.[13-18] The nature of the terminal substituent groups are found to influence the liquid crystalline behaviour in some Schiff bases. The high nematic thermal stabilities of the 3-pyridyl compounds suggest that the diminution in conjugation between a terminal phenyl ring and the CH of the Schiff base linkage that must occur when this ring is replaced by 3-pyridyl, are offset by the enhanced axial polarizability resulting from the 3-heteronitrogen. *Young* et al[17] studied the effect of the presence of terminal 5-membered hetorcyclic rings on the liquid crystalline behaviour of Schiff bases. In Schiff bases having hydroxy-substitution in the ortho-position, lateral substitution was found to enhance the Nematic-Isotropic (N-I) temperatures.

At the phase transitions, due to application of fields and with other alignment procedure, the materials exhibiting liquid-crystalline property undergo changes in refractive index and optical constants. Such changes when interpreted from a macroscopic point of view may reveal important conclusions regarding such materials. While drawing conclusions about molecular rotations from a study of vibrational band shapes, it is essential to know the assignment of the mode under

consideration. The assignment of vibrational bands, therefore, appears to be of utmost importance for studies of such systems. Vibrational assignments of molecular systems which show structural resemblence to the liquid crystals may therefore be useful. The aromatic Schiff bases, are excellent systems for this purpose and are, therefore, chosen to be systems for the present studies. The Raman spectra in solution phase, the excitation profile in the pre-resonance region and the IR spectral data are expected to provide useful information for assignment of the important vibrational modes in the Schiff bases. A comparative study with the analogous molecules is also of significance for assigning the observed vibrational features in these systems.

From the point of view of molecular Physics and Chemistry, the biological materials are extremely complicated systems. However, these systems function in a systematic way and their functions may be treated in terms of dynamic rather than static properties of molecules. As a next step, one may be tempted to introduce a known interaction between the atoms and ions of the system and based on the known structure, calculate their dynamic properties. This may, however, not result in the general theory of the relevant processes. In looking to Physics for guidance to find a concept capable of describing biological order we are led to the concept of coherence which applies to cases as different as lasers, masers, superconductors and superfluids. In biological systems periodic processes are very

common. Among them the periods may extend from that of life-cycles to very high frequency electric vibrations. In contrast to most physical periodic processes, periods of biological processes often vary from case to case. Thus the period of the life-cycles of cells grown under exactly the same conditions vary with certain limits i.e. each cell exhibits a certain amount of personality. Random energy supplied to certain systems need not lead to heating but may result in the excitation of ordered (coherent) states. In looking for a physical characteristic common to most biological systems, one is at once led to their dielectric properties. High electric fields of about 10^5 V/cm is present in many biological systems. This field acts in the range of non-linear response and the materials in the system are therefore, strongly non linearly polarized. Many ions contained in biomolecules provide essential contribution to their stabilization, to their interaction[19] as well as to their interaction to the surrounding medium.[20]

The dielectric properties of water associated with biological structures are of considerable relevance to many biological systems. Dielectric measurements[21] on lysozyme have shown that 36 water molecules are so bound to the protein structure that they are prevented from rotating under the influence of applied electric fields and another 70 water molecules are so bound that they exhibit a dielectric dispersion at a lower frequency than expected for normal bulk water.

Measurements at microwave frequencies for DNA at various stages of hydration have shown[22] that around 280 water molecules per helix turn are so influenced by the electrostatic forces associated with the DNA structure that they do not freeze until temperatures of -100°C and lower, are attained.

Dielectric behaviour of hydrated biological materials exhibits interesting features at low frequency range i.e. at $\leq 10^6$Hz. The variation of relative permittivity as a function of frequency in this range shows a fall and is indicative of a dielectric relaxation.

In order to get a deeper insight into the behaviour of complex molecules, time-dependent dielectric studies may be of significant value. Studies related to polarization, dielectric relaxation and dielectric losses in complex molecular systems are capable of providing valuable information in this context. The dielectric behaviour of complex biological molecules in living organism is substantially influenced by the effects associated with dissolved ionic salts and other chemicals. The concentration of ions in biological fluids can be quite high. In some systems such as mammalian plasma, the concentration of Na^+ is of the order of 0.15M. The typical ionic concentrations for the higher plant cells, in general, are K^+ (0.119M), Cl^- (0.065M), and Na^+ (0.014M).[23] The presence of ions with such concentration range in the neighbourhood of biomolecules, therefore, greatly

influence the behaviour of biomolecules. As such, it seems logical that systematic studies of complex molecular systems embedded in ionic environment are of utmost significance for better understanding of their behaviour. In an attempt to get better insight into the dielectric behaviour of molecules of biological significance, dispersed in a strong ionic matrix (e.g. KBr matrix), we considered it worthwhile to study the time-dependent dielectric behaviour of aromatic Schiff bases with various substituent groups. The Schiff base molecules, dispersed in KBr matrix may be regarded as randomly oriented and as such the dispersed system may be assumed to be a heterogenous system. In order to avoid possible complications arising due to intermolecular interactions in liquid phase, we prefered to carry out the investigations related to dielectric studies in the solid phase. Studies of these systems in solid phase, however, are more advantageous in the sense that the solid phase properties are sometimes able to explain the biological processes.

References

1. L. Rimai, R.G. Kilponen and D. Gill *Biochem. Biophys Res. Commun.* 41, 492 (1970).
2. M.E. Heyde, D. Gill, R.G. Kilponen and L. Rimai *J. Ann. Chem. Soc.* 93, 6776 (1971).
3. A.R. Oseroff and R.H. Callender *Biochemistry* 13, No 20, 4243 (1974) and references therein.
4. G. Eyring and R. Mathies *Proc. Nat. Acad. Sci.* 76, 33 (1979).
5. B. Aton, A.G. Doukas, D. Narva, R.H. Callender, U. Dinur and B. Hunig *Biophys. J.* 29, 79 (1980).
6. A. Lewis *Int. Conf. Raman Spectrosc.* W.F. Murphy, Ed. p. 556, North Holland, Amsterdom and New York (1980).
7. A.G. Doukas, B. Aton, R.H. Callender and T.G. Ebrey *Biochemistry* 17, 2430 (1978).
8. R. Mendelson, A.L. Verma, H.J. Bernstein and M. Kates *Can. J. Biochem.* 52, 774 (1974).
9. A. Lewis, J. Spoonhower, R.A. Bogomolni, R.H. Lozier and W. Stoeckenius *Proc. Nat. Acad. Sci.* 11, 4462 (1974).
10. H.J. Terner, C.L. Burns and M.A. El-Sayed *Proc. Nat. Acad. Sci.* 76, 3046 (1979) and references therein.
11. M. Stockburger, W. Klusmann, H. Gattermann, G. Massig and R. Peters *Biochemistry* 18, 4886 (1979).
12. A.C. Albrecht and M.C. Hutley *J. Chem. Phys.* 55, 4438 (1971).

13. I. Teucher, C.M. Paleos and M.M. Labes *Mol. Cryst. Liquid Cryst.* 11, 187 (1970).

14. (a) R.A. Champa *Mol. Cryst. Liquid Cryst.* 16, 175 (1972).
(b) *"Liquid Crystals and Ordered Fluids"* J.F. Johnson and R.S. Porter, Eds., vol. 2, p. 507, Plenum Press, New York (1974).

15. C.S. Oh *Mol. Cryst. Liquid Cryst.* 19, 95 (1972).

16. S. Jen, N.A. Clork and P.S. Pershan *Phys. Rev. Letts.* 31, No 26 p. 1552 (1973).

17. W.R. Young, I. Haller and L. Williams *"Liquid Crystals and Ordered Fluids"* J.F. Johnson and R.S. Porter, Eds., p. 383, Plenum Press, New York (1970).

18. *"Advances in Liquid Crystals"* Ed. Glenn H. Brown, vol 2, Academic Press, New York (1976).

19. A. Wada and H. Nakamura *"Nature of the Charge Distribution in Proteins" Nature* 293, 757-758 (1981).

20. A. Warshel *Acc. Chem. Res.* 14, 284-290 (1981).

21. S. Bone and R. Pethig *J. Mol. Biol.* 157, 571-575 (1982).

22. T.E. Cross and R. Pethig *Int. J. Quantum Chem. Quantum Biol. Symp.* 10, 143-152 (1983).

23. *"Dielectric and Electronic Properties of Biological Materials"* R. Pethig, p. 107, John Wiley and Sons, Chichester (1979).

CHAPTER – II

THEORETICAL ASPECTS

2.1 Introduction

The Raman effect is an inelastic scattering phenomenon in which the illuminated sample absorbs a photon and simultaneously emits another photon of a different frequency. When the emitted photon is of lower frequency than the absorbed photon, the process is termed Stoke's Raman scattering, while if the emitted photon is of higher frequency, the process is called anti-Stoke's Raman scattering. Fig. 2.1 depicts schematically two Raman scattering processes. The Figure also shows that Raman scattering is a two-photon process which connects the molecular energy-levels m and n. The dashed line in the diagram indicates the virtual electronic states (electronic levels that are not real) of the molecule and states o and p represent the lowest-lying excited electronic levels of the molecule. Raman scattering, therefore, is very much like a two-photon absorption process taking the system from state m to n or vice versa, except that instead of two photons being absorbed, one is absorbed and one emitted. Raman spectroscopy generally is carried out in the visible and near-UV range of excitation frequencies. Since most of the molecular systems do not display absorption at these

optical frequencies, the virtual level lies well below the excited eigenstates, o and p. The level m and n are most often molecular vibrational levels for which the transition frequencies are much smaller than the optical excitation frequencies. The resonance Raman effect arises when the excitation frequencies are equal to the frequencies of one photon allowed transition between states n or m and states o or p as shown in Fig. 2.1(B). This electronic resonance enhancement can increase the efficiency of the Raman scattering by a factor of 100 or more. This phenomenon is particularly important in biophysical applications of Raman spectroscopy, since many proteins have chromophores with visible absorption bands.

The process depicted in Fig. 2.1(A) is often referred to as spontaneous Raman scattering, in analogy to spontaneous emission phenomena. In contrast, the inelastic light scattering processes such as coherent anti-Stokes Raman scattering (CARS) and stimulated Raman scattering (SRS) is marked by stimulated or coherent emission. In these coherent Raman spectroscopies, laser fields at both the excitation frequency and the Stokes-shifted frequency are incident on the sample, and they coherently drive the light scattering. In stimulated Raman scattering the Raman process coherently adds photons to the laser field at ω_s and coherently absorbs photons from the laser field at ω_L. The Raman signal is detected as a gain in the intensity at ω_s or as a loss in the intensity at ω_L. The former is the basis for stimulated

Raman gain spectroscopy (SRGS) and the latter in the basis for inverse Raman spectroscopy (IRS). The laser field at which the gain or loss in intensity is measured is referred to as the "probe" laser, while the other is called the "pump" laser.

The phenomenon of the Raman effect arises because molecular vibrations modulate the frequency of the dipole induced in a molecule by an incident field. The electric dipole moment induced in a molecule by the electric field E can be expanded in a power series:[1]

$$\mu = \alpha E + \beta E^2 + \gamma E^3 \qquad \ldots\ (2.1.1)$$

where the field E and induced dipole μ are vectors which, in general, are not oriented in the same direction, since α, β and γ are tensor quantities. In Eqn. (2.1.1) α is the polarizability tensor of rank 2, while β, γ, etc. are the hyperpolarizabilities of rank 3, 4, etc. While the tensor properties of α, β and γ are intrinsic feature of the Raman effect, they rarely need to be explicitly considered in applications of Raman spectroscopy in physical and chemical analysis. Spontaneous Raman scattering arises due to the linear term in Eqn. (2.1.1) while coherent Raman effects are connected with term cubic in E.

2.2 Spontaneous Raman Scattering

Although a quantum mechanical treatment is necessary

for a complete explanation of Raman scattering, many aspects of the phenomenon can be described reasonably well by the classical electromagnetics of the induced dipole and the molecular vibration. Following the treatment of *Placzek*[2], the polarizability can be expanded in a *Taylor* series as a function of the vibrational normal coordinate q.

$$\alpha = \alpha_o + (\frac{\partial \alpha}{\partial q})_o q + \frac{1}{2}(\frac{\partial^2 \alpha}{\partial q^2})_o q^2 + \ldots\ldots \quad \ldots (2.2.1)$$

where the subscript "o" indicates that the expansion is centered at the equilibrium molecular configuration. In order to understand the nature of the Raman effect it is only necessary to consider the first derivative term in Eqn. (2.2.1). Treating the molecular vibration as simple harmonic motion it can be shown that the oscillating dipole radiates energy not only at the incident frequency ω_L, but also at the frequencies $\omega_L - \omega_M$ (Stokes) and $\omega_L + \omega_M$ (Anti-Stokes) where ω_L is frequency of electric field, ω_M is the harmonic vibrational frequency. The power radiated by the molecule at the Stokes frequency is given by the classical relation[1]

$$P(\omega_s) = \frac{\omega_s^4}{3c^3} (\frac{1}{2} \alpha' q_o E_L)^2 \quad \ldots. (2.2.2)$$

where $\alpha' = (\frac{\partial \alpha}{\partial q})_o$ and q_o is the vibrational amplitude and E_L is the amplitude of electric field. This expression can be presented in terms of the phenomenological Raman differential

cross section per unit solid angle, $d\sigma/d\Omega$, given by[3]

$$\frac{d\sigma}{d\Omega} = (\alpha' q_o)^2 \left(\frac{\omega_s}{c}\right)^4 \quad \ldots\ldots (2.2.3)$$

and the relationship between the scattered light at ω_s and the incident light at ω_L is[1]

$$P(\omega_s) = Nl\frac{d\sigma}{d\Omega}\Delta\Omega\, P(\omega_L) \quad \ldots\ldots (2.2.4)$$

where N is the density of molecules in the molecular energy level responsible for the scattering, l is the sample length and $\Delta\Omega$ is the solid angle over which the light is collected. Raman scattering cross sections are typically of the order of 10^{-30} cm^2Sr^{-1} and as such is of extreme feeble nature. The scattered light is incoherent as the phase factor of independently radiating dipoles are random.

The classical electromagnetism also reveals the principal selection rule for Raman scattering. For a particular vibrational normal mode to be Raman active, the derivative of the polarizability with respect to the normal coordinate, evaluated at the equilibrium position must be nonzero ($\alpha' \neq 0$). For polyatomic molecules, establishing whether α' is zero or non-zero for a specific vibration is complicated. However, a general selection rule holds for vibrational transitions from the ground state to the first excited state. These transitions are Raman

active only if at least one cartesian component of α' is of the same symmetry species as the vibration itself. The significance of this selection rule is that many vibrations which are not infrared active such as totally symmetric vibrations, are Raman active.

Although classical electromagnetic theory provides considerable insight into the nature of Raman effect, a classical picture is not adequate to describe this process. A time-dependent quantum mechanical analysis is required to describe this inelastic light scattering process.

2.3 Pre-resonance Raman Intensity of vibrational bands

For randomly oriented molecules, the total intensity (over the solid angle 4π) of the scattered light resulting from a molecular transition between vibrational states m and n is given by[4,5]

$$I_{mn} = \frac{2^7\pi^5}{3^2c^4}(\nu_o \pm \nu_{mn})^4 I_o \sum_{\rho,\sigma} |(\alpha_{\rho\sigma})_{mn}|^2 \qquad \ldots (2.3.1)$$

where I_o is the incident intensity, ν_o is the frequency of the incident wave, c is the velocity of light, ν_{mn} is the frequency corresponding to the vibrational energy separation between the states m and n and $\alpha_{\rho\sigma}$ represents the $\rho\sigma$ th component of the transition polarizability tensor, where ρ and σ denote the cartesian co-ordinates. The $\rho\sigma$ th component of the transition

polarizability tensor between the states m and n, $(\alpha_{\rho\sigma})_{mn}$, may be derived by using second-order perturbation theory and is given by[6]

$$(\alpha_{\rho\sigma})_{mn} = \sum_{e} \left[\frac{\langle m|M_{\sigma}|e\rangle\langle e|M_{\rho}|n\rangle}{E_e - E_m - E_o} + \frac{\langle m|M_{\rho}|e\rangle\langle e|M_{\sigma}|n\rangle}{E_e - E_n + E_o} \right] \quad \ldots\ldots\ldots (2.3.2)$$

where the summation is over all vibronic states and the operators M_{σ} and M_{ρ} are defined by $M_{\sigma} = R_{\sigma} - \langle g|R_{\sigma}|g\rangle$. R_{σ} and R_{ρ} denote the electronic dipole moment operators[6] e.g. $R_{\sigma} = -\sum_{k} e(r_k)_{\sigma}$ with $(r_k)_{\sigma}$ being the σth component of the position vector of the kth electron. The molecule in this case is considered to be in the molecular state m which is perturbed by the electromagnetic wave and thus causing the transition to another state n, hence giving rise to the scattered light of frequency $(\nu_o - \nu_{mn})$. From Eqn. (2.3.2) it is obvious that when E_o approaches the energy of an allowed molecular transition [Fig. 2.2], the term $E_e - E_m - E_o$ becomes smaller and thus making the first term in Eqn. (2.3.2) very large. This is the condition for resonance. In order to have a closer view of the phenomenon, the molecular states m and n have to be broken down into their electronic and vibrational components which can be achieved by writing the total wave functions as products of electronic and vibrational parts[6] as follows:

$$|m\rangle = |g\rangle\!|i\rangle,\ |n\rangle = |g\rangle\!|j\rangle \text{ and } |r\rangle = |e\rangle\!|v\rangle \ . \quad (2.3.3)$$

[within Born-Oppenheimer approximation].

where $|g\rangle$ and $|e\rangle$ are the ground and excited electronic states respectively, $|i\rangle$ and $|j\rangle$ are the vibrational states associated with the ground electronic state and $|v\rangle$ is a vibrational state associated with the excited electronic state. Albrecht and Hutley have derived[7] an explicit form for the frequency-dependent Raman scattering in pre-resonance region.

$$(\alpha_{\rho\sigma})_{gi,gj} = \sum_{e} \sum_{s} [(\nu_e \nu_s + \nu_o^2)/h^2(\nu_e^2 - \nu_o^2)(\nu_s^2 - \nu_o^2)] \langle i|Q_a|j\rangle [\{(g^o|R_\rho|e^o)(e^o|h_a|s^o)(s^o|R_\sigma|g^o)\} + \{(g^o|R_\sigma|e^o)(e^o|h_a|s^o)(s^o|R_\rho|g^o)\}] \quad \ldots (2.3.4)$$

where $h_a = \left(\frac{\partial H}{\partial Q_a}\right)_o$ with H denoting the electronic part of the molecular Hamitonian and subscripts e and s refer to virtual electronic states with eigenfrequencies at ν_e and ν_s respectively and subscript o corresponds to the nuclear co-ordinate parameters at the ground state equilibrium configuration. In Eqn. (2.3.4) the diagonal terms (i.e. e=s) have been designated as A' term whereas the off-diagonal terms ($e \neq s$) as B' term. Albrecht and Hutley[7], in order to simplify the summation over virtual states, considered the special case where the incident frequency ν_o gradually approaches the molecular absorption band involving an excited electronic state which serves as an active virtual state for the vibrational mode responsible for the scattering. Assuming that only one component, $\alpha_{\rho\rho}$ of the polarizability is active[7,8]

and that e, is the major active electronic state in the near resonance condition, they obtained the following form

$$(\alpha_{\rho\rho})_{ij} = A_{\rho\rho} + B_{\rho\rho} \qquad \ldots\ (2.3.5)$$

where $$A_{\rho\rho} = 2[(\nu_e^2 + \nu_o^2)/(\nu_e^2 - \nu_o^2)^2][(e^o|R_\rho|g^o)^2/h^2]$$

$$\times(e^o|h_a|e^o)\langle i||Q_a||j\rangle \qquad \ldots\ (2.3.6)$$

and $$B_{\rho\rho} = 4 \sum_s [h^{-2}(\nu_e \nu_s + \nu_o^2)/(\nu_e^2 - \nu_o^2)(\nu_s^2 - \nu_o^2)]$$

$$(g^o|R_\rho|e^o)(s^o|R_\rho|g^o)(e^o|h_a|s^o)\langle i||Q_a||j\rangle \quad \ldots\ (2.3.7)$$

Again, assuming that the active virtual states, s lie at energy values which are sufficiently high to permit use of some average ν_s in term $B_{\rho\rho}$, both the terms A and B can be rewritten[7] as follows :

$$A_{\rho\rho} = \left(\frac{2e^2}{h^2}\right)\left[\frac{(\nu_e^2 + \nu_o^2)}{(\nu_e^2 - \nu_o^2)^2}\right] \sigma_e \varepsilon_{ee}(a_{ij}) \qquad \ldots\ (2.3.8)$$

and $$B_{\rho\rho} \approx \left(\frac{2e^2}{h^2}\right)\left[\frac{2(\nu_e \nu_s + \nu_o^2)}{(\nu_e^2 - \nu_o^2)(\nu_s^2 - \nu_o^2)}\right] \sum_s R_e R_s \varepsilon_{es}(a_{ij})$$

$$\ldots\ (2.3.9)$$

where a new notation has been introduced for the cross-section for electronic transitions.

$$\sigma_k = |R_k|^2 \quad \text{with} \quad R_k = e^{-1}(k^o|R_\rho|g^o) \quad \ldots\ (2.3.10)$$

and the vibronic energy is given by

$$\varepsilon_{kl}(a_{ji}) = (k^o|h_a|l^o)\langle i||Q_a||j\rangle \quad \ldots\ (2.3.11)$$

Defining the Raman scattering cross-section σ_{RAM}, as

$$\sigma_{RAM}(m.n) = \frac{2^7\pi^5}{3^2}\left(\frac{\nu^4}{c^4}\right)(\alpha_{mn})^2 \quad \ldots\ (2.3.12)$$

where $\nu = (\nu_o - \nu_{mn})$ the frequency of scattered light,
Eqn. (2.3.1) can be re-expressed in a simpler form as follows:

$$I_{mn} = \sigma_{RAM}(m,n)I_o \quad \ldots\ (2.3.13)$$

Albrecht and Hutley expressed σ_{RAM} in the following form:[7]

$$\sigma_{RAM} \approx 0.88778[F_A \sigma_e^* \varepsilon_{ee}(a_{ij}) + F_B \sum_s R_e^* R_s^* \varepsilon_{es}^*(a_{ij})]^2 \quad \ldots\ (2.3.14)$$

where asterisk denotes use of the dimensionless atomic unit (hartree) and F_A and F_B are the dimensionless frequency factors given by[7]

$$F_A = \nu^2(\nu_e^2 + \nu_o^2)/(\nu_e^2 - \nu_o^2)^2$$

$$F_B = 2\nu^2(\nu_e\nu_s + \nu_o^2)/(\nu_e^2 - \nu_o^2)(\nu_s^2 - \nu_o^2)$$

.... (2.3.15)

In Eqn. (2.3.14) the Raman scattering cross-section σ_{RAM} is expressed in units of barns (per orientally averaged scattering centre).

The functions F_A and F_B carry the frequency-dependence of Raman intensity and can be evaluated[7] for real examples.

It is worth mentioning in this context that the positions of the Raman bands (including resonance Raman) are solely governed by the electronic ground state. The Raman band intensities, however, can only be understood in terms of the excited electronic states of the molecule. A study of resonance Raman or pre-resonance Raman intensities, then, can provide unique information regarding excited state geometry of the system under study. This holds great promise for understanding several biological processes where chemical transformations take place in the excited states rather than the ground states.

2.4 Depolarization Ratios

The components of the electric moment vector induced by

the scattering molecule by the electric field of the incident light is given by

$$\begin{aligned} P_x &= \alpha_{xx} E_x + \alpha_{xy} E_y + \alpha_{xz} E_z \\ P_y &= \alpha_{yx} E_x + \alpha_{yy} E_y + \alpha_{yz} E_z \\ P_z &= \alpha_{zx} E_x + \alpha_{zy} E_y + \alpha_{zz} E_z \end{aligned} \qquad \ldots\ldots (2.4.1)$$

where P_x, P_y and P_z represent the components of the induced electric moments and E_x, E_y and E_z denote the components of the electric field of the incident electromagnetic wave along x, y and z axes, relative to a space-fixed coordinate system. The tensor α is defined by an array of nine components α_{xx}, α_{xy} etc. It may be shown that in all cases of our present interest the tensor is a symmetric one i.e. the off-diagonal components are related by

$$\alpha_{xy} = \alpha_{yx}, \quad \alpha_{yz} = \alpha_{zy} \text{ and } \alpha_{zx} = \alpha_{xz} \qquad \ldots\ldots (2.4.2)$$

Out of the nine components of the polarizability tensor, the number of distinct components, thus, is reduced to six. In fluids, the orientation of the molecule changes due to continuous rotation. The observed scattering in such case, corresponds to the average over all molecular orientations. The result can be expressed in terms of the quantities defined as follows:

$$\bar{\alpha} = \frac{1}{3} (\alpha_{xx} + \alpha_{yy} + \alpha_{zz}) \qquad \ldots\ldots (2.4.3)$$

and $$\gamma^2 = \frac{1}{2}\left[(\alpha_{xx} - \alpha_{yy})^2 + (\alpha_{yy} - \alpha_{zz})^2 + (\alpha_{zz} - \alpha_{xx})^2 + 6(\alpha_{xy}^2 + \alpha_{yz}^2 + \alpha_{zx}^2)\right] \quad \ldots\ (2.4.4)$$

where $\bar{\alpha}$ and γ are the mean value and anisotropy invariants of the molecular polarizability tensor .

In case of Raman scattering using plane polarized incident radiation observed at right angles to the incident direction, the degree of polarization ρ_1 is given by

$$\rho_1 = \frac{3(\gamma')^2}{45(\bar{\alpha}')^2 + 4(\gamma')^2} \quad \ldots\ (2.4.5)$$

where α' and γ' represent the first derivatives with respect to the normal coordinate Q. It follows that the line is only polarized (i.e. $\rho_1 < 3/4$) if $\bar{\alpha}$ does not vanish.

The Raman polarization rule is that only fundamentals of totally symmetric vibrations give polarized Raman lines ($\rho_1 < 3/4$). The Raman lines of fundamentals belonging to all other species are depolarized i.e. $\rho_1 = \frac{3}{4}$.

Under resonance conditions,[2,9] the depolarization ratio

$$\rho_1 = \frac{3G^s + 5G^a}{10G^o + 4G^s} \quad \ldots\ (2.4.6)$$

where $G^o = 3\bar{\alpha}^2 = \frac{1}{3}(\alpha_{xx} + \alpha_{yy} + \alpha_{zz})^2$

$$G^s = \frac{1}{3}[(\alpha_{xx} - \alpha_{yy})^2 + (\alpha_{yy} - \alpha_{zz})^2 + (\alpha_{zz} - \alpha_{xx})^2$$

$$+ \frac{1}{2}[(\alpha_{xy} + \alpha_{yx})^2 + (\alpha_{xz} + \alpha_{zx})^2 + (\alpha_{yz} + \alpha_{zy})^2]$$

and $G^a = \frac{1}{2}[(\alpha_{xy} - \alpha_{yx})^2 + (\alpha_{xz} - \alpha_{zx})^2 + (\alpha_{yz} - \alpha_{zy})^2]$

Here G^o, G^s and G^a are called isotropic, the quadrupole and the magnetic dipole components of the scattering tensor respectively. It therefore follows[9] that when all other terms except a single diagonal component of the polarizability is zero, depolarization ratio ρ_l has the value 0.33.

2.5.1 Introduction to Dielectric Properties

The electrical properties of a material held between two electrodes of area A and separation d can be completely characterized by its electrical conductance and capacitance given by

$$G = \sigma A/d \; ; \qquad C = \epsilon_o \epsilon A/d$$

where ϵ_o is the dielectric permittivity of free space, ϵ is the permittivity of the material relative to free space and σ is the

conductivity of the material. The conductivity σ is a measure of the ease with which delocalized electric charge can migrate through the material under the influence of the electric field whereas the permittivity reflects the extent to which localized charge distributions can be distorted through polarization by an external electric field.

2.5.2 Dielectrics and Capacitors

In order to understand the mechanism of how dielectrics work, we must look at their molecular structure in general. Most dielectrics have zero net charge and have no free charges that can migrate to either capacitor plate. If free charges in the dielectric are eliminated, then the other electrical structure which can explain the change in capacitance, is the electric dipole.[10] The permanent dipole moment of the molecules when placed in an electric field tends to align itself with the electric field. The dielectric, in this condition is said to be polarized. The amount of orientation each dipole receives depends on a number of factors e.g. the strength of the electric field, the magnitude of the dipole moment, the structural constraints placed on the mobility of the dipoles and the disorienting effects of thermal agitation. Since there are many molecular dipoles distributed throughout the volume of the dielectric and since each is electrically neutral, the net change in charge of the dielectric under the influence of the capacitor's field is zero.

However, if we consider an infinitesimal volume of the dielectric that is one-half a dipole's length thick and adjacent to the positive side of the capacitor plate, we see that the surface of the dielectric acquires a net negative charge. Although the dielectric material itself remains electrically neutral, there are surface charges built up on the areas immediately next to the capacitor plates. These charges have the effect of neutralizing or diluting the charge on either plate, which in turn reduces the electric field or voltage between the plates and hence increases the capacitance. The orientation of an aligned molecular dipole is always such that its electrical field opposes the field orienting it. The net effect of the aligned dipoles in the dielectric is to reduce the applied field.

2.5.3 Dielectric Constant and Frequency

The dielectric constant depends largely on how fast the electric field changes. If the field changes slowly enough, the dipoles will be able to reorient themselves to the new situation every time the field changes. In order to move, however, the molecules comprising the dielectric have to overcome frictional effects that retard the reorientational motion.[10] The extent of these frictional forces depends on the size and shape of the molecules and the amount of association they have with one another. Larger and asymmetric molecules generally move more slowly as compared to others. As the frequency of the field increases, the frictional forces become relatively large compared

to the electrical force reorienting the dipoles, and hence the dipole oriention tends to lag the changes of the field, i.e., the dipoles can not become completely reoriented before the field reverses again and the dielectric constant of the material, as such is lowered. When the frequency of the external field is very high, the frictional forces are overwhelmingly large compared to orienting electrical forces; hence the dipoles hardly move at all. In this situation, the contribution of aligned permanent dipoles to the dielectric constant becomes negligible. The only remaining contribution to the dielectric constant comes from the induction of dipoles through distortion of charge centers. It should, however, be realized that these slight shifts of electronic charge centers are not dependent on shape or size of the molecules but depends on how tightly the electrons are held by the atomic structure of the molecule.

For a two-components system with polar molecules in which one is substantially larger in size than the other, the variation of the dielectric constant with frequency can be classified into following characteristic regions:

1. At low frequencies of the field reversals, the large molecules have plenty of time to reorient themselves in the alternating field. The retarding frictional forces acting on the molecules are small compared to the electrical orienting forces. The value of the dielectric constant is essentially identical to the static dielectric constant and it is at a

maximum value.

2. As the frequency of the field reversals increases, the frictional forces are no longer negligible, and complete reorientation and equilibrium is not achieved. The dielectric constant, therefore decreases with the increase of the frequency of the field. This region is particularly interesting because the extent of the reorientation of the molecule is dependent upon the hydrodynamic properties of the molecule itself; hence this region can potentially provide information regarding the size and shape of molecules. This region where the dielectric constant decreases with increasing field frequency is called the dielectric dispersion region.

3. At these frequencies the frictional forces retarding the reorientation of the molecules have completely overwhelmed the electrical orienting forces, so the permanent dipole of the molecules make no contribution to the dielectric constant.

4. As the frequency of the field is further increased, the solvent molecules begin to lag the fluctuations of the field and complete orientation of solvent dipoles is decreased and as a result, the dielectric constant decreases.

5. When the frequency of the field reversal is very high, only the atomic distortions of induced dipoles can keep pace with it and hence the dielectric constant is very small.

2.5.4 Charge-Dipole Interaction

The interaction between a positive charge and an immobile dipole is schematically shown in Fig. 2.3.

If the dipole is free to rotate, then the dipole will assume a statistical orientation about the configuration of lowest energy with respect to the charge q. The amount of orientation the dipole will assume depends on the strength of interaction between the dipole and the charge. If the interaction is very strong, then the dipole will essentially be aligned collinearly with the charge; however, if the energy of interaction is small compared to the thermal energy $k_B T$, it is then possible to calculate the energy of interaction on statistical basis.

The potential energy for this situation is given by[10]

$$U = \frac{-q^2 \mu^2}{3k_B T r^4 K^2} \qquad \text{..... (2.5.1)}$$

where K denotes the dielectric constant of the medium and the negative sign indicates an attractive force. The potential V is given by[10]

$$V = \frac{-(69.11 n \mu \cos\theta)}{K r^2} \quad \text{kcal/mole} \qquad \text{.... (2.5.2)}$$

and Eqn. (2.5.1) can be written as

$$U = \frac{-(80.1 \times 10^4)\, n^2 \mu^2}{r^4 k_B T} \qquad \ldots\ldots (2.5.3)$$

where n is the number of electronic charges on q, μ is the dipole moment in debyes and r is the distance from the dipole center to the charge in angstrom units.

In the event that a charge-dipole interaction exists where the distance of separation is very small, it is necessary to use a more exact expression. For this situation, the potential energy is given by[10]

$$U = \frac{qq_1}{K} \left[\frac{1}{r_+} - \frac{1}{r_-} \right] \qquad \ldots\ldots (2.5.4)$$

where r_+ and r_- are the distances from the positive and negative charges of the dipole respectively, q is the charge on each particle in the dipole and q_1 is the charge interacting with the dipole. It should be remembered that as a free charge moves closer and closer to a freely rotating dipole, the dipole will orient itself so that the free charge is collinear with it.

2.5.5 Dipole-Dipole Interaction

The potential energy of interaction of two dipoles[10] is given by

$$U_{tot} = \frac{\mu_1 \mu_2}{l_1 l_2 K}\left[\frac{1}{L + \frac{1}{2}(l_1 - l_2)} - \frac{1}{L + \frac{1}{2}(l_1 + l_2)}\right.$$

$$\left. - \frac{1}{L - \frac{1}{2}(l_1 + l_2)} + \frac{1}{L - \frac{1}{2}(l_2 - l_1)}\right] \quad \ldots\ (2.5.5)$$

where μ_1 and μ_2 denote the dipole moments of the interacting dipoles whose centres are separated by a distance L, l_1 and l_2 represent the distance of separation of the charges in the two dipoles. For a typical case as shown in Fig. 2.4(A) the potential energy is given without approximation[10] as

$$U = \frac{2\mu_1 \mu_2}{l_1 l_2 K}\left[\frac{1}{\{L^2 + \frac{1}{4}(l_1+l_2)^2\}^{1/2}} - \frac{1}{\{L^2 + \frac{1}{4}(l_2-l_1)^2\}^{1/2}}\right]$$

$\ldots\ (2.5.6)$

For large distance of separation between the centres of the two dipoles compared to their lengths, the energy of interaction[10] is given by

$$U = -\frac{\mu_1 \mu_2}{Kr^3}\,(2\mathrm{Cos}\theta_1\mathrm{Cos}\theta_2 - \mathrm{Sin}\theta_1\mathrm{Sin}\theta_2) \quad \ldots\ (2.5.7)$$

where the angles θ_1 and θ_2 are defined in Fig. 2.4(B).

If one or both dipoles are able to fluctuate, then the potential energy of interaction between the dipoles can be calculated provided the electrical energy of interaction is small compared to the thermal energy. Considering the situation depicted in Fig. 2.5 in which dipole 1 is fixed and dipole 2 is free to rotate in the field of dipole 1, the average component of dipole-moment of dipole 2 in the field due to dipole 1 can be written as[10]

$$\bar{\mu}_2 = \frac{\mu_2^2 E_1}{2k_B T} = \frac{\mu_2^2 \mu_1 (1 + 3\cos^2\theta)^{1/2}}{3k_B T K r^3} \qquad \ldots\ (2.5.8)$$

and hence the energy of interaction is[10]

$$U = - \frac{\mu_1^2 \mu_2^2}{3k_B T r^6 K^2} (1 + 3\cos^2\theta) \qquad \ldots\ (2.5.9)$$

The negative sign in Eqn. (2.5.9) indicates the fact that the fluctuating dipole will always be aligned in the most stable state, and hence the energy will be negative. When both the dipoles are free to rotate, the energy of interaction between the two dipoles can be obtained by averaging Eqn. (2.5.9) over all possible values of $\cos^2\theta$ and can be expressed as follows:[10]

$$U = - \frac{2\,\mu_1^2 \mu_2^2}{3k_B T r^6 K^2} \qquad \ldots\ (2.5.10)$$

Eqn. (2.5.9) and (2.5.10) can be rewritten as

$$U = - \frac{(3.5 \times 10^4)\mu_1^2 \mu_2^2 (1 + 3\cos^2\theta)}{K^2 T r^6} \quad \text{Kcal/mole} \qquad \ldots\ (2.5.11)$$

and

$$U = - \frac{(7.0 \times 10^4)\mu_1^2 \mu_2^2}{r^6 K^2 T} \quad \text{Kcal/mole} \qquad \ldots\ (2.5.12)$$

where μ_1 and μ_2 are the respective dipole moments in debyes and r is in anstroms.

One would naturally expect that dipole-dipole interactions would be relatively weak when encountered over relatively large distances of separation because of the $1/r^6$ distance dependence. However, over short distances of separation dipole-dipole interactions can be quite important.

2.6 Dielectric Relaxation and Loss

The rates at which polarizations can occur are limited. Therefore, as the frequency of the applied electric field is increased, some polarizations can no longer be able to attain their low frequency or dc values. The slowest polarization mechanism, usually corresponds to that of dipolar orientation and as such, is the first polarization term to disappear as the frequency is increased.[11] The dipole moments in this case, are just not able to orient fast enough to keep in alignment with the applied electric field and hence the total polarizability falls

from α_T to $(\alpha_T - \alpha_o)$ where α_T, in general, is given by[11]

$$\alpha_T = \alpha_e + \alpha_a + \alpha_o \quad \ldots\ (2.6.1)$$

where α_e, α_a, and α_o are the electronic, atomic and orientational polarizability respectivily. The fall of the total polarizability α_T with its related reduction of permittivity and the occurrance of energy absorption is referred to as dielectric relaxation or dispersion. The frequency at which this fall in orientation polarization occurs usually vary from very low frequency of the order of 10^{-1} Hz and below for large hindered macromolecules to frequencies upto 10^{12} Hz for small molecules[11]. Since the dispersion due to the fall-off of the atomic polarization occurs at frequencies comparable with the natural frequencies of vibrations of the atom in a molecule (i.e. $\sim 10^{14}$ Hz), and that for electronic polarization occurs at still higher frequencies corresponding to electronic transition between different energy levels in the atom (visible, uv and X-ray frequencies), the atomic and electronic polarization practically remain constant in the frequency range of dielectric relaxation due to orientation polarization. The frequencies at which electronic and atomic dispersions occur are determined by the inertial properties of the molecules or atoms and have the form of a resonance dispersion. The dipolar orientation process, on the other hand, gives rise to relaxation dispersions where the frequency as well as the shape of the dielectric loss characteristic depend mainly on the immediate environment of the molecular dipole, and the

corresponding changes in permittivity are very different from that of the resonance dispersion.

A mathematical model for such an orientational relaxation process may be derived[11] by assuming that the polarization P is composed of two parts P_1 and P_2, where P_1 arises from atomic and electronic displacements and P_2 arises from the much slower process of dipolar orientation. For the frequency range of interest it is assumed that P_1 responds instantly to an applied electric field E and has a constant value given by

$$P_1 = \chi_1 E \qquad \ldots\ (2.6.2)$$

The part P_2, however, lags behind E in such a way that at any instant P_2 approaches its final value at a rate given by[11]

$$\frac{dP_2}{dt} = \frac{1}{\tau}\,(\chi_2 E - P_2) \qquad \ldots\ (2.6.3)$$

where χ_1 and χ_2 represent the relative dielectric susceptibility corresponding to P_1 and P_2 respectively. If the electric field E is applied as a step-function at t = 0 when P_2 = 0, then by integrating the above Eqn. we have

$$P_2 = \chi_2[1 - \exp(-\frac{t}{\tau})]E \qquad \ldots\ (2.6.4)$$

so that

$$P = [\ \chi_1 + \chi_2\{1 - \exp(-\frac{t}{\tau})\}]E \qquad \ldots\ (2.6.5)$$

which shows that the polarization approaches its final value *exponentially with a time constant* τ . *In other words, the* dielectric material gradually responds or relaxes to the polarizing influence of the applied field with a characteristic relaxation time τ . The correponding solution for P_2, in an alternating electric field $E = E_o\exp(jwt)$ gives

$$P = (\ \chi_1 + \frac{\chi_2}{1 + jw\tau}\ )E \qquad \ldots\ (2.6.6)$$

For small and relatively simple molecular structures, usually there is a single orientational process, but for polymers the dielectric dispersion can consist of several components associated with small side-chain movements ranging upto whole macromolecular motions. Other complications may arise for macromolecular systems associated with its heterogeneity, where as a result of the Maxwell-Wagner effect apparent dielectric relaxation may occur at low frequencies.

The real and imaginery components of the complex permittivity are given by

$$\epsilon^* = \epsilon' - j\epsilon'' \qquad \ldots\ (2.6.7)$$

which shows that the real and imaginery parts of the permittivity are 90^{o} out of phase with each other. The real part ϵ' is given by

$$\epsilon' = \epsilon_{\infty} + \frac{\epsilon_s - \epsilon_{\infty}}{1 + j\omega^2\tau^2} \qquad \ldots\ (2.6.8)$$

and the imaginery component ϵ'' given by

$$\epsilon'' = \frac{(\epsilon_s - \epsilon_{\infty})\omega\tau}{1 + \omega^2\tau^2} \qquad \ldots\ (2.6.9)$$

These Eqns. are commonly known as the Debye dispersion formulas and are applicable to the situation where equilibrium is attained exponentially with time when a constant external field is imposed on a dielectric. The transition from the low frequency to the high frequency dielectric behaviour extends roughly over about four decades in frequency.

A simple mathematical manipulation of the Debye dispersion formula may lead to the following equations:[11]

$$\epsilon''\omega = (\epsilon_s - \epsilon')/\tau \qquad \ldots\ (2.6.10)$$

and $$\frac{\epsilon''}{\omega} = (\epsilon' - \epsilon_{\infty})\tau$$

where the relaxation time τ represents the reciprocal of the mean rate coefficient of the dielectric relaxation process and since

such molecular processes usually follow an Arrhenius temperature low , then one can write[11]

$$\tau = A \exp(\Delta H/RT) \qquad \ldots\ (2.6.11)$$

where ΔH is the Arrhenius activation enthalpy per mole and A is a constant.

The phase lag between the polarization and the applied electric field leads to an absorption of energy and joule heating. The rate of conversion of electrical energy to heat in the material is represented by the imaginery component ϵ'', and is referred to as the dielectric loss factor. The ratio $\frac{\epsilon''}{\epsilon'} = \tan\delta$ have values ranging from less than 10^{-4} for low-loss polymers up to 1 for very lossy materials. Other synonyms used for $\tan\delta$ are the dissipation factor defined as the ratio of energy lost to energy stored and the reciprocal of the Q-factor 1/Q.

The relationship between the relaxation time, the frequency of maximum loss, and the maximum loss value can be found by differentiating Eqn. (2.6.10) with respect to w and equating to zero.

$$\frac{d\epsilon''}{d\omega} = 0 \qquad \text{at} \quad \omega_{max} = \frac{1}{\tau}$$

and

$$\epsilon''_{max} = \frac{(\epsilon_s - \epsilon_\infty)}{2} \qquad \ldots\ (2.6.12)$$

Another factor to be considered is that since dielectric absorption is a measure of the energy dissipated in the material, then processes which are usually related to d.c. conductivity σ can also contribute to the total dielectric absorption. At a frequency f the total dielectric loss ϵ''_T will be given by

$$\epsilon''_T = \epsilon'' + \frac{\sigma}{2\pi f \epsilon_o} \qquad \ldots\ (2.6.13)$$

from which it can be seen that the d.c. conductivity could contribute significantly to the absorption at low frequencies.

Deviations from an ideal Debye-type single relaxation are likely to occur for macromolecular systems as a result, for example, of such effects as combinations of cooperative and isolated movements of side-chain molecular groups. This gives rise to a spread of relaxation times each contributing to a Debye-type dispersion. For a set of closely spaced relaxation times the resultant ϵ'' loss curve as a function of frequency will be much broader. A method of checking for a single relaxation time can be obtained[11] by rearranging Eqns. (2.6.8) and (2.6.9) to eliminate $\omega\tau$ giving

$$\left[\epsilon' - \frac{(\epsilon_s - \epsilon_\infty)}{2}\right]^2 + (\epsilon'')^2 = \left[\frac{(\epsilon_s - \epsilon_\infty)}{4}\right]^2 \qquad \ldots\ (2.6.14)$$

which is of the form $X^2 + Y^2 = r^2$ i.e. the equation of a circle of radius r, but as only positive values for ϵ'' are possible, a plot of ϵ' against ϵ'' produces a semicircle of radius $(\epsilon_s - \epsilon_\infty)/2$ with the centre at $\{(\epsilon_s - \epsilon_\infty)/2, 0\}$. Such a plot of ϵ' against ϵ'' is referred to as a Cole-Cole plot. If a symmetrical distribution of relaxation times occurs about a mean relaxation time, then a depressed semicircle is found in the Cole-Cole plot of ϵ' against ϵ''.

2.7 The Macroscopic and Microscopic Relaxation Time

For materials exhibiting a single decay or macroscopic relaxation time τ, it was shown[11] that the intrinsic microscopic relaxation time τ_i is given by

$$\tau_i = \frac{(2\epsilon_s + \epsilon_\infty)\,\tau}{3\epsilon_s} \qquad \ldots\ (2.7.1)$$

where τ represents a decay time or time constant determined as an experimental parameter, and is equivalent for example to the circuit time constant function RC describing the decay of charge from a capacitor C through a resistor R. The intrinsic or microscopic relaxation time τ_i is the quantity required if dielectric relaxation phenomena are to be interpreted at the molecular level. The microscopic relaxation time τ_i is related to the mean square angular deviation of a molecule over a given period of time. It is of the order of magnitude of time required

for a given molecule if fixed and then released to result to random orientation in the absence of any macroscopic polarization which might result from external fields or surrounding polar molecules for example. If the molecule is envisaged to change position by jumps over an energy barrier, then τ_i can be defined as one-half the average time a molecule waits before jumping.

Since the difference between the macroscopic and microscopic relaxation time results from local field effects and orientation correlation between the dipoles, it is not immediately clear whether one should expect that a single microscopic relaxation time will always lead to a process governed by a single macroscopic relaxation time.

2.8 Conduction and Dielectric Polarization in Disordered Solids

The bulk electrical conductivities and low-frequency dielectric properties of disordered samples are understood in terms of the hopping of charge carriers between localised sites.[12,13] The relaxation time characterizing a low-frequency dielectric dispersion for such materials is related to the steady-state electrical conductivity σ as follows:

$$\tau \approx \frac{\epsilon_o \epsilon_\infty}{\sigma} \qquad \ldots\ (2.8.1)$$

where ϵ_o denotes the permittivity of free space and ϵ_∞ represents

the relative permittivity of the material at the high-frequency limit of the dielectric dispersion. The above empirical expression relating the dielectric relaxation time and the steady-state electrical conductivity has been observed[14,15] in a number of pseudo-crystalline disordered systems in which conduction properties can be described in terms of phonon-assisted hopping of charge carriers between spatially localised, weakly-overlapping electronic states. The steady-state conductivity σ in such a process is given by

$$\sigma = Nqu \qquad \ldots\ (2.8.2)$$

where N represents the density of charge carriers, each carrying charge of magnitude q and u denotes the effective mobility which can be considered as an activated process in which the lattice phonons supply the required energy (E_j-E_i) to the charge carriers for hopping from a low-lying occupied site i to a high-energy empty site j. The average transition time t between sites i and j given by

$$t = t_o \exp[(E_j - E_i)/k_BT] \exp(2\alpha s) \qquad \ldots\ (2.8.3)$$

where t_o is a constant which depends on the lattice phonon frequency, the phonon density of states and the charge-carrier-phonon coupling strength, α is the reciprocal of the length which describes the spatial extent of the electronic wavefunctions

localised at sites i and j and s is the mean distance between the sites. The effective diffusion constant D is given by the Einstein relation as follows:

$$D = (\mu k_B T)/q \qquad \ldots\ (2.8.4)$$

where k_B is the Boltzmann constant and T is the temperature in absolute unit. At the steady-state conduction limit, the effective diffusion constant D for charge carriers hopping between localised sites was given[16] by

$$D = s^2/6t \qquad \ldots\ (2.8.5)$$

Using these Eqns. the steady-state conductivity can be expressed as

$$\sigma = \frac{Nq^2s^2}{6k_BTt} \qquad \ldots\ (2.8.6)$$

By recognising the fact that a charge-carrier hopping between two sites i and j separated by a mean distance s is dielectrically indistinguishable from the relaxing of a classical dipole of moment m = qs, the steady-state conductivity can be rewritten[16] as:

$$\sigma = \frac{Nm^2}{6k_BT\tau} \qquad \ldots\ (2.8.7)$$

where the relaxation time τ for the dipole is given by $\tau = t$. For a material containing N dipoles of moment m, the limiting low-frequency relative permittivity ϵ_s is given by[16]

$$(\epsilon_s - 1)\epsilon_o = \frac{Nm^2}{3kT} \frac{E_L}{E} \qquad \ldots\ (2.8.8)$$

where E_L and E denote the microscopic local electric field and the macroscopic applied electric field respectively. Combining Eqn. (2.8.7) and (2.8.8), the relaxation time can be written as[16]

$$\tau = \frac{(\epsilon_s - 1)\epsilon_o}{2} \frac{E}{E_L} \qquad \ldots\ (2.8.9)$$

For materials containing a small number of non-interacting dipoles, the local electric field can be regarded to be equal to that of the externally applied electric field and as such the modified expression for τ becomes independent of the electric field and is given by

$$\tau = \frac{(\epsilon_s - 1)\epsilon_o}{2} \qquad \ldots\ (2.8.10)$$

The experimental data[12-14], however, do not show satisfactory agreement with the above modified form of τ and hence suggests that the local field E_L exceeds the externally applied field E as a result of dipole-dipole interactions. This consideration yields[16]

$$\frac{(\epsilon_s - \epsilon_\infty)(2\epsilon_s + \epsilon_\infty)}{\epsilon_s(\epsilon_\infty + 2)^2} = \frac{Nm^2}{9\epsilon_o kT} \quad \text{.... (2.8.11)}$$

Eqns. (2.8.11) and (2.8.7) give

$$\tau = \frac{3\epsilon_o(\epsilon_s - \epsilon_\infty)(2\epsilon_s + \epsilon_\infty)}{2\epsilon_s(\epsilon_\infty + 2)^2 \sigma} \quad \text{.... (2.8.12)}$$

The Eqn. (2.8.12) has been found to describe the dielectric and conductive properties of the weakly conducting materials.[16]

References

1. *"Laser Spectroscopy and its Applications"* L.J. Radziemski, R.W. Solarz and J.A. Paisner, Eds., Marcel Dekker, p. 514, New York (1987).
2. *"Rayleigh and Raman Scattering"* G. Placzek, UCRL Transl. No. 526(L) from "Handbuch der Radiologie, Ed., E. Marx [Akademische Veriagsgesellschaft, Leipzig, (1934)].
3. W.M. Tolles, J.W. Nibler, J.W. MoDonald and A.B. Harvey *Appl. Spectrosc.* 31, 253 (1977).
4. H.A. Kramers and W. Heisenberg *Z. Physik* 31, 681 (1925).
5. P.A.M. Dirac *Proc. Roy. Soc., London* 114, 710 (1927).
6. *"Raman Spectroscopy, Theory and Practice"* Ed., H.A. Szymanski, vol. 2, p. 36, Plenum Press, New York-London (1970).
7. A.C. Albrecht and M.C. Hutley *J. Chem. Phys.* 55, 4438 (1971).
8. P.P. Shorygin *Pure Appl. Chem.* 4, 87 (1962).
9. K. Kumar and P.R. Carey *J. Chem. Phys.* 63, No 9, 3697 (1975) and references therein.
10. *"Electrical Interactions in Molecular Biophysics"* Raymond Gabler, p. 155 (1978) Academic Press.
11. *"Dielectric and Electronic Properties of Biological Material"*, R. Pethig p. 15-19, John Wiley and Sons, Chichester (1979).

12. P. Carnochan and R. Pethig *J. Chem. Soc. Faraday Trans. 1* 72, 2355 (1976).

13. S. Bone and R. Pethig *J. Chem. Soc. Faraday Trans. 1* 74, 720 (1978).

14. J. Eden, P.R.C. Gascoyne and R. Pethig *J. Chem. Soc. Faraday Trans. 1* 76, 426 (1980).

15. D.D. Eley, N.C. Lockhart and C.N. Richardson *J. Chem. Soc. Faraday Trans. 1* 75, 323 (1979).

16. S. Bone, J. Eden, P.R.C. Gascoyne and R. Pethig *J. Chem. Soc. Faraday Trans. 1* 77, 1729 (1981).

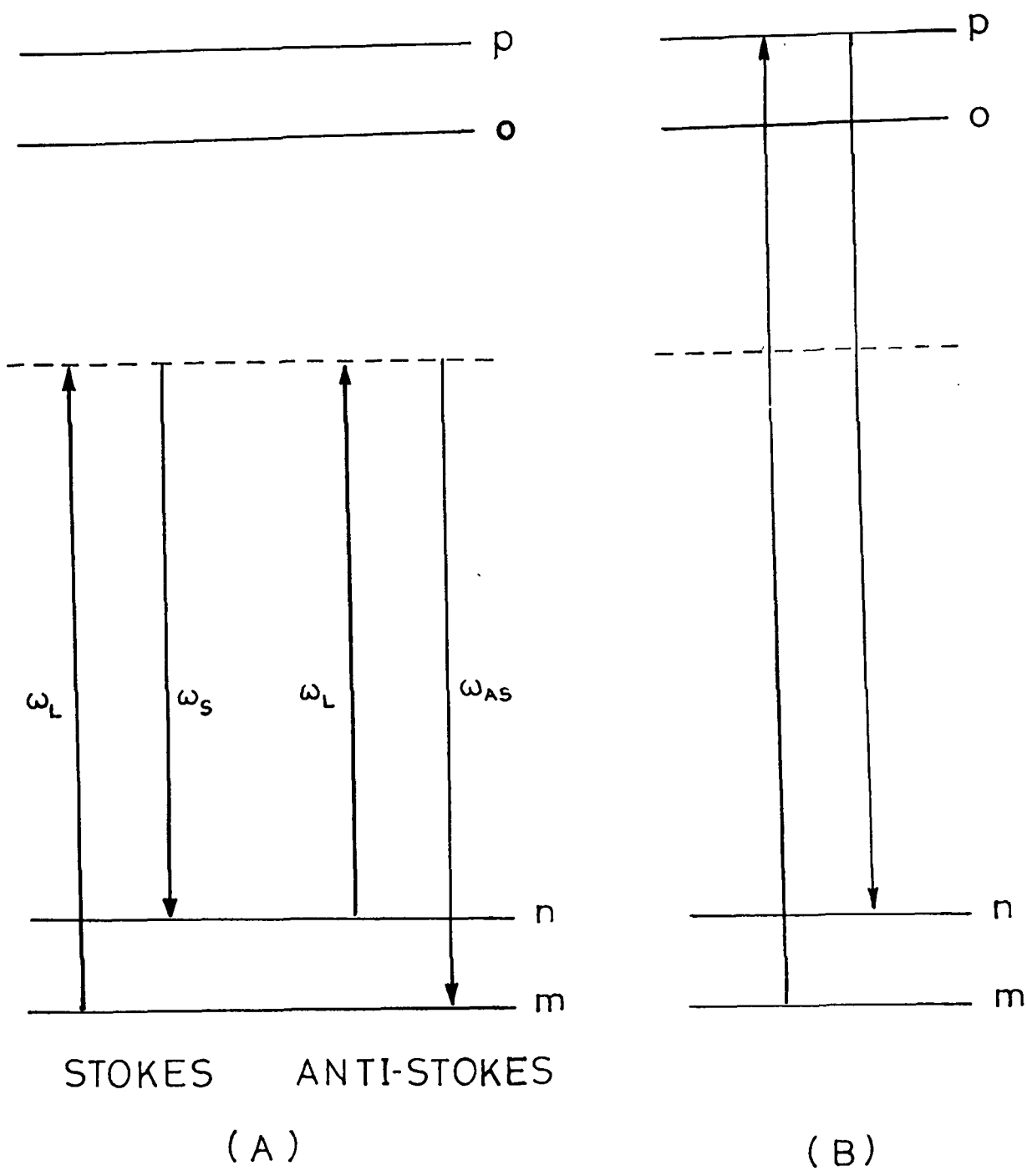

Fig.2.1(A) Energy-level diagram for spontaneous Raman scattering. States labeled m, n, o and p are real molecular eigenstates. The dotted line represents the virtual state.

(B) Resonance Raman effect

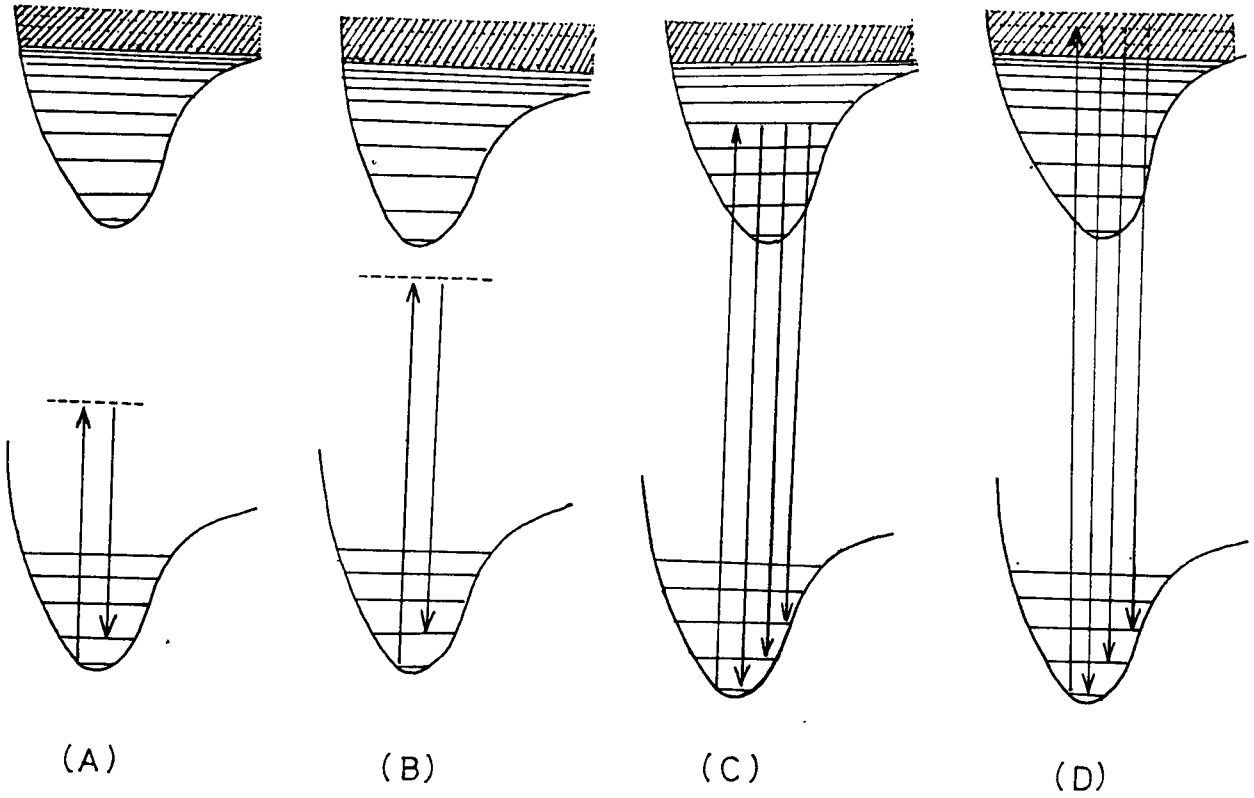

Fig.2.2 Illustration of various light scattering processes (A) Normal Raman Scattering, (B) Pre-resonance Raman Scattering, (C) Discrete Resonance Raman Scattering and (D) Continuum Resonance Raman Scattering.

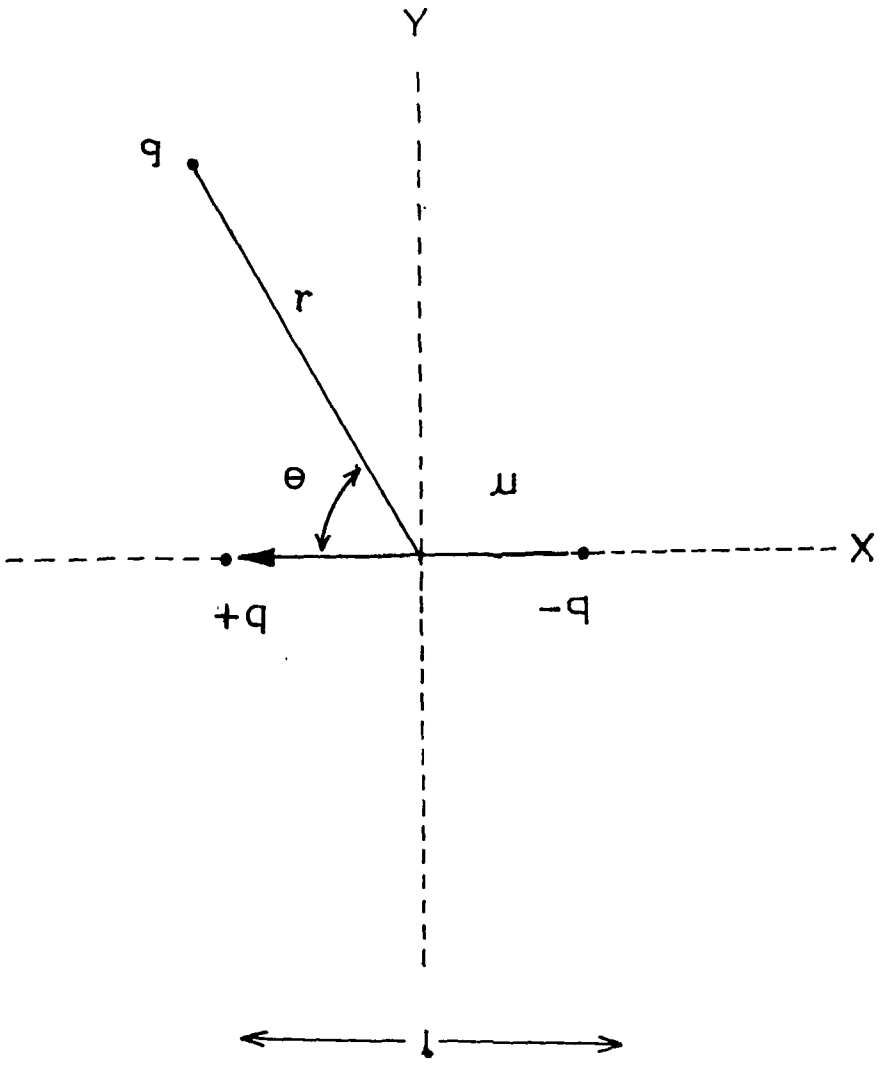

Fig.2.3 A schematic diagram illustrating the interaction between positive charge q and a dipole of moment μ .

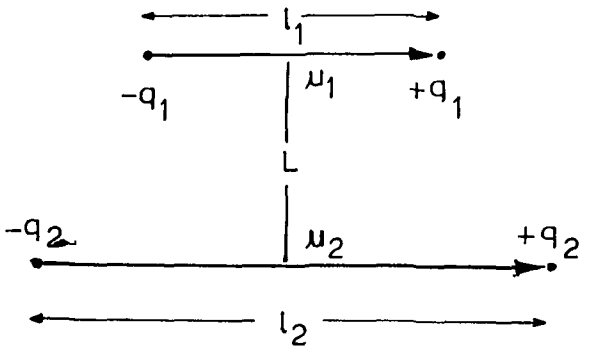

(A)

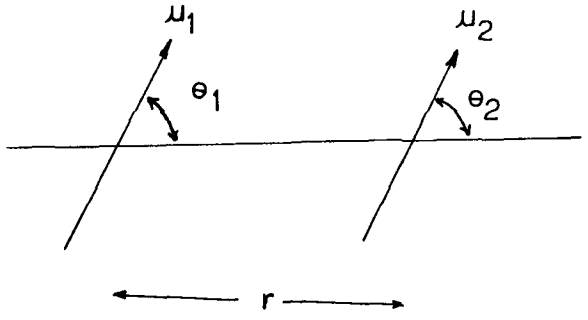

(B)

Fig.2.4 (A) Two parallel dipoles whose centres are separated *by a distance* L

(B) A generalised situation where two dipoles are interacting with one another. The angles θ_1 and θ_2 define the orientation of the two dipoles with respect to a reference line and r is the distance between the dipole centres.

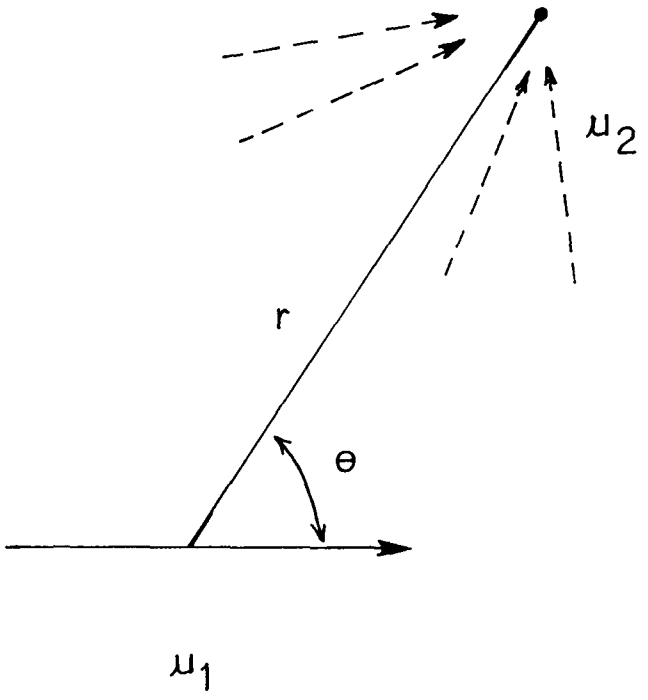

Fig.2.5 Dipole 1 is fixed and dipole 2 is free to rotate. Dipole 2 can assume one of a number of statistically accessible positions in the field of dipole 1.

CHAPTER – III

EXPERIMENTAL TECHNIQUES

In this chapter we present a brief discussion of the experimental techniques and the instruments used to obtain the spectra (Raman, IR and UV-vis) for the present studies. The salient features of the multifrequency LCR meter which is used for obtaining the dielectric data have also been presented in this Chapter.

3.1 Basic Optics of the Raman Experiment

In a standard Raman instrument, an intense monochromatic radiation is focussed onto the sample. The scattered light is gathered by the collecting optics and is directed to a dispersing system (usually a double monochromator), which selects the scattered light of particular frequency range. At the exit port of the monochromator the Raman spectrum displays in the form of a series of faint lines. These signals are detected by a photomultiplier tube and recorded after electronic processing on a chart recorder. The block diagram of a Raman instrument is given in Fig. 3.1.

3.2 Laser Sources

The Spectra Physics model 165 Ar^+ laser and the Liconix model 4240 He-Cd laser are the laser sources used for recording

the Raman spectra, presented in this thesis.

3.2.1 Spectra Physics model 165-09 Argon-ion Laser (5 Watts)

The Spectra Physics model 165-09 Argon ion laser is a continuous wave (CW) laser. It essentially consists of a laser head and an exciter (Spectra Physics model 265). The laser head consists of a Beryllium oxide plasma tube closed at each end by the Brewster angle windows, a solenoid and an optical resonator. The optical resonator is formed by a reflector (spherical) at the output end together with a prism assisted by a flat reflecting mirror at the back end. The prism is placed in the optical path of the resonator in such a way that it selects the correct wavelength. The plasma tube is supported on a kinematically adjustable mount so that the plasma tube is positioned exactly along the central line of the mirror. External thumb wheel controls are provided for the selection of wavelength of the emitted radiation and for changing the intra-cavity aperture. The emitted light from this laser source is polarized and the plane of polarization can be changed to any desired plane by using the $\lambda/2$ plate. The available laser lines along with typical power outputs are summarized in Table III-1.

The Spectra Physics model 265 Exciter contains the necessary electric and electronic circuitries in order to create, sustain and monitor the ionic discharge in the plasma tube. It

also monitors and controls the output power and regulates the solenoid current of the 165 Argon ion laser head. The 265 exciter runs on a 230 volts three phase (phase to phase) power line which is provided by a power transformer supplied with a three phase 400 volts stabilized power from the main line. The input power stabilization was achieved with the help of three single phase 8.3 KVA (each) Nelco voltage stabilizers connected in the star (Y) configuration. Both the 165 Ar^+ laser head and the 265 exciter are continuously cooled by flowing chilled deionised distilled water at a constant temperature of 15^oC and at a pressure of 40 PSIG from the Neslab HX-500 (Air cooled) Water Chiller Plant.

The specifications of Spectra Physics Model 165 Ar^+ laser have been presented in Table III-2.

3.2.2 Liconix Model 4240 Helium-Cadmium Laser

Liconix Model 4240 Helium-Cadmium laser, essentially consists of a laser head and a power supply. The optical section of the laser head is formed by two mirrors mounted on adjustable plates and held at a precise separation by three invar rods that run along the length of the laser tube made of pyrex glass. The mirrors are adjusted to reflect the laser light down the bore of the laser tube and to allow the emission of a precise amount of light as an output beam. The laser head is an air cooled system and requires no external cooling device. The output power at 4416

A is about 40 mW.

Coherent emission or lasing occurs in a helium cadmium laser by way of a mechanism rather similar to that of the helium neon laser. As a result of the low current (65 mA) dc discharge, electrons in the bore or positive column collide with helium atoms, thus transferring energy to them and raising the helium atoms to a metastable state. The metastable helium atoms in turn collide with cadmium atoms and transfer their energy to the cadmium which in the process is left in an excited ionized state (Penning collision). Some cadmium atoms are ionized by direct electron impact. The excited cadmium ions lose energy by emission of photons at 4416 A which in turn can, by stimulated emission, cause other excited cadmium ions to excite photons with identical wavelength, momentum and polarization.[1] The coherent lasing radiation is built up in the resonant optical cavity by multiple reflections between the retro reflecting cavity mirrors. A small fraction of the resonant energy is coupled out as a useful beam through the partially transmitting output mirror.

In order to maintain the photon producing conditions the helium pressure and the cadmium vapour pressure must be maintained within certain limits. Cadmium vapour pressure is maintained by electronically controlling the temperature of a heater surrounding the cadmium reservoir. Helium is consumed by entrapment in the cathode and under cadmium deposits inside the

laser tube. The cleaned-up helium is replaced and pressure maintained by use of a heat-controlled leak between a small (higher pressure) and the helium ballast. The helium gas heater is electronically controlled, using the voltage drop across the tube as pressure indicator.

The power supply Model 4240 PS utilizes AC power from the primary source and converts it into different DC levels for maintaining a constant output power by controlling the gas pressure (both helium pressure and cadmium vapour pressure).

The specifications of Liconix Model 4240 He-Cd laser are tabulated in Table III-3.

3.3 Optics around the Sample

A laser filter or the `lasermate' is placed in the light path before it enters the focussing system. The laser filter is a small grating monochromator which allows the excitation wavelength to pass through but blocks weaker non-lasing lines from the laser plasma. It is therefore able to provide a clean Raman spectrum uncluttered by the laser-plasma lines, especially for a strongly scattering sample.[2]

The filtered laser beam is deflected upward through 90^{o} by a mirror and is focussed onto the sample to a spot of diameter

~10 μm by the fused silicon condensing lens. Scattered radiation from the sample passes through a polarization analyzer, a device based on birefringence and total reflection or on dichroism. The polarization analyzer transmits light of a particular polarization depending on the orientation of the polarizer. Use of polarization, therefore provides direct information regarding the state of polarization of the observed Raman band. The scattered radiation is collected by an elliptical mirror which ascertains a large solid angle about the focal volume and hence collects the optimum amount of scattered light. Fig. 3.2 shows the optical diagram of the light collecting system.

The collected scattered light is now passed through a polarization scrambler which essentially consists of a wedge of birefringent material. This device is used to scramble the polarization of the light entering the entrance slit of the spectrometer. In polarization scrambler, in contrast to the half-wave ($\lambda/2$) plate, the retardation varies from place to place and as such the emerging radiation is depolarized. The polychromatic scattered radiation is focussed onto the entrance slit of the spectrometer. The optical ray-diagram is illustrated in Fig. 3.3.

3.4 The Spectrometer : SPEX Ramalog model 1403

The function of the spectrometer is to separate the spatially scattered photons from the sample on the basis of their frequency. The light dispersing process is repeated by linking

two single monochromators to form a double monochromator. The double monochromator also separates the Raman photons from the overwhelming number of Rayleigh photons.

All the Raman spectra in the present study have been recorded with the help of SPEX Ramalog 1403 double monochromator coupled with a water cooled photomultiplier tube RCA C-31034-02.

The SPEX 1403 double monochromator is f/7.8 instrument with a spectral coverage from $3.1X10^4$ cm^{-1} to $1.1X10^4$ cm^{-1}. An accuracy of +1 cm^{-1} in the 10,000 cm^{-1} range, a resolution of 0.15 cm^{-1} and a spectral repeatability of +0.2 cm^{-1} can be achieved by this instrument. The 1800 grooves/mm holographic gratings are used in this instrument. The gratings are mounted on a modified Czerny-Turner mount as shown in Fig. 3.4. Use of fundamental grating equation yields[3]

$$m\lambda = d(\sin\alpha + \sin\beta) \qquad \ldots\ (3.4.1)$$

where m, λ and d denote the spectral order, wavelength and grating spacing respectively whereas α and β represent the angle of incidence and the angle of diffraction respectively.

Substituting $\alpha = \theta + \phi$

and $\beta = \theta - \phi$

where θ denotes the angle of rotation of the grating from zero as illustrated in Fig. 3.4 and ϕ represents the constant angle which

depends on the design of the instrument, Equation (3.4.1) can also be written as

$$m\lambda = 2d\sin\theta\cos\phi \qquad \ldots\ (3.4.2)$$

Since in the Ramalog 1403 instrument, the Raman bands are observed only in terms of frequency shift (in cm^{-1}) on a linear scale, it utilizes a cosecant drive for the grating rotation with $\phi = 10^{o}$ and $\cos\phi = 0.984$ (according to the manufacturer's supplied data).[3]

The scattered radiation focussed onto the entrance slit of the spectrometer gets dispersed by the 1800 grooves/mm holographic gratings. Nearly monochromatic radiation of frequency ν for a particular tuning of the spectrometer reaches the exit slit of the double monochromator by the grating mirror combination.

The details of specifications of the 1403 double monochromator has been presented in Tables III-4 and III-5.

3.5 Theoretical Resolving Power

The theoretical resolving power R_T is given by[3]

$$R_T = \frac{\lambda}{\Delta\lambda} = \frac{\nu}{\Delta\nu} = 2\sin\theta\cos\phi\, W/\lambda = mN \qquad \ldots\ (3.5.1)$$

where λ = wavelength

ν = wavenumber

N = total number of grating grooves

W = width of grating ruling

and m = order of diffraction

3.6 Factors Influencing Resolution

Source — From Eqn. (3.5.1), since resolution depends linearly on the grating width (i.e. optical path difference), resolution deteriorates if the source illuminates less than the full width of the grating. As a result, the source or condensing lens should fully illuminate the collimating mirror. This can usually be checked visually by opening the spectrometer or, in the case of energy outside the visible spectrum, by making certain that throughput is reduced when the edges of the collimating mirror are obstructed.

Slit width — Spectral bandpass is a function of the reciprocal linear dispersion which, in turn, depends on the wavelength, the grating constant, the focal length of the instrument and the spectral order. Approximate bandpass for 1800 grooves/mm gratings in a 1403 double monochromator is tabulated in Table III-4.

Slit height — Increase in the heights of straight slits reduces the instrumental resolution. As the height of the

slits is increased the ends of the exit slit begin to pass portions of adjoining wavelengths. The variation of resolution as a function of slit height has been presented as follows along with the Recommended Minimum Entrance Slit Width:

Slit Height (mm)	Resolution A	Recommended Minimum Slit Width (μ)
2	0.1	10
5	0.1	10
10	0.1	15
20	0.2	20

3.7 Spectrometer Control and Data Processing

Data processing and control of the spectrometer were carried out by a 8-bit microcomputer `SPEX DATAMATE'. With the help of the inbuilt software, it was possible to manipulate the spectral data by background addition, subtraction, division, frequency range and intensity range expansion/reduction, integration, differentiation etc., wherever necessary. The spectral data as well as the manipulated data array could be stored in the 4K data point storage in any of its eight variable length files. The stored data could be plotted in a strip chart recorder or could be transfered to external peripherals, e.g., floppy discs or to a general computer through the standard IEEE port for further data processing. It is also possible to bypass

the data storing option and record the spectra directly on the strip chart recorder. The high voltage required for operating the photomultiplier tube is also supplied by the datamate.

3.8 The Photomultiplier Tube

RCA C-31034-02 photomultiplier tube, cooled to $-30^{o}C$ by a thermo-electric cooling device was used for obtaining the Raman spectral data. The photomultiplier tube having an almost linear absolute responsivity 3000 A to 8500 A wavelength range was operated for a current gain of 10^{6} with a maximum dark pulse summation of 12 cps. The RCA C-31034-02 photomultiplier tube consists of a gallium arsenide chip placed at its photocathode, an ultraviolet transmitting glass window and an inline copper beryllium dynode structure consisting of eleven dynodes.

The raw data is obtained from the output of the preamplifier (pc Dam) of gain 400. The anode of the PMT is the input of the pc Dam. The high voltage of -1750 volts required for operating the PMT is supplied by the datamate with a stability of +0.002% after 30 minutes of warm up.

3.9 Sampling Techniques

A laser beam, being a narrow and unidirectional, entity, can be manipulated in a variety of sample-cell configurations thus providing considerable ingenuity in

exercising the design and use of sample cells. A substantial advantage stemming from the geometric simplicity of the Raman experiment, is that samples may be examined in any physical state. For liquid samples, which we have used more frequently a cell consisting of around 1 cm path length is adequate, provided the cell bottom is transparent. In order to minimise the amount of scattered light from the interface reaching the spectrometer, the cell should be toped around the meniscus.

3.10 Perkin-Elmer Model 983 IR Spectrophotometer

The Perkin-Elmer model 983 IR spectrophotometer records the transmittance of infrared radiation through a sample during a selected time-period in either the single or the double-beam mode. After the radiation passes through the sample a monochromator is used to produce a spectrum (expressed in wavenumber units), during the recording period. Each spectrum can be entered in the memory system of the instrument and can also be simultaneously plotted by the instrument Flowchart recorder. The instrument has the following data processing facilities:

1. Spectral subtraction or addition, which gives the difference between a spectrum being scanned and the spectrum in the memory system.

2. Spectral averaging, which increases the amplitudes of the spectral peaks and reduces random noise components.

3. Absorbance expansion, which provides for the expansion of spectral intensities.

4. Automatic full scale replotting, which increases the amplitudes of the peaks of a spectrum to fill the chart ordinate scale. Functionally, in Perkin-Elmer model 983-IR spectrophotometer the IR radiation is emitted by a heated ceramic tube and is divided into two beams, which are blocked alternately by a presample chopper to produce pulses of radiation. One beam passes through the sample which absorbs radiation of a wavenumber corresponding to its characteristic molecular vibrational frequencies, while the other beam serves as a reference. The two beams are combined in the photometer section by rotating sector mirror, which is synchronized with the presample chopper. The radiation passes through one of a set of optical filters where the correct filter is automatically selected for the spectral region being scanned. The combined pulsed beam passes into the monochromator where it is dispersed by a grating into its spectral components. Finally the transmitted radiation is focussed onto a thermocouple detector. The resultant signal from the thermocouple detector is converted to digital form for processing by the instrument microprocessor system.

The specifications of the instrument are presented in Table III-6. and the optical diagram is given in Fig. 3.5.

3.11 Cary Model 2390 UV-VIS Double-beam Spectrophotometer

The Cary model 2390 is a double-beam, digital reading and recording instrument for measuring absorbance/transmittance at specified wavelengths. This model employs a broad band tungsten halogen lamp in the NIR and visible range of spectrum and a deuterium lamp in the ultraviolet range of the spectrum. At all stages, the analog signal is processed by a ADC and the results are displayed directly on the screen. Continuous scan i.e. the spectrum over a wavelength range can be plotted on a Y-T plottor. The digital absorbance/transmittance vs wavelength values can also be obtained through an attached dot-matrix printer. The entire instrumental control as well as automatic background correction etc. are achieved through a microprocessor.

Some of the important specifications of the instrument have been presented in Table III-7.

3.12 Multifrequency LCR-meter, HP-4274A

The multifrequency LCR-meter HP-4274A was used for the measurement of capacitance and loss tangent at 10 discrete frequencies. The four terminal fixture HP-16034B was used for all measurements. It can measure resistance and capacitance in series equivalent circuit or parallel mode.

The salient features of this instrument is presented in Table III-8.

References

1. Instruction Manual for Liconix Model 4240 He-Cd Laser (1982).
2. "Biochemical Applications of Raman and Resonance Raman Spectroscopy" P.R. Carey, p. 53, Academic Press, New York (1982).
3. Operation and Maintenance Instruction Manual for SPEX Model 1403 Spectrometer (1982).

Table III-1

Spectra Physics Model 165-09 Argon-ion Laser Power

Wavelength (A)	Power in watts
Multi-Line	
4579 - 5145	5.00
Single-Line	
5145	2.00
5017	.40
4965	.70
4880	1.50
4765	.75
4727	.30
4658	.20
4579	.35

Table III-2

The specifications of Spectra Physics Model 165 Ar^+ laser

Noise, Light control RMS, 10 H_Z - 20 MH_Z		0.2%
Noise, Current control RMS, 10 H_Z - 2 MH_Z		1%
Frequency stability		60 $MH_Z/^oc$
Beam Diameter		1.25 mm
Beam Divergence (Full angle)		0.69 mrad.
Cavity Configuration		Long radius output, Flat High Reflector
Cavity length	w/o prism	1 + 0.003 meter
	w/prism	1.05+0.003 meter
	Folded cavity	N/A
Polarization		Vertical
Mode-spacing	w/o prism	149.6-150.5 MH_Z
	w/prism	142.5-143.3 MH_Z
	Folded cavity	N/A

Table III-3

Few specifications of Liconix Model 4240 He-Cd Laser

Power	40 mW at 4420 A
Mode	TEM_{oo}
Beam diameter ($1/e^2$)	1.2 mm
Beam divergence	0.5 mrad.
Polarization, Vert. +5%	>500:1
Power stability	$\pm$2 %
Noise, rms, $10H_z$-$10MH_z$	<3%
Pointing stability	25 rads/^oc

Table III-4

Spectral Band pass for 1800 grooves/mm grating in SPEX 1403 Double Monochromator.

Spectral Band pass (cm^{-1})	Ar^+ 5145 A (19435 cm^{-1})	Ar^+ 4880 A (20492 cm^{-1})
	80 $/cm^{-1}$	70 $/cm^{-1}$
0.5	40	35
1.0	80	70
2.0	160	140
5.0	400	350

Note: The above values are for first order dispersion only.

Table III-5

Optical specifications of SPEX 1403 Double Monochromator

Mount	Czerny-Turner, additive dispersion
Focal length	0.85 m
Aperture	f/7.8
Mirrors	MgF_2 over coated aluminized.
Slits	Four straight, bilaterally adjustable.
Max width (mm)	3 at entrance and exit. 5 at centre
Max Height (mm)	20
Gratings (Holographic)	1800 grooves/mm
Range	uv - visible
Spectral purity (I/I_o)	10^{14} at > 20 cm^{-1}
Spectral coverage	31000 - 11000 cm^{-1}
Dispersion at 5145 Å	10 cm^{-1}/mm
Resolution, Hg 5791 Å (FWHM)	0.15 cm^{-1}
Readout, 5 digits	cm^{-1} and cm^{-1}
Accuracy	+1 over 10000 cm^{-1}
Repeatability	+0.2 cm^{-1}

Table III-6

The following specification refers to the full range scan mode of the Model 983 Spectrophotometer. Measurements and calibration are made at an ambient temperature of approximately 20°C with the instrument purged with dry air and supplied by the manufacturer.

Principle	Real-time, double-beam, ratio recording with pre-sample chopping and integral data handling facilities.
Optics	F4.2 monochromator with 4 gratings and 9 filters, purgable.
Screen Readouts	Digital display of wavenumber, ordinate value resolution slit width and scan time.
Abscissa Range	5000 cm^{-1} to 180 cm^{-1}
Abscissa Accuracy	± 3 cm^{-1} 5000 to 4000 cm^{-1} ± 2 cm^{-1} 4000 to 2000 cm^{-1} ± 1 cm^{-1} 2000 to 180 cm^{-1} Maintained independently of scan conditions.
Abscissa Repeatability	Run-to-run repeatability after warm-up of 0.005 cm^{-1}.
Abscissa Expansion	x0.25, x0.5, x1, x2, x10, x20.
Scan Time	5 speeds for Scan Modes 1 to 4 4 speeds for Scan Modes 5 to 7
Time Drive	0.1 to 50 cm per minute.
Ordinate Scales	Double Beam: Transmission; Absorbance (0 - 3 A.U.); Emission Single Beam: Transmission; Absorbance
Ordinate Accuracy and Repeatability	Better than 0.1%T, typically limited by noise level.
Ordinate Scale Expansion	Up to x100 with appropriate offsets available.
I_o Flatness	Better than ± 0.5%T
Resolution	Best resolution for each Integrated Scan Mode. Mode: 1 2 3 4 5 6 7 Resolution: 10 7 5 3 2 1 0.5 cm^{-1}

Table III-7

Few specifications of Model 2390 UV-Vis Double Beam Spectrophotometer.

Wavelength Range Limits	185 to 3152 nm
Spectral Bandwidths	0.07 to 3.6 nm in UV-Vis; 0.16 to 14.4 in NIR
Reference Modes	Autoselect., Autogain, Autoslit Single Beam
Baseline Correction	±0.001 Abs at 187 to 875 nm; ±0.002 Abs at 800 to 3100 nm
Resolution	0.07 nm; 0.35 nm at 1200 nm
Wavelength Accuracy	±0.20 nm
Wavelength Repeatability	±0.05 nm
Wavelength Drive	Stepper Motor, 0.01 nm/step
Slewing Speed	50 nm/sec

Table III-8

Few specifications of Multifrequency LCR-meter, HP-4274A

Measurement Circuit Modes:		Auto, Series and parallel.
Measurement Terminals	:	Four terminal pair configuration with guard terminal.
Range Modes		Auto and Manual (up-down).
Measurement Frequencies	:	100Hz, 120Hz, 200Hz, 400Hz, 1KHz, 2KHz, 4 KHz, 10 KHz, 20 KHz, 40 KHz and 100 KHz.
Test Signal Level	:	1mV to $5V_{rms}$, continuously variable in 4 ranges.
Offset Adjustment	:	Stray capacitance, residual inductance, resistance and conductance of test fixture or test leads can be compensated for as follow: C: up to 20pF. L: up to 2000nH. R: up to 0.5 ohm. G: up to 5 S.
Operating Temperature and Humidity	:	0°C to 55°C at 90% RH (to 40°C).

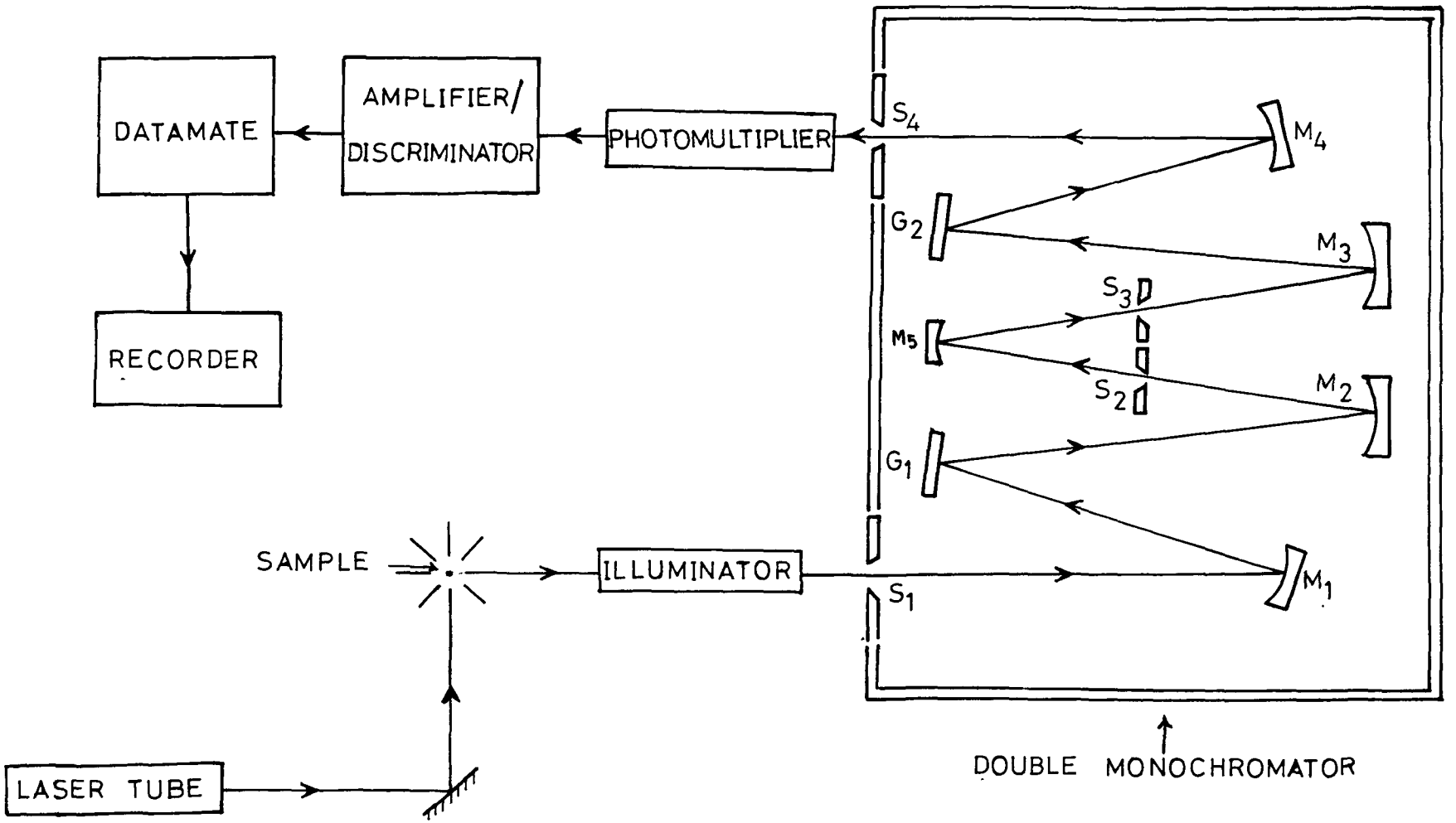

Fig3.1 Block diagram of a Raman Instrument.

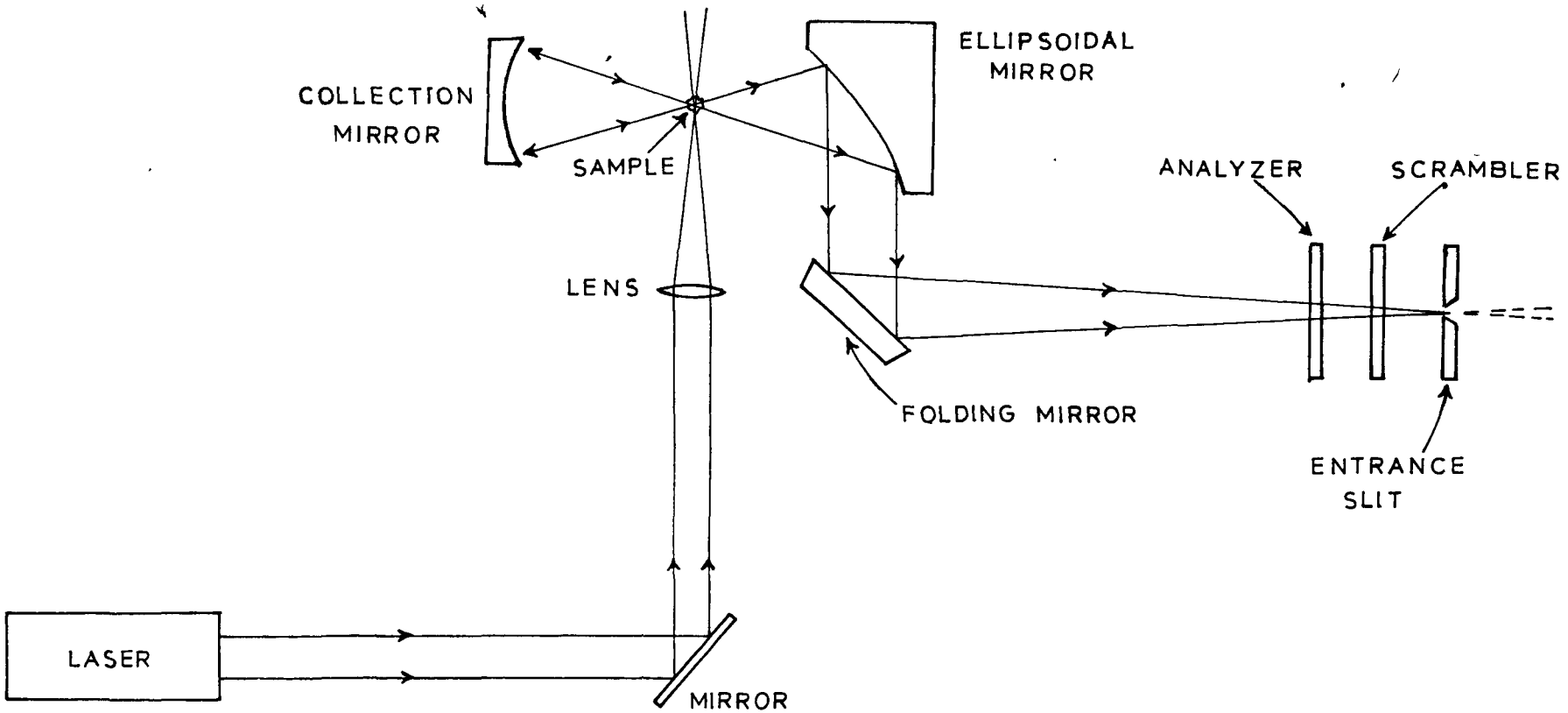

Fig.3.2 Optical diagram of the light - collecting system of a Raman Instrumennt.

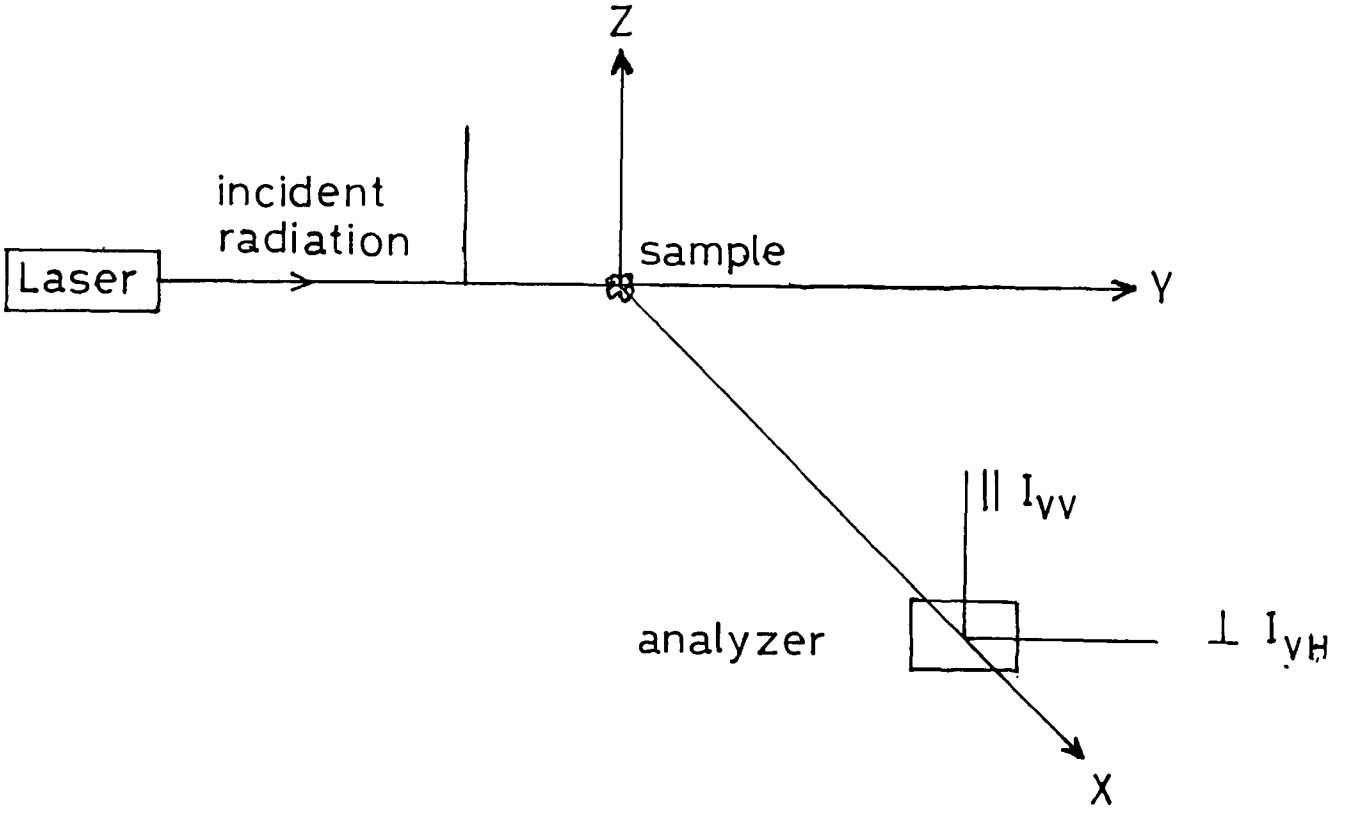

Fig.3.3 Optical diagram showing the two components of scattered intensity I_{VV} and I_{VH}

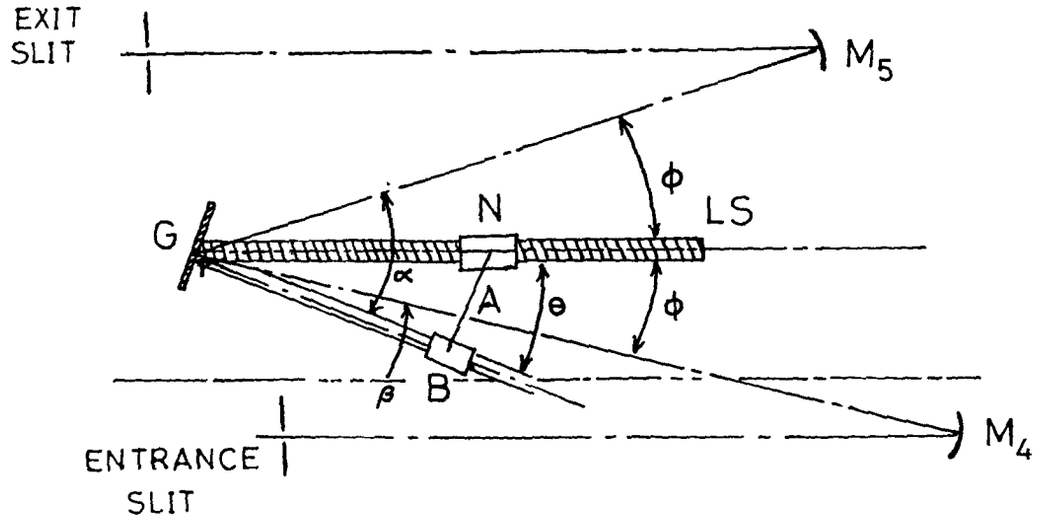

Fig.3.4 Mechanical cosecant drive mechanism for the Czerny Turnur mount of gratings for the SPEX Model 1403 Ramalog. The nut N moves along the lead screw LS while the slide B moves along a bar held at right angles to the grating G. The grating rotates as the arm A moves along the bar.

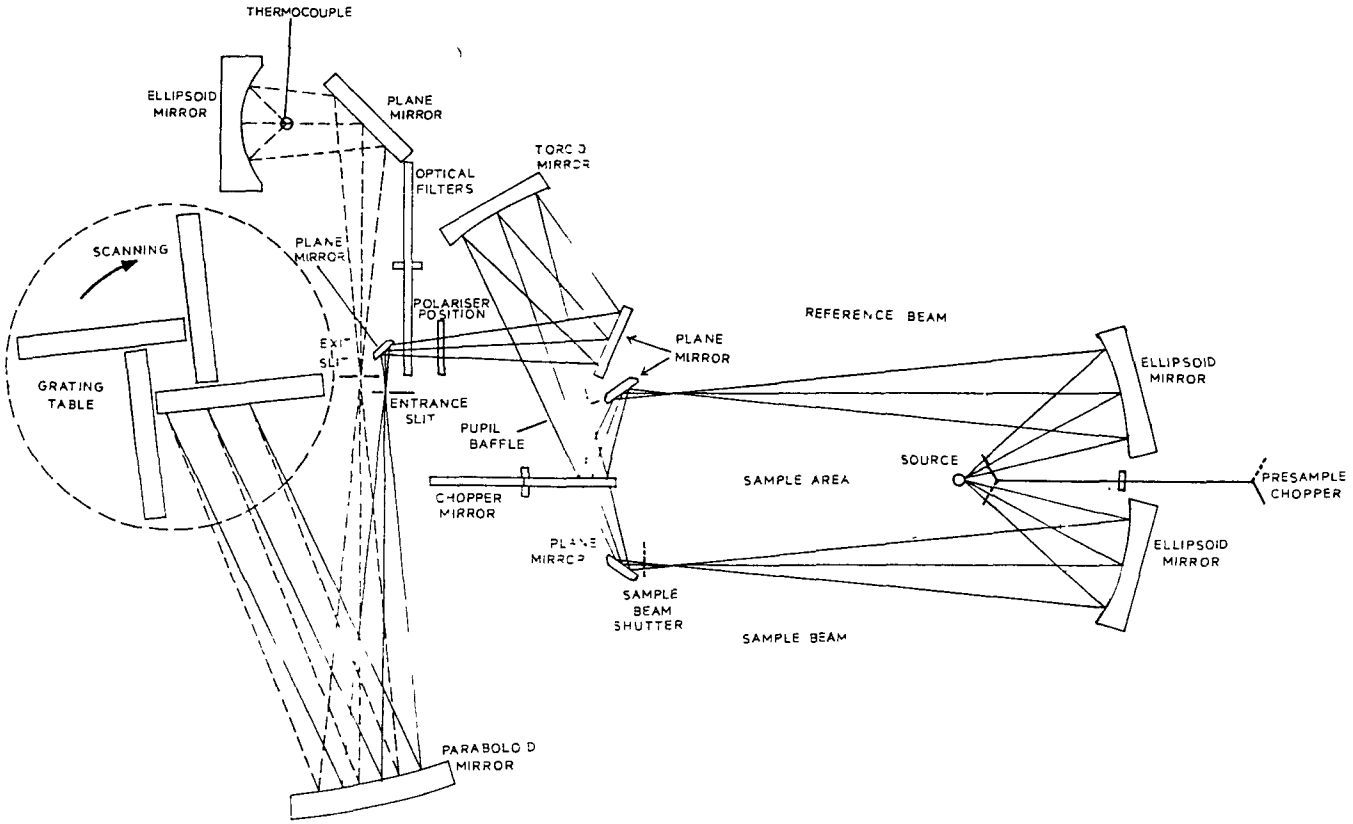

Fig.3.5 Optical ray-diagram of Perkin-Elmer Model 983 IR Spectrophotometer.

CHAPTER – IV

SYNTHESIS AND SAMPLE PREPARATION

4.1 Synthesis of p-Dimethylaminobenzylidene-p'-methoxyaniline (DABPMA)

The procedure followed[1] while synthesizing the compound DABPMA, has been outlined briefly as follows:

Para-dimethylaminobenzaldehyde (DMAB) and Para-methoxyaniline (PMA) were used as the parent compounds for the preparation of the schiff-base, DABPMA. The commercially available powdered sample of DMAB was purchased from E. Merck (India) and was further purified by crystallizing the powdered sample in dilute ethyl alcohol at room temperature. The purified sample of DMAB was obtained in transparent hexagonal crystal form. The crystals were washed in distilled water (distilled three times) and were dried in blowing air. The other parent compound para-methoxyaniline (PMA) was purchased from Thomas Baker and Co. London, and was used without further purification.

2.99 gms of the purified crystalline sample of DMAB and 2.46 gms of PMA were dissolved in sufficient quantity (about

40ml) of absolute ethyl alcohol. The reaction mixture was purified by slow filtration process. The filtrate was then refluxed continuously in a round bottom flask fitted to a leibig condenser through which cold water was circulated using an electrically-controlled water circulator (MK-70). The process of reflux was carried out at a constant temperature of 90^{o}C and was continued for three hours. The completion of the reaction was checked by using thin-layer-chromatography technique (TLC). The sample, after the completion of the reaction, was left untouched for about ten hours. The solid compound (light greenish yellow in colour) was then separated from ethanol containing traces of the unreacted parent compounds. The solid deposit was collected by filtration and was washed well with cold aqueous alcohol. The product was obtained in sufficiently pure form by crystallizing the sample three times from aqueous methanol. The pure sample was preserved in a dessicator.

4.2 Synthesis of Benzylidene-o-hydroxyaniline (BOHA)

The parent compounds ortho-amino-phenol (OAPH) and Benzaldehyde, used for the synthesis of the Schiff-base Benzylidene-o-hydroxyaniline (BOHA) were obtained from Aldrich with 99% purity of OAPH and 99% of Benzaldehyde and were used without further purification. 2.18 gms of ortho-aminophenol and 2.3 gms of benzaldehyde were dissolved in absolute ethyl alcohol and the procedure mentioned in 4.1 was followed except that the

reaction was continued for four hours in this case. The product, after the completion of the reaction was separated from ethyl alcohol, washed with distilled water and then extracted with chloroform. The compound thus obtained, was finally purified by using silica gel column chromatography(120 mesh size). The compound is light yellow in colour.

4.3 Synthesis of Benzylidene-p-nitroaniline (BPNA), p-Dimethylaminobenzylideneaniline (DABA), Benzylidene-m-hydroxyaniline (BMHA), p-methoxybenzylidene-p'-nitroaniline (PMBPNA) and p-Dimethylaminobenzylidene-p'-hydroxyaniline (DABPHA)

Extrapure AR grade p-nitroaniline was obtained from Sisco Research Lab and was used without further purification. The procedure followed for synthesizing the compound BPNA is same as that mentioned in 4.1. The compound was purified by using the method as mentioned in 4.2. The compound is bright yellow in colour.

The compounds DABA, BMHA, PMBPNA and DABPHA were synthesized by using parent compounds:

Aniline was a product of E. Merck (India), m-amino phenol was a product of Aldrich, Benzaldehyde (chlorine free) was a product of Sigma, p-anisaldehyde was a product of Sigma and p-amino phenol was obtained from Aldrich. The other chemicals are the same as mentioned earlier.

4.4 Elemental Analysis of the Synthesized Schiff bases

In order to confirm the formation of the desired compounds and to check the extent of their purity, the elemental analysis of Carbon, Hydrogen and Nitrogen was performed for all the Schiff bases, synthesized for present studies. The elemental analysis was performed by microanalytical technique using Heraeus Elemental Analyzer CHN-O-Rapid. The percentage weight of Carbon, Hydrogen and Nitrogen were obtained and were compared with those of the theoretically estimated values. They were found to be in good agreement.

4.5 H^1 NMR Spectral Analysis of Schiff bases

H^1 NMR spectra of the synthesized Schiff bases were recorded by using Varian EM-390 NMR Spectrometer at 90 MHz. The conclusions drawn from the H^1 NMR spectral studies of the compounds synthesized, were utilised to extend support to the mode of bonding containing H-atoms and to provide confirmatory evidences, in favour of their chemical structures.

4.6 Sample Preparation and Recording of Raman Spectra

The solid samples were dissolved in spectroscopic grade solvents, purified earlier by distillation process, to make a solution of concentration $\sim 10^{-4}$M. The solutions were purified by slow filtration process. To record the Raman spectra, about 2.3

ml of the prepared solution was taken in a cylindrical cell, which was positioned in a proper mount. The laser at a selected wavelength was made to strike the bottom edge of the cell. The spectrometer was routinely calibrated with known CCl_4 line in lower region i.e. 100 - 500 cm^{-1} and with Indene in the higher frequency range i.e. 1300 - 1675 cm^{-1} and some times with known Raman lines of solvents that were being used. Other spectral parameters such as laser power, integrating time, wavenumber increment, slit-width etc. were adjusted from time to time in order to optimise the signal to noise ratio. For weak Raman signals, the spectra were run several times and were averaged with the help of the Datamate.

The cell was cleaned to free it from grease and finger prints as they can cause a considerable increase in the fluorescent background of the spectrum and from air bubbles which increase the scatter of the laser beam.[2]

The fluorescent background in the Raman spectra was reduced by purifying the samples by the process of recrystallization. The photodecomposition was found to be minimum and was further avoided by using rotating cell technique.[3,4] This technique also avoids the local heating leading to thermal lens effect.

References

1. P.J. McCarty, R.J. Hovey, K. Veno and E. Martell *J. Am. Chem. Soc.* 77, 5820 (1955).
2. *"Basic Laser Raman Spectroscopy"* Jack Loader, p. 6, Heyden and Sons (1970).
3. W. Kiefer and H.J. Bernstein *J. Appl. Spectrosc.* 25, 500 (1971).
4. W. Kiefer and H.J. Bernstein *J. Appl. Spectrosc.* 25, 609 (1971).

CHAPTER – V

ASSIGNMENT OF VIBRATIONAL BANDS IN AROMATIC SCHIFF BASES

ABSTRACT

The Raman spectra have been recorded for four aromatic Schiff bases DABPMA, BPNA, DABA and BOHA in acetonitrile solution. The prominent vibrational Raman bands in the frequency range 1100 - 1700 cm^{-1} have been assigned. Special emphasis has been given to the assignment of the ν_{8a} , ν_{8b} (Wilson's notation) and $\nu_{C=N}$ modes of vibration involving the aniline moiety of the Schiff bases. These assignment are also aided by the available data on other substituted benzene molecules. The Raman and Infrared intensities of the bands have been used in identifying the vibrational modes. The relative intensity of the $\nu_{C=N}$ Raman band in these molecules in general, is indicative of the extent of conjugation in aromatic Schiff bases.

---

*Contents of this Chapter form part of the paper published:

R. Das and K. Kumar *Spectrochimica Acta* 45A,pp.705-709 (1989).

5.1 Introduction

The assignments for some important vibrational bands of aromatic Schiff base molecules are presented in this chapter. These assignments are based on correlation and are mostly aided by the assignments of modes of analogous molecules. The vibrational analysis is presented on the basis of the frequency ranges expected for each mode of vibration alongwith a general comparision with the vibrational spectra of the di-light and di-heavy substituted benzenes and other related molecular systems. Comparative studies of the vibrational spectra of different aromatic Schiff base molecules have also contributed significantly while assigning some vibrational bands. At times, the Raman and IR band intensities have been taken into account for identifying certain vibrational modes. For all the molecules under study, C_1 point group symmetry has been assumed while assigning the vibrational bands.

As pointed out by *Hester et al*[1] the obvious difficulty in assigning bands of para-substituted benzenes arises due to

individual substituent-effects on the forms of normal modes. Ample evidence for the complex nature of the normal modes of substituted benzene molecules is available.[1,2]

The important vibrational assignments have been presented in tabular form in Table V-1. The results being self-explanatory, the following discussion is confined to some of the important modes. Throughout the entire discussion, the benzenoid moiety vibrations are numbered according to Wilson's vibrational notations.[3]

5.2 Assignment of C-C Stretching Vibrations of Benzenoid Moiety

So far as the frequency range of vibrational bands of benzenoid moiety are concerned, the molecules, p-Dimethylamino benzylidene-p-methoxyaniline (DABPMA) is expected to behave as a para-disubstituted benzene molecule, whereas the molecules p-Dimethylamino benzylidene aniline (DABA), Benzylidene-p-nitroaniline (BPNA) and Benzylidene-O-hydroxyaniline (BOHA) may exhibit behaviour similar to that of di-substituted or/and mono-substituted benzene molecule. Benzene has two doubly degenerate modes ν_8 (1596 cm^{-1}) and ν_{19} (1485 cm^{-1}) having symmetries e_{2g} and e_{1u} respectively in the point group D_{6h}. Under C_1 point group symmetry each of these two doubly degenerate modes splits into two totally symmetric components, the first two are denoted by ν_{8a} and ν_{8b} whereas the other two are represented by ν_{19a} and

ν_{19b}. For disubstituted benzene molecules, according to Wilson's vibrational forms,[3] Carbon atoms in position 1 and 4 have zero amplitude[4] in normal mode ν_{8a}. Hence the frequency of mode ν_{8a} is less influenced by substituents than that of mode ν_{8b}. The frequency of ν_{8a} mode is, therefore, expected to be higher than the frequency of ν_{8b} in para-disubstituted type of molecules. Earlier observations[5-8] on similar molecules are in agreement with this. Among the molecules, presently studied, the molecules DABPMA, DABA and BPNA contain benzene rings where substitutions are in para-positions. The Raman spectra of these molecules [Figs. 5.1-5.4] show the presence of a medium to strong band in the range of 1591 - 1609 cm^{-1}. This Raman band is assigned to the ν_{8a} mode of C-C stretching vibration in benzene molecule. A comparative study of this Raman band reveals that the band is not shifted to a considerable extent (the magnitude of shift 18 cm^{-1}) even though the nature of substituents is quite different. The Raman band lying in a lower frequency range and having a comparatively lower intensity may be attributed to the ν_{8b} mode. This band with moderate intensity is observed at 1557 cm^{-1} and 1562 cm^{-1} in the Raman spectra of DABPMA and DABA respectively. For the molecule BPNA, this Raman band appears as a very weak feature at 1554 cm^{-1}.

For benzene molecules having di-substitution in ortho and meta-positions the vibrational amplitude in ν_{8a} normal mode[4] is $\sqrt{3/2}$ and the corresponding amplitude in the ν_{8b} normal mode

is 1/2. Since in mode ν_{8a} Carbon atoms linked with the substituents have bigger vibrational amplitude in ortho- and meta-disubstitutions, the frequency of mode ν_{8a} is expected to be smaller than that of ν_{8b}. The same inference was obtained[4-10] from normal co-ordinate analysis and related studies on similar molecular systems. The result of the normal co-ordinate analysis on orthosubstituted nitrobenzenes[9] reveals that the frequency corresponding to mode ν_{8b} may not necessarily be more than that of mode ν_{8a}. For O-fluoro nitrobenzene and O-iodonitrobenzene the normal co-ordinate analysis shows the frequency values of mode ν_{8a} to be 1604 cm^{-1} and 1599 cm^{-1} respectively whereas that of mode ν_{8b} was found to occur at 1593 and 1586 cm^{-1} respectively. The Raman spectra of the molecule BOHA, which is incidently, the only molecule studied by us, containing an ortho-substituted benzene ring shows a strong Raman band at 1597 cm^{-1}. This band is assigned to the ν_{8a} mode whereas the other Raman band having medium intensity and occuring at 1577 cm^{-1} is attributed to the ν_{8b} mode of benzene C-C stretching mode.

So far as the substitution effects on the frequency of mode ν_{8a} and ν_{8b} are concerned, the former appears to be less influenced by the nature of the substituting group on benzene rings. Vibrational mode ν_{8b}, on the other hand, seems to be influenced by both the nature and position of the substituting group in the benzene rings. From observations of the Raman spectra of the molecular systems having different substituting

groups, it appears that, it is not the mass of the substituent groups but their perturbing effects on the electronic system of the benzene ring which play the role while influencing the frequency of mode ν_{8b} in these molecules. It is probable that the substituent groups on the benzenoid moiety influences the π-electron distribution of the aromatic rings through their inductive and mesomeric properties. The electron distribution in the benzenoid moiety, is therefore, expected to be significantly perturbed by the electron donating and accepting properties of substituent groups. The dependence of frequency on the chemical nature of the substituents has also been reported by several authors.[11-19]

It is relevent to note here that in one of the samples DABPMA the vibrations ν_{8a} and ν_{8b} are influenced by the electrostatic environment of the molecule. The positions of both the vibrations are affected in a more or less, similar manner with the change in polarity of the solvent molecules.

The degenerate pair of vibrational modes of benzene ring ν_{19a} and ν_{19b} are mainly the C-C stretching vibrations, although the normal co-ordinate analysis[20,21] reveals that the mode can not be described only by stretching force constants. Vibration ν_{19} has e_{1u} symmetry in benzene and being an IR active mode had become known in the IR spectroscopic studies.[22-26] The vibrational forms of modes ν_{19a} and ν_{19b}

show that for para-disubstitution the frequency of ν_{19a} is expected to be at a higher value than that of ν_{19b}. This was also supported by theoretical calculations.[21] *Garrigou-Lagrange et al*[6] assigned ν_{14}, ν_{19b} and ν_{19a} in increasing order of frequency in the frequency interval of 1400 - 1500 cm^{-1}. In Katritzky's opinion[7], the frequency range for ν_{19a} in para-disubstituted benzene derivatives is 1480 - 1520 cm^{-1} and that of ν_{19b} is 1409 $\pm$ 8 cm^{-1}. For alkylbenzenes *Mc Murry and Thornton*[22] put the frequency of ν_{19a} into the range 1510 - 1521 cm^{-1}. For p-ethoxybenzaldehyde, p-carboxybenzaldehyde and p-cyanobenzaldehyde the IR bands at 1523, 1498 and 1500 cm^{-1} were assigned[8] to the mode ν_{19a}.

The Raman spectra of all the four molecules under study, show a band of varying intensity in the frequency region around 1500 cm^{-1}. In DABPMA and DABA this band appears at 1507 and 1495 cm^{-1} respectively whereas in BOHA it occurs at 1487 cm^{-1}, all the bands having low intensity. In BPNA molecule, however, the band appears as an intense one at 1507 cm^{-1}. These Raman bands for the four molecules are attributed to ν_{19a} mode of ring. The intensity of this Raman band, in general, is found to be low, the only exceptional case being that of BPNA molecule where it appears as an intense band. The gain in intensity of this Raman band in BPNA is probably due to the lowering of symmetry by a heavy substituent group such as nitro-group (mass of the substituent being 46 amu) which permits

the ν_{8b} mode to interact with other vibrations. The asymmetric nitro-stretching vibration of BPNA which happens to occur in the vicinity of the same range of frequency, may be of considerable significance in this context. The gain in intensity in the ν_{19a} mode of benzene vibration, therefore, may be due to the mixing of these two vibrations. The mixing of C-C stretching vibration with the symmetric stretching vibration of nitrogroup has also been found while attempting the normal co-ordinate analysis[9] in monohalogenated nitrobenzenes. The comparative study of the Raman spectra of the molecules studied, reveals that the frequency of ν_{19a} band is affected by substituent groups. A closer look at the difference in the band positions in different molecules reveals that the substituent-effect on the frequency of ν_{19a} is more or less dominated by the chemical nature of the substituting group on the aniline ring of the aromatic Schiff bases. The position of the substituent group in the aniline ring also contributes to a significant extent while influencing the frequency of mode ν_{19a}.

The weak Raman band observed in the frequency range 1443-1457 cm^{-1} may be attributed to ν_{19b} vibration of ring. This band has frequency of 1443 cm^{-1} in both DABPMA and DABA molecules and 1457 cm^{-1} in BPNA. The band is too weak in the Raman spectra of BOHA. The IR spectra of all the molecules, however, show the presence of this vibrational band. This occurs as a weak feature at 1445, 1438, 1448 and 1456 cm^{-1} in DABPMA, DABA, BPNA and BOHA respectively.

5.3 Assignment of C-H in-plane Bending Vibrations

In the frequency range 1114 - 1195 cm^{-1}, all the molecules under study, show two overlapping Raman bands. The band occuring at higher frequency is observed to be comparatively more intense than that occuring at lower frequency. These pair of Raman bands are observed at 1169 cm^{-1} & 1176 cm^{-1} in DABPMA and at 1168 cm^{-1} & 1177 cm^{-1} in DABA molecule. However in case of molecules BOHA and BPNA, the same pairs are observed at 1173 cm^{-1} & 1195 cm^{-1} and at 1114 cm^{-1} & 1182 cm^{-1} respectively. The lower frequency Raman band could be attributed to the normal mode δ_{15} (benzene C-H in-plane bending vibration). In Raman spectra its intensity is expected to be low which is in consistency with the observations. The intensity of the Raman band at 1114 cm^{-1} in BPNA, however, is much larger than that of the 1182 cm^{-1} Raman band. This assignment of mode δ_{15} is done in accordance with earlier work[23] on similar systems. The other Raman band which occurs at higher frequency with a comparatively high intensity could be assigned to mode δ_9 (benzene C-H in-plane bending vibration). The Raman bands at 1176 cm^{-1}, 1195 cm^{-1}, 1182 cm^{-1} and 1177 cm^{-1} for DABPMA, BOHA, BPNA and DABA respectively are, therefore, attributed to mode δ_9. This vibration in D_{6h} point group belongs to the symmetry species e_{2g} and is a Raman active mode. This vibration, in benzene is supposed[24] to be the most pure CH in-plane bending vibration. The assignment of mode δ_9 in the molecules, under study is in agreement with the available

literature[24] values.

5.4 Assignment of C=N Stretching Vibration

A significant amount of work dealing with the position of the -C=N- stretching vibration in IR spectra has been done in variety of molecules, the details of which are reviewed by *Fabian et al.*[25] The effect of conjugation on the -C=N- stretching vibration, in ring systems, in particular, is probably to mix them with C=C vibrations. The frequencies of the two are so close that, it is sometimes doubtful whether either can be regarded to retain its individual character. The -C=N- stretching vibration was located for non-conjugated compounds (of the type R-CH=N-R) to be around 1650 cm^{-1} and was confirmed by others[23] working on similar systems. The conjugation effect on the position of -C=N stretching band, due to an aromatic ring is variable and depends partly on the point of its attachment.[23] The -C=N band moves to about 1630 cm^{-1} in IR spectra when the aromatic ring is attached to the nitrogen atom of the -C=N- linkage, whereas an attachment of an aromatic ring to the carbon atom promotes its position to 1640 cm^{-1}. The influence of the aryl conjugation on the position of the -C=N- stretching band, in general, is found[23] to lower the frequency of its occurance.

The Raman spectra of the four aromatic Schiff bases

show a band in the frequency interval 1623 - 1633 cm^{-1} which vary in intensity from moderate to weak. This Raman band is observed at 1623 cm^{-1}, 1629 cm^{-1}, 1633 cm^{-1} and 1626 cm^{-1} in DABPMA, DABA, BPNA and BOHA respectively, in acetonitrile solution. In molecules DABPMA and BPNA its relative intensity is observed to be lower than that in BOHA and DABA. The change in the relative intensity of this Raman band due to the difference in character of the substituting groups and their position in the benzene ring, shows the sensitivity of the band towards the environmental change. It appears that the electronic distribution of the aromatic ring linked to the nitrogen atom of the Schiff base linkage has a prominent role to play while perturbing the conjugation effect on this band. It also seems to be governed by the extent of π-electron delocalisation by the substituting groups on the benzene ring. Although the internal co-ordinates are likely to be mixed to a considerable extent, the -C=N- stretching vibration seems to have the highest contribution to this Raman band. This Raman band could, thus be assigned to the -C=N- stretching mode which is also in agreement with the available literature values[26,27] in analogous molecular systems.

The position of the -C=N stretching band appears to be less influenced by the electrostatic environment in comparision to the ν_{8a} mode of vibration.

5.5 Assignment of other Important Vibrations

The vibrational modes which are not concerned collectively with all the Schiff base molecules, under study, but are restricted only to individual molecules of interest are discussed here. The nitro-stretching vibration in BPNA and Ph-$N(Me)_2$ stretching vibration in DABPMA deserve mention in this context.

The NO_2 group stretching vibrations splits into two components. One of them is the symmetric mode and the other one is antisymmetric. *Randle and Whiffen*[28] assigned the symmetric stretching to a band between 1333 and 1370 cm^{-1} and the antisymmetric one between 1494 and 1539 cm^{-1} in the spectra of 23 aromatic nitrobenzene derivatives. It was reported[29] that conjugation-effect changes the frequency of both the symmetric and antisymmetric vibrations. The normal co-ordinate analysis on p-nitrobenzaldehyde[30] shows that the symmetric nitro-stretching vibration has its highest contribution at 1352 cm^{-1} against the experimentally observed Raman band at 1349 cm^{-1}. The same vibrational band in monohalogenated nitrobenzenes[9], is observed at 1353 cm^{-1}. Data reported[23,27] on the Raman spectra of several nitroaromatic molecules also show the same range of frequency for the symmetric nitro-stretching vibration. Based on these data, the Raman band at 1393 cm^{-1} with medium intensity is assigned to the symmetric stretching mode of the nitro group in BPNA. The

antisymmetric nitro stretching is probably mixed to a considerable extent with the ν_{19a} mode of C-C stretching vibration and appears as a strong Raman band at 1507 cm^{-1}.

A band of very weak intensity occuring at 1417 cm^{-1} in the Raman spectra of molecule DABPMA in acetonitrile is probably due to the Ph-$N(Me)_2$ stretching vibration. This band was found to occur at 1370 cm^{-1} in case of sulfonamide molecule by earlier workers.[31] The shift in the band position might be due to the conjugation taking place between the phenyl system and the dimethylamino group attached to the benzene ring of molecule DABPMA.

5.6 Infrared Spectra

We list, as a part of Table V-1, the positions and intensities of some of the bands in IR spectra of the Schiff base molecules discussed earlier.

References

1. E. Ernsfbrunner, R.B. Girling, W.E.L. Gossma, E. Mayer, K.P.J. Williams and R.E. Hester *J. Raman Sperctrosc.* 10, 161 (1981).
2. P.N. Gates, D. Steele, R.A.R. Pearce and K. Radcliffe *J. Chem. Soc. Perkin Trans.* 2, 1607 (1972).
3. "*Molecular Vibrations*" E.B. Wilson, J.C. Decius and P.C. Cross, McGraw-Hill, London (1955).
4. "*Vibrational Spectra of Benzene Derivatives*" G. Varsanyi Academic Press, New York, London (1969).
5. N. Herzfeld, J.W. Hobden, C.K. Ingold and H.G. Poole *J. Chem. Soc.* 272 (1946).
6. C. Garrigou-Lagrange, J.M. Lebas and M.L. Josien *Spectrochim Acta* 12, 305 (1958).
7. A.R. Katritzky *Quart. Rev.* 13, 353 (1959).
8. P. Venkoji *Spectrochim Acta* 42A, 1301 (1986). and references therein.
9. P. Muralidhar Rao and G.R. Rao *J. Raman Spectrosc.* 20, 529 (1989).
10. M.A. Kovner and A.M. Bogomolov *Opt. Spek.* 4, 301 (1958).
11. T. Anno and I. Matubara *J. Chem. Phys.* 23, 796 (1955).
12. C.D. Cooper and L.N. Sastri *J. Chem. Phys.* 20, 607 (1952).
13. W.F. Forbes and J.J. Myron *Can. J. Chem.* 39, 2452 (1961).
14. M. Ito and T. Shigeoka *Spectrochim Acta* 22, 1029 (1966).
15. R.J. Jakobsen *Spectrochim Acta* 21, 433 (1965).

16. R.J. Jakobsen and E.J. Brewer *Appl. Spectrosc.* 16, 32 (1962).

17. S.L.N.G. Krishnamachari *Ind. J. Phys.* 31, 447 (1957).

18. J.M. Lebas, C. Garrigou-Lagrange and M.L. Josien *Spectrochim. Acta* 15, 225 (1959).

19. N.A. Puttnam *J. Chem. Soc.* 48, 5100 (1960).

20. M.A. Kovner *Zhur. Exp. Teor. Fiz.* 26, 598 (1954).

21. J.R. Scherer *Spectrochim. Acta* 19, 601 (1963).

22. H.L. McMurry and V. Thornton *Anal. Chem.* 24, 318 (1952).

23. *"The Infrared Spectra of Complex Molecules"* L.J. Bellamy, John Wiley and Sons, New York (1959).

24. J.R. Scherer and J. Overend *Spectrochim. Acta* 17, 719 (1961).

25. J. Fabian, M. Legrand and P. Poirier *Bull. Soc. Chim. Fr.* 23, 1499 (1965).

26. *"Liquid Crystals, Ordered Fluids"* J.F. Johnson and R.S. Porter, Eds., vol. 2, p. 507, Plenum Press, New York (1974).

27. *"Introduction to Infrared and Raman Spectroscopy"* N.B. Colthup, L.H. Daly and S.E. Wiberley, p. 326, Academic Press, New York (1975).

28. R.R. Randle and D.H. Whiffen *J. Chem. Soc.* 4153 (1952).

29. E. Lippert *Elektrochem.* 59, 534 (1955).

30. S. Mohan and A.R. Prabakaran *J. Ram. Spectrosc.* 20, 263 (1989).

31. K. Kumar and P.R. Carey *Can. J. Chem.* 55, 1444 (1977).

Table V-1

Tentative assignments of vibrational bands in Aromatic Schiff bases

Band positions in cm^{-1}								Vibrational Assignments
DABPMA		DABA		BPNA		BOHA		
Raman	IR	Raman	IR	Raman	IR	Raman	IR	
1169w	1171sh	1168w	1170m	1114m	1116s	1173w	1172w	δ_{15}
1176w	1181s	1177w	1185m	1182w	1185s	1195sh	1196w	δ_{9}
-	-	-	-	1393w	1397w	-	-	Symmetric-NO_2 stretch
1417vw	1417w	-	-	-	-	-	-	Ph-$N(Me)_2$ stretch
1443w	1445sh	1443sh	1438w	1457w	1448m	-	1456w	ν_{19b}
1507w	1505s	1495vw	1487m	1507s	1507w	1487w	1479sh	ν_{19a}
1557m	1557m	1562m	1557m	1554vw	1582sh	1577m	1580sh	ν_{8b}
1595s	1597sh	1591s	1590s	1601s	1607s	1597s	1591m	ν_{8a}
-	-	1609m	1605s	-	-	-	-	
1623m	1625sh	1629m	1625sh	1633w	1623s	1626m	1631m	C=N stretch

Abbreviations: w = weak, m = medium, s = strong, vw = very weak, sh = shoulder

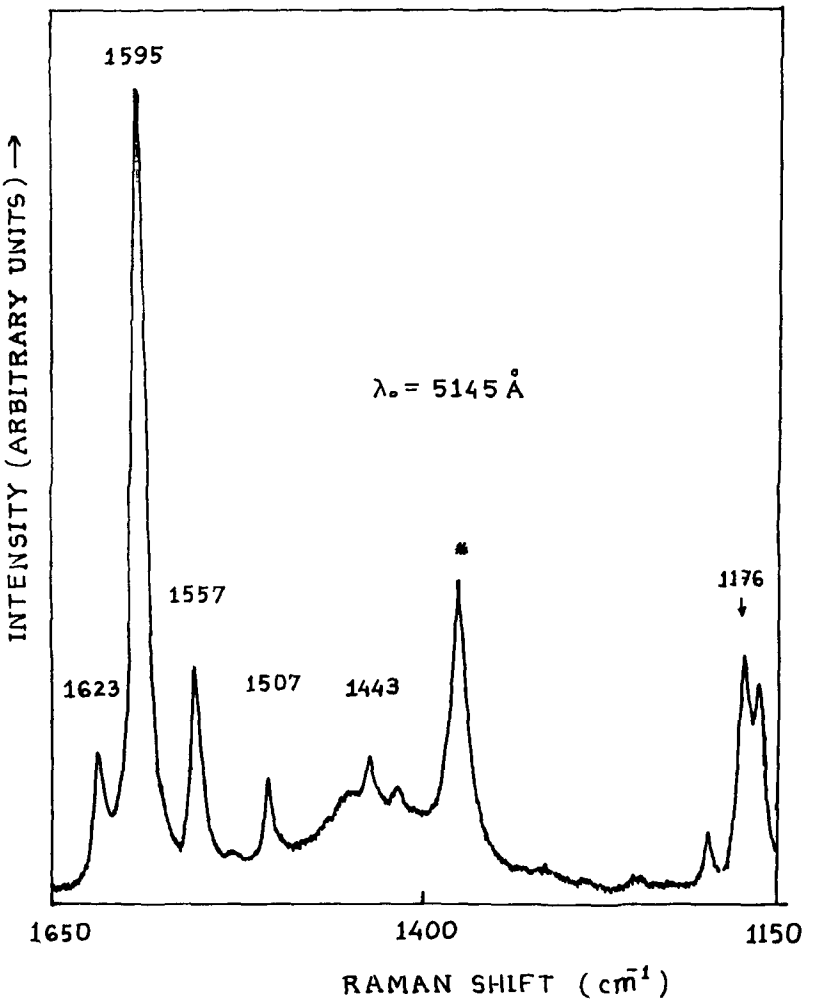

Fig.5.1 Raman spectrum of DABPMA in acetonitrite soln.

λ_o = 5145 Å , conc. $\sim 10^{-4}$M

* mark shows the acetonitrile band (1375 cm^{-1})

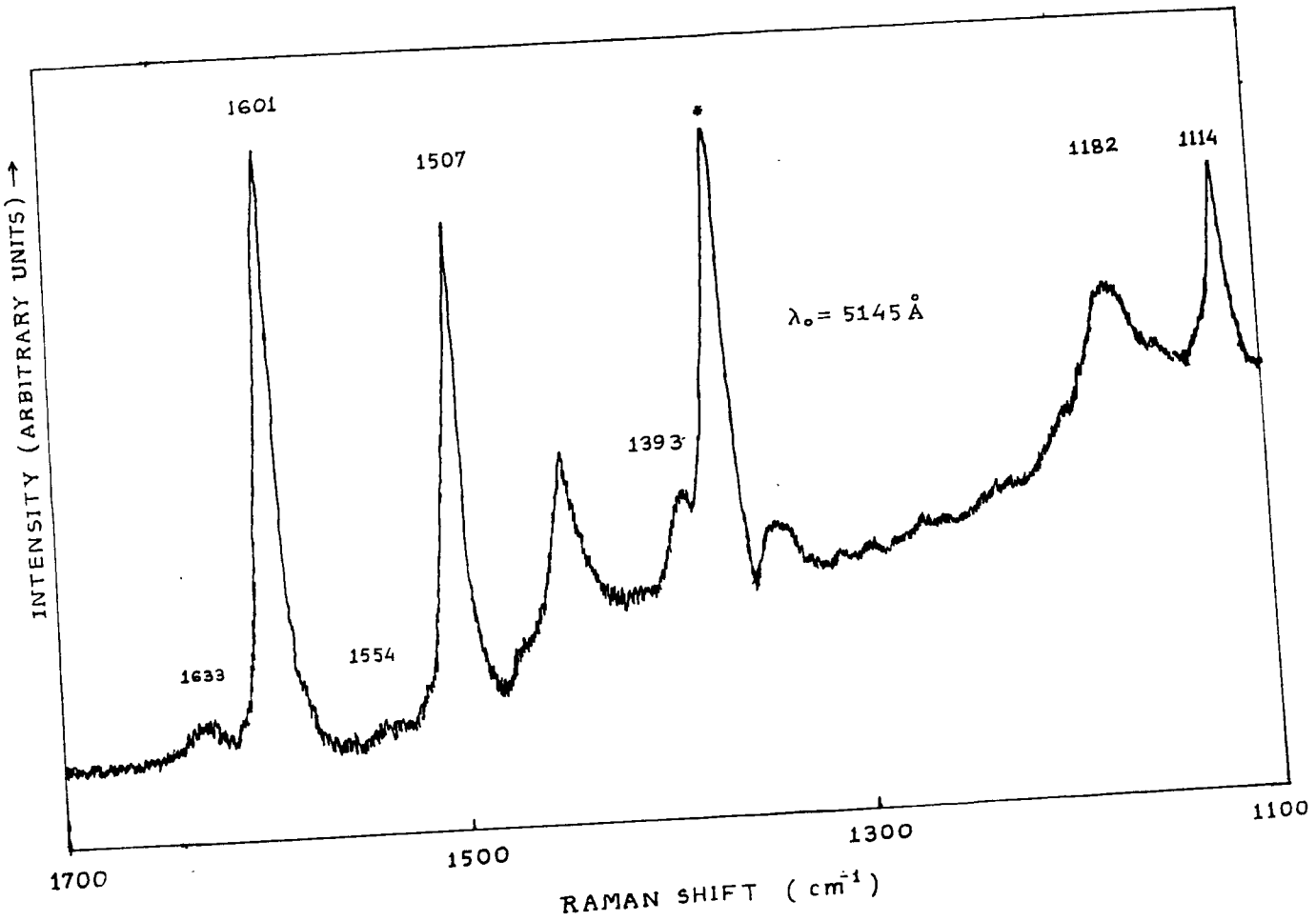

Fig.5.2 Raman spectrum of BPNA in acetonitrite soln.

λ_o = 5145 Å conc. ~ 10^{-4} M

* mark shows the acetonitrile band (1375 cm^{-1})

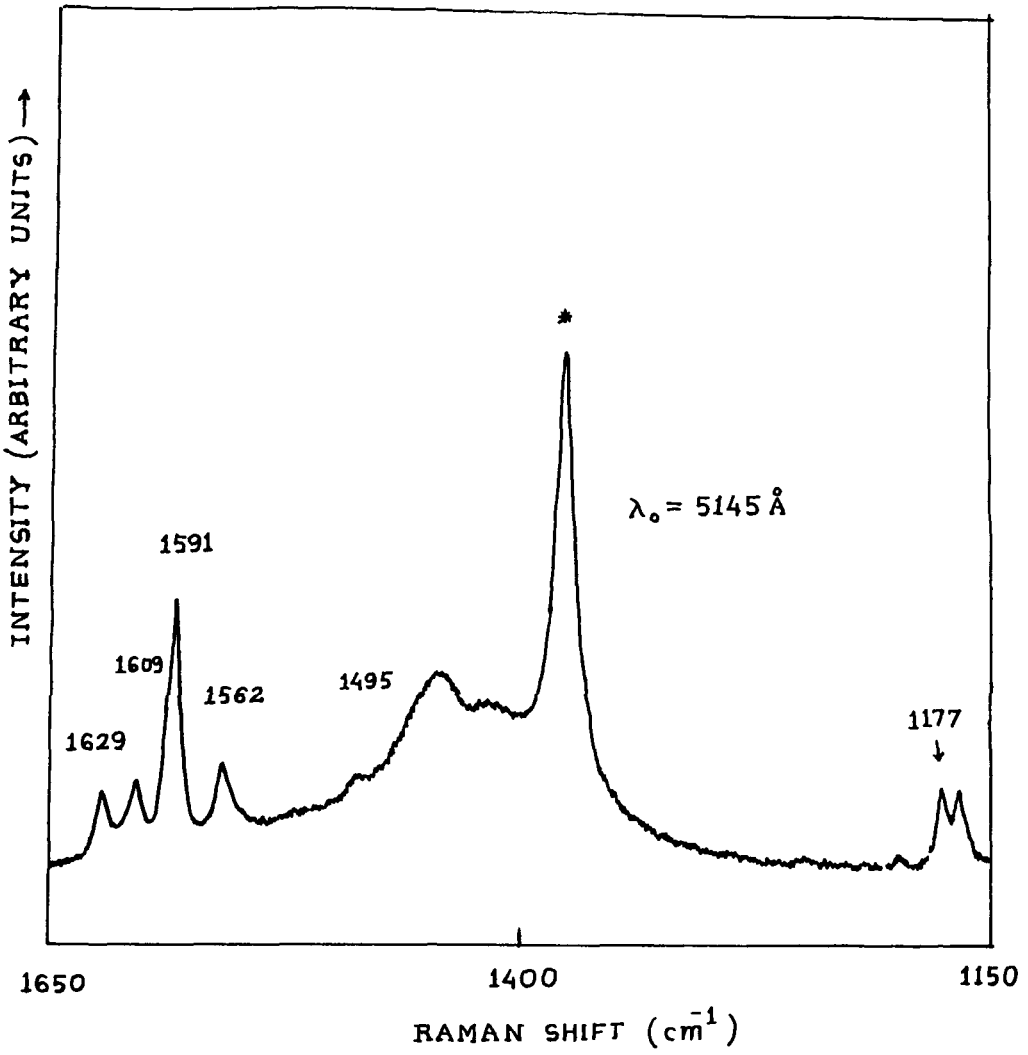

Fig.5.3 **Raman** spectrum of DABA in acetonitrite soln.

λ_0 = 5145 Å , conc. $\sim 10^{-4}$ M

* mark shows the acetonitrile band (1375 cm^{-1})

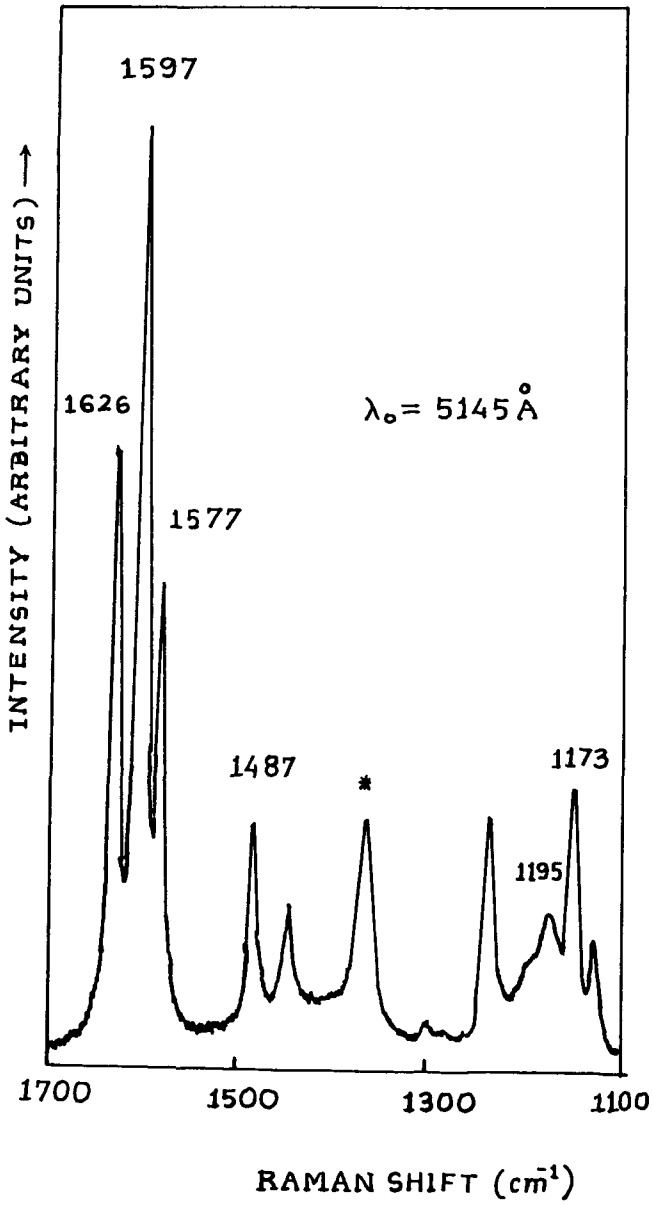

Fig.5.4 Raman spectrum of BOHA in acetonitrite soln.

λ_0 = 5145 Å , conc. ~ 10^{-4}M

* mark shows the acetonitrile band (1375 cm^{-1})

CHAPTER – VI

RAMAN EXCITATION PROFILES OF AROMATIC SCHIFF BASES

ABSTRACT

The pre-resonance Raman spectra of aromatic Schiff bases have been recorded at various exciting wavelengths. The excitation profiles of the Raman bands corresponding to ν_{8a}, ν_{8b} and $\nu_{C=N}$ vibrational modes have been presented. The theoretical Raman intensity factors have been calculated using Albrecht and Hutley's approach. The observed and calculated intensity factors, normalized with respect to the λ_0=4880Å exciting line has been presented. The pre-resonance in bands (i.e. ν_{8a}, ν_{8b}, and $\nu_{C=N}$) is interpreted in terms of vibronic coupling between the excited electronic states.

*Contents of this chapter form a part of the paper published:

R. Das and K. Kumar *Spectrochimica Acta* 45A, pp. 705-709 (1989).

6.1 Introduction

The dependence of Raman intensity and the depolarization ratio on the exciting frequency has been used to account for many important aspects of molecular systems.[1] Intensity enhancement of the chromophore vibrations occurs when the exciting frequency approaches the electronic absorption band of the chromophore. The intensities of those vibrations, which contribute to the vibrational structure of the electronic absorption band, even if it is not resolved, are enhanced in this process.[2,3] The variation of Raman intensity with the exciting frequency gives the Raman excitation profile (REP) and resembles an absorption spectrum for the mode being monitored. Preresonance Raman excitation profiles may, therefore, provide a lot of detailed information about the nature of the lowest electronic excited states of molecules. The preresonance Raman technique requires the knowledge of the chromophore structure as well as the correlation of changes in its Raman spectrum with perturbation to the geometry and environment of the molecule.[3]

The dispersion of the depolarization ratio (ρ) with the exciting frequency can give valuable information regarding the structure and symmetry of the molecule. The value of ρ becomes the 0.33 in the extreme case, when only one component of the scattering tensor (α_{xx} or α_{yy} or α_{zz}) contributes and all

the others are zero.[1]

Aromatic Schiff bases [Fig. 6.1] exhibit electronic transition in the UV region of the spectrum. Consequently the preresonance Raman technique is useful for the study of structural features of these molecules whose lowest electronic transition lies in the UV region. The structurally sensitive Raman lines of Schiff bases are, therefore, expected to undergo intensity enhancement when the frequency of the exciting radiation approaches the frequency corresponding to the electronic absorption maxima. The vibrational modes of aromatic Schiff bases arising from N=C group and phenyl rings could be useful as Raman probes in preresonance Raman technique. In order to get a deeper insight into the behaviour of such molecular systems, we have determined the experimental excitation profiles of the structurally sensitive Raman lines of four Schiff bases. The Raman spectra of all the Schiff bases are recorded in acetonitrile solution and the 1375 cm^{-1} Raman band of acetonitrile is used as the internal standard for relative intensity measurements. In order to avoid probable perturbation effects due to varying solvents, only acetonitrile is used as the solvent in all cases.

6.2 Electronic Absorption Spectra

The electronic absorption spectra of the aromatic Schiff bases, in acetonitrile solution, in general exhibit two

absorption bands in the wavelength range 290 - 370 nm [Fig. 6.2]. One of them is observed as a strong band in the wavelength range 330 - 370 nm whereas the other appears as a weak feature in the lower wavelength region (~300 nm). It is possible that the electronic transitions are mixed to a significant extent and as such, each of the two electronic absorption bands are expected to contain contributions from more than a single transition. The absorption band appearing in the lower wavelength range, may be arising mainly due to the excitation of n, π-electrons of the aromatic system. The strong absorption band appearing in the higher wavelength region, however, is expected to contain[4] major contribution due to the charge-transfer (C-T) transition.

6.2.1 Substitution in Benzylidene ring

The positions of both the electronic absorption bands are observed to be influenced by the chemical nature of the substituent groups in the benzylidene ring of the Schiff base molecule. The electronic absorption maximum λ_{max} is observed at 336 nm in acetonitrile solution when there is a strong electron donating dimethylamino group, substituted in the para-position of the benzylidene ring (DABA). The position of λ_{max} does not appear to be affected much when the aniline ring is substituted by another strong electron donating methoxy group in the para-position of the aniline ring. The λ_{max} value in such a case is observed at 334 nm in acetonitrile

solution (DABPMA).

6.2.2 Substitution in Aniline ring

It is observed that when the aniline ring is substituted by a strong electron withdrawing nitro group, the absorption band in the higher wavelength range is red-shifted by approximately 30nm relative to the same band of DABPMA and DABA. The absorption maximum, λ_{max} in this case, is observed at 364nm in acetonitrile solution (BPNA). Because of the high electron-withdrawing power of the nitro-group it behaves as an intramolecular charge-transfer acceptor centre. The charge-transfer interactions as such, is expected to be more probable when the nitro-substitution occurs in the ortho or para-position of the aniline ring.

Substitution by a hydroxyl-group on the ortho-position of the aniline ring shows a tendency of red shift in the electronic absorption band due to C-T transitions. This absorption band is observed at 340 nm in acetonitrile solution. The other electronic absorption band arising mainly due to the $n-\pi^*$ electronic transition in this compound appears as a comparatively stronger band at 265 nm.

The electronic absorption spectra of all the four aromatic Schiff bases in acetonitrile solution are shown in Fig. 6.2.

6.3 Influence of Absorption on Observed Raman Band Intensities

During passage of light through the scattering substances, both the exciting and the scattered light undergo absorption which also depends on wavelength and distances traversed.[1] All the measurements are taken for dilute solutions hence no corrections are necessary for absorption of radiation by the solution.

Unless otherwise specified, we shall use the integrated Raman band intensity values referred to a scale in which the 1375 cm^{-1} Raman band of acetonitrile is adopted as the reference standard. This intensity scale, however, presupposes identical operating conditions for the sample and the reference substance. The simplest possible way to ascertain identical operating conditions with sufficient accuracy is to use an appropriate reference substance as the internal standard in liquids. In this method, however, care should be taken to guard against the solvent effects in liquids. The intensity values in the following sections may be taken on the average to be subject to an uncertainty of not more than 10%.

6.4 Selection of Raman Bands

It was empirically established and was confirmed by several workers[1,5-7] that the vibrations, which determine the vibrational structure of the absorption band whose maximum is

nearest to the exciting line, appear with high intensity in Raman spectra under preresonance excitation. The vibrations which characterize the vibrational structure of the electronic band nearest to the exciting frequency are particularly intensified in preresonance Raman spectra, even when the vibrational structure of the absorption band is latent because of broadening or overlapping of several absorption bands. When the exciting frequency approaches the region of electronic absorption, the intensity increase of different Raman lines of the same molecule, generally appears to be non-uniform.[2] The properties of the superimposed individual vibrational bands which influence preresonance Raman intensity may also play role in governing non-uniform behaviour of preresonance Raman intensity.

In order to study the excitation profile, only those vibrational Raman bands which are well-separated and have d epolarization ratio (ρ) = 0.33 are chosen. This enables us to measure relative intensity accurately and the theory of Albrecht and Hutley[8] can also be applied to compare the experimental values with the theoretically calculated ones.

On the basis of the foregoing discussions the Raman bands corresponding to the ν_{8a}, ν_{8b} modes of C-C stretching vibrations of benzene ring and $\nu_{C=N}$ (C=N stretching vibration) were chosen for the present study as these bands were satisfying the condition necessary for the study of the excitation profile.

The intensity of the selected vibrational Raman bands of Schiff bases were measured relative to the intensity of 1375 cm^{-1} Raman band of acetonitrile. Since the reference Raman line (1375 cm^{-1}) is fairly close to the Raman bands of interest (1550 - 1630 cm^{-1}), no correction is required for the spectrometer response. Again since the preresonance Raman spectra were recorded at a low concentration of solute ($\sim 10^{-4}$M), the correction due to intensity-dependence on excitation wavelength of the solvent band, used as the internal standard, was not of utmost necessity. The average band areas were, therefore, taken to be the corrected integrated vibrational intensities. The ratio of the band areas for a given vibration of the solute and for the solvent band was taken to give a relative integrated intensity of the particular Raman band. Such intensities were then normalised relative to the intensity corresponding to the exciting wavelength λ_o = 4880 A°.

6.5 Calculation of Theoretical Intensity Variations

The dependence of the intensity of Stoke's Raman scattering on the exciting frequency ν_o is given by:

$$I \propto (\nu_o - \nu_M)^4$$

where ν_M indicates the wavenumber of the molecular vibration in question. When resonance or preresonance effects are taken into account, a number of additional factors, corresponding to the

excited electronic levels, play dominant role in the modifying the frequency-dependence of Raman intensity. If only one or two electronic levels are considered to play a predominant role in the scattering process, then the intensity of vibrational Raman scattering has a relatively simple frequency-dependence [discussed in details in 2.3]. In case only one electronic level is important, the total frequency dependence of the scattered intensity associated with a particular molecular vibration including both the normal fourth power law dependence and the frequency dependence of the scattering tensor is given by[8,9]

$$F_A^2 = \left[\frac{\nu^2(\nu_e^2 + \nu_o^2)}{(\nu_e^2 - \nu_o^2)^2}\right]^2 \qquad \ldots\ldots 6.5.1$$

where ν_e in the eigenfrequency associated with the dipole allowed transition from the ground electronic state to the electronic state in question. ν_o is the exciting line frequency and ν is the frequency of scattered radiation such that

$$\nu = \nu_o - \nu_M$$

where only Stokes scattering is considered.

However, if two electronic levels are important, then the frequency dependence of the scattered Raman intensity is given by[8]

$$F_B^2 = \left[\frac{2\nu^2(\nu_e\nu_s + \nu_o^2)}{(\nu_e^2 - \nu_o^2)(\nu_s^2 - \nu_o^2)} \right]^2 \quad \ldots\ldots 6.5.2$$

where ν_e and ν_s are the frequencies associated with the dipole-allowed transitions from the ground electronic state to the two electronic states in question.

The theoretical intensity factors are calculated using Eqn. (6.5.1) and (6.5.2) where all the entities on the right hand side are obtained from the experimental data. The dependence of vibrational Raman intensities predicted by F_A^2 and F_B^2 terms are presented in Tables VI-1-4 along with the experimentally determined frequency-dependent intensity values. A comparision of the two may provide insight into the electronic-vibrational coupling phenomena in the electronic state(s), involved predominantly in the preresonance intensity enhancement.

6.6 Excitation Profiles

An excitation profile can be obtained for those molecules only which are free from intrinsic luminescence and are highly soluble so as to yield a good Raman spectrum. In addition to these, the Raman bands of interest should be sufficiently separated to allow careful intensity measurements. The four Schiff bases BPNA, DABPMA, BOHA and DABA were found to satisfy these criteria and hence the excitation profiles were obtained

for three Raman bands in all the four molecules. Under preresonance condition, the extension of conjugation from a benzenoid nucleus to its side chains can give rise to intensity enhanced modes from the side chains. However, the extension of conjugation effect, though a necessary one is not a sufficient condition to induce preresonance Raman features from the side chains. In addition, another prerequisite condition is that the vibrational modes of the side chains must be vibronically coupled to the electronic transition.

6.6.1 Excitation Profiles for Benzylidene-p-nitroaniline (BPNA)

The electronic absorption spectrum of Benzylidene-p-nitroaniline (BPNA) is shown in Fig. 6.2. The absorption spectrum shows that the absorption maximum (λ_{max}) for this molecule occurs at 364 nm. This absorption maximum contains major contribution from the C-T electronic transition.[4] The otherwise forbidden electronic transition n—— π^*, may also gain some intensity due to the mixing with C-T or π—— π^* transition and intensity borrowing. Hence it may contribute to intensity enhancement of the chromophore vibrations. The preresonance Raman spectra of BPNA [Fig. 6.3A and 6.3B] reveals that the spectra are dominated by three Raman bands which correspond to ν_{8a}, ν_{8b} and $\nu_{C=N}$ modes. From the preresonance spectra one can note that both ν_{8a} and ν_{8b} gain intensity as the exciting wavelength changes from 5145A° to 4579A°. Far from resonance, one finds that this profile tends to decrease rapidly.

As far as the conjugative effects of the substituent group are concerned, the molecule BPNA has close resemblence with trans-4-Benzylidene 2-phenyl- Δ^2-Oxazolin-5-one. For such a system, it was shown[9] that the electronic dipole transition responsible for the intense low frequency absorption band as well as the vibrational modes responsible for the intense Raman bands are localized in the -C=C-N=C-Ph part of the molecule. Further, it was also observed that the substituents in the benzylidene ring have little influence on the Raman spectra and as such, have minor perturbations in the factors responsible for Raman intensity. In BPNA which has a somewhat similar structure a similar behaviour is probable. However, in BPNA molecule, substitutions in the aniline ring are likely to influence the Raman spectra whereas the contribution of the substituents in benzylidene ring is expected to be restricted due to steric hindrance suffered by the benzylidene moiety. The molecule BPNA contains a nitro-group in the para-position of the aniline ring. Although the nitro group has a high value of polarizability, it does not conjugate much with the benzene ring and therefore may not be responsible for strong vibronic coupling.[3] However the conjugation extended may be strong enough so that the ν_{8a} and ν_{8b} vibrational modes can perturb the π-conjugative system of the molecule. As a result the bands corresponding to these modes may be intensity enhanced in the preresonance Raman spectra of BPNA [Figs. 6.3A,6.3B].

The experimental and calculated relative Raman intensities for the normal modes ν_{8a} and ν_{8b} of BPNA as a function of the exciting wavelengths have been presented in Table VI-1.

6.6.2 Excitation Profiles for p-Dimethylaminobenzylidene-p'-methoxyaniline (DABPMA)

The electronic absorption spectra of p-Dimethylaminobenzylidene-p'-methoxyaniline (DABPMA) shows the absorption maximum λ_{max} at 334 nm and arises mainly due to the C-T electronic transition [Fig. 6.2]. The preresonance Raman spectra of DABPMA are also dominated by the features in the 1550 - 1630 cm^{-1} region [Figs. 6.4A, 6.4B]. The variation in Raman intensity in the ν_{8a} and ν_{8b} modes as a function of exciting frequency in shown in Table VI-2. The intensities of both the Raman lines increase steadily as the exciting wavelength progressively approaches the absorption band (from 5145A° to 4579A°). It is apparent that the electron rearrangement caused by the dimethylamino group in the benzylidene ring has minor effect on the vibrational coupling schemes. Moreover, the extension of conjugation effect due to the dimethylamino group is likely to be limited because of steric hindrance suffered by the benzylidene ring. It is therefore probable that the conjugation due to methoxy group is only responsible for the perturbation of the π-electron system of the aniline moiety. It is also likely that the intensity enhancement for bands due to the modes ν_{8a} and

ν_{8b} is influenced by a supposedly active preresonance phenomenon involving the $n - \pi^*$ transition which, although a forbidden transition, may gain sufficient intensity due to intensity borrowing from the C-T/ $\pi - \pi^*$ electronic transition.

6.6.3 Excitation Profiles for p-Dimethylamino Benzylideneaniline (DABA)

The electronic absorption maximum, λ_{max} for p-Dimethylamino Benzylideneaniline (DABA) occurs at 336 nm [Fig. 6.2] and is expected mostly to be due to C-T electronic transition. The preresonance Raman spectra of DABA has been presented in Figs. 6.5A, 6.5B which reveals that unlike in other molecules (i.e. DABPMA, BPNA and BOHA), this molecule shows four Raman bands in the region 1550 - 1630 cm^{-1}. These bands occur at 1562 cm^{-1}, 1591 cm^{-1}, 1609 cm^{-1} and 1629 cm^{-1} and are attributed to ν_{8b}, ν_{8a}, ν_{8a} and $\nu_{C=N}$ modes of vibration respectively. Two ν_{8a} represent the two vibrations of two benzene rings. From the preresonance Raman spectra one can note that all the four bands show a more or less steady increase in intensity as the exciting wavelength gradually approaches the absorption maximum. Although the molecule DABA contains a strong electron-donating dimethylamino group in para-position of the benzylidene ring, due to steric hindrance, again, this group has little influence in perturbing the vibronic coupling scheme. The p-dimethylamino group in the benzylidene ring, therefore, has negligible contribution towards preresonance intensity enhancement [Table

VI-3]. On the other hand the portion of the molecule containing the aniline ring i.e. Ph-N=C, seems to play a leading role in affecting the preresonance Raman intensity to the bands corresponding to the vibrational modes ν_{8a}, ν_{8b} and $\nu_{C=N}$. The N=C site in this portion of the molecule may be regarded as an electron-accepting centre. Therefore it is likely to perturb the π-conjugative system of the aniline system which in turn influences the vibrational coupling scheme in the molecule.

6.6.4 Excitation Profiles for Benzylidene-O-hydroxyaniline (BOHA)

The electronic absorption spectra of Benzylidene-O-hydroxyaniline (BOHA) shows that the molecule absorbs at 340 nm [Fig. 6.2]. The C-T transition provides the major contribution to the electronic maximum. The preresonance Raman spectra of BOHA [Figs. 6.6A, 6.6B] shows that the intensity enhancement is maximum for three Raman bands at 1577 cm^{-1}, 1597 cm^{-1} and 1626 cm^{-1} which are attributed to [see Chap. 5] modes ν_{8b}, ν_{8a} and $\nu_{C=N}$ respectively. Since the molecules contains a hydroxyl group in the o-position the possibility of extending mesomeric effects and forming intramolecular hydrogen bond may exist, depending on the energetically favoured interaction. The formation of hydrogen bond in this system is expected to play a dominant role to bring about substantial perturbation to the π-electron system of the aniline moiety. The intensity factors are shown in Table VI-4.

6.7 Comparision of Experimental and Theoretical Intensity Variations

The experimentally measured and theoretically calculated variations of Raman intensities as a function of exciting wavelengths are presented in Table VI-1, VI-2, VI-3 and VI-4 respectively. The results show that in all the four cases, the intensity variation is better determined by the F_B^2-terms of Albrecht and Hutley's theory.[8] Although The intensity factors represented by F_B^2 terms are closer to those of the experimentally measured values as compared to the F_A^2 terms, the F_B^2 terms are deviated from the experimentally measured intensity factors. This discrepancy which arises due to damping phenomena may be taken care of by making use of the damping constant Γ. The absence of vibrational structure in the electronic absorption spectra and overtones in the Raman spectra restricted the experimental determination of the damping constant and thus restricted the application of damping corrections to the intensity factors for their closer approach to the observed values.

6.8 Conclusion

Raman intensity as a function of excitation wavelength (the excitation profiles) are presented for four aromatic Schiff bases. The profiles identify the electronic absorption bands

participating in vibronic coupling and have been used to test the theory of pre-resonance Raman effect. Due to the close relationship between the electronic absorption band and the excitation profile the electronic absorption spectra have been recorded and their interpretation has also been attempted. The chromophore responsible for the electronic transition is also related to the bands which show resonance enhancement when the wavelength of the exciting radiation approaches the electronic absorption band. What follows is the conclusion regarding these relationships in various Schiff bases having different substituent groups.

The electronic absorption spectra of the four aromatic Schiff bases show that all the four molecules investigated have two main absorption bands in the wavelength region 200 - 400 nm. The first absorption band observed in the lower wavelength region is assigned to the excitation of the π-electrons of the aromatic system ($\pi - \pi^*$ transition). It is also observed that the position of this band is not significantly shifted with changes in the nature of the substituents in the aniline ring. With no substituent group in the benzylidene ring and an electron-acceptor nitro-group in the para-position of the aniline ring, this absorption band is observed at 225 nm. When the $-NO_2$ group is replaced by an electron donor -OH group in the ortho-position, the transition is observed at 223 nm. Substituting the benzylidene ring at the para-position by electron donor $-N(Me)_2$

group and keeping the aniline ring as such, the band is observed at 256 nm. The electron-donor $-OCH_3$ group at the para-position does not shift the band position significantly and it is observed at 256 nm. These observations indicate that the electronic absorption band in the uv region i.e. 220 - 260 nm is arising due to the excitation of the π-electrons.

At longer wavelengths i.e. in the region 300 - 370 nm, three aromatic Schiff bases show a relatively intense absorption band with a weak feature appearing as a shoulder around 300 nm. The strong absorption band is likely to be due to the charge-transfer (C-T) transition which is similar to the one observed in nitroanilines and other related molecules. It is expected that the carbon atomic orbitals interact with the appropriate p components of nitrogen atomic orbitals (lone pair) and consequently lead to enhanced interaction between the π and the n-orbitals. Substituent groups of varying chemical characters placed at different sites reveal that the aniline moiety plays, more or less, the central role in determining the position of the strong electronic absorption band. With no substituent group in the benzylidene ring and an electron-donor hydroxyl group in the ortho-position of the aniline ring, the band is observed at 340 nm whereas substituting the aniline ring by the electron-accepting nitro-group, the C-T band shows a red-shift of 30 nm. These results indicate the sensitivity of the long wavelength absorption band towards the nature of the substituent groups (in

the aniline ring) which supports the assignment of this electronic absorption band to the C-T band.

The pre-resonance Raman spectra of the above mentioned substituted aromatic Schiff bases i.e. BPNA, BOHA, DABPMA and DABA indicate that the Raman bands corresponding to ν_{8a} and ν_{8b} vibrational modes show significant enhancement in intensity in comparison to other vibrations in the benzenoid moiety. Similar intensity enhancement is also observed in the Raman band due to $\nu_{C=N}$ mode. A comparative study of the observed variation of Raman intensity with those of the theoretically calculated values reveals that the symmetric vibrational modes ν_{8a}, ν_{8b} and $\nu_{C=N}$ gain intensity via the F_B^2-term of Albrecht and Hutley.[8] The mixing of the electronic states is via C-C stretching modes ν_{8a} and ν_{8b} of the aniline moiety and also the $\nu_{C=N}$ vibrational mode. The Raman bands due to all the three modes are enhanced in the pre-resonance region. Only those vibrations which couple the excited electronic states are intensity enhanced. The main electronic absorption band contributing to the intensity enhancement is the charge transfer band observed at higher wavelengths. The active electronic states for the Raman lines due to ν_{8a}, ν_{8b} and $\nu_{C=N}$ have been taken to be in the range 330 - 370 nm and also the one around 300 nm. The most important contribution comes from the C-T electronic transitions. These results show that the aromatic Schiff base molecules suffer relatively little displacement along the ν_{8a}, ν_{8b} and $\nu_{C=N}$

normal modes when the molecules are excited in the near uv region.

The source of pre-resonance Raman intensities for the $\nu_{8a'}$ ν_{8b} and $\nu_{C=N}$ modes in these molecules is the vibronic mixing of the excited states through these vibrational modes.

References

1. J. Behringer *in "Raman Spectroscopy, Theory and Practice"* H.A. Szymanski, Ed., vol. 1, Plenum Press, New York (1967).
2. K. Kumar and P.R. Carey *Can. J. Chem.* 55, 1444 (1977) and references therein.
3. K. Kumar and P.R. Carey *J. Chem. Phys.* 63, 3697 (1975) and references therein.
4. *"Electronic Absorption Spectra and Geometry of Organic Molecules"* H. Suzuki, Academic Press, New York (1967).
5. J. Tang and A.C. Albrecht *in "Raman Spectroscopy, Theory and Practice"* H.A. Szymanski, Ed., vol. 2, Plenum Press, New York (1970).
6. R.S. Cataliotti, S.M. Murgia, G. Paliani, A. Poletti and M.Z. Zgierski *J. Raman Spectrosc.* 16, 251 (1985) and references therein.
7. C. Kosmidis, A. Bolovinos and P. Tsekeris *J. Raman Spectrosc.* 21, 737 (1990) and references therein.
8. A.C. Albrecht and M.C. Hutley *J. Chem. Phys.* 55, 4438 (1971).
9. K. Kumar, D.J. Phelps and P.R. Carey *Can. J. Chem.* 56, 232 (1978) and references therein.

Table VI-1

Excitation Profiles for BPNA

λ_o(A) ν_o(kK)$_{vac}$	ν_{8a}			$\nu_{C=N}$		
	R_A	R_B	R_I	R_A	R_B	R_I
5145 (19.429)	0.5	0.5	0.6	0.5	0.5	0.4
4880 (20.486)	1.0	1.0	1.0	1.0	1.0	1.0
4765 (20.981)	1.5	1.4	1.2	1.5	1.4	1.1
4727 (21.149)	1.7	1.5	1.3	-	-	-
4579 (21.830)	3.1	2.5	1.9	3.1	2.5	1.4
4416 (22.642)	6.6	4.5	2.1	4.8	3.3	1.7

Table VI-2

Excitation Profiles for DABPMA

λ_o(A) ν_o(kK)$_{vac}$	ν_{8a}			ν_{8b}			$\nu_{C=N}$		
	R_A	R_B	R_I	R_A	R_B	R_I	R_A	R_B	R_I
4965 (20.135)	0.8	0.8	0.9	0.7	0.8	0.8	0.8	0.8	0.9
4880 (20.486)	1.0	1.0	1.0	1.0	1.0	1.0	1.0	1.0	1.0
4579 (21.830)	2.8	2.4	1.3	2.4	2.1	1.4	2.8	2.4	1.3
4416 (22.642)	5.5	4.4	1.5	4.2	2.2	1.5	5.5	4.4	1.5

Table VI-3

Excitation Profiles for DABA

λ_o(A) ν_o(kK)$_{vac}$	ν_{8a}			ν_{8b}			$\nu_{C=N}$		
	R_A	R_B	R_I	R_A	R_B	R_I	R_A	R_B	R_I
5145 (19.429)	0.5	0.6	0.7	0.5	0.5	-	0.5	0.6	0.9
4965 (20.135)	0.8	0.8	0.9	0.7	0.8	0.8	0.8	0.8	1.0
4880 (20.486)	1.0	1.0	1.0	1.0	1.0	1.0	1.0	1.0	1.0
4765 (20.981)	1.4	1.3	1.2	1.3	1.1	1.2	1.4	1.4	1.1
4727 (21.149)	1.6	1.5	1.4	1.5	1.5	1.3	-	-	-
4579 (21.830)	3.6	3.2	1.6	2.5	2.4	1.6	2.8	2.4	1.4
4416 (22.642)	5.3	4.3	2.3	4.5	4.3	2.7			

Table VI-4

Excitation Profiles for BOHA

λ_o(A) / ν_o(kK)$_{vac}$	ν_{8a}			ν_{8b}			$\nu_{C=N}$		
	R_A	R_B	R_I	R_A	R_B	R_I	R_A	R_B	R_I
5145 (19.429)	0.5	0.6	0.8	0.5	0.6	0.8	0.5	0.6	0.8
5017 (19.926)	0.7	0.7	0.9	0.7	0.7	0.9	0.7	0.7	0.9
4965 (20.135)	0.8	0.8	1.0	0.8	0.8	0.9	0.8	0.8	0.9
4880 (20.486)	1.0	1.0	1.0	1.0	1.0	1.0	1.0	1.0	1.0
4765 (20.981)	1.4	1.3	1.1	1.4	1.3	1.1	1.4	1.3	1.1
4727 (21.149)	1.6	1.5	1.1	1.6	1.4	1.2	1.6	1.5	1.1
4579 (21.830)	2.5	2.1	1.2	2.5	2.1	1.2	2.5	2.1	1.2

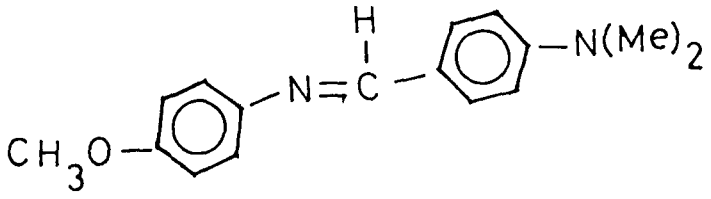

DABPMA

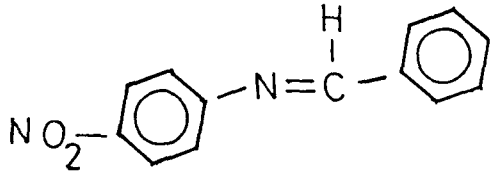

BPNA

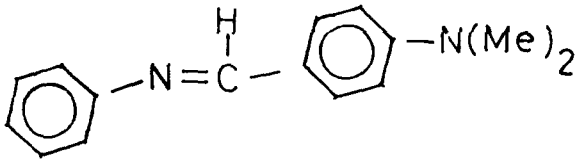

DABA

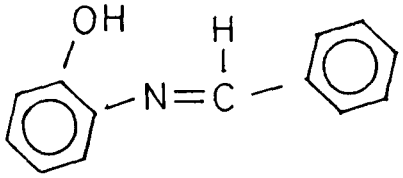

BOHA

Fig.6.1 Aromatic Schiff bases used in Raman studies.

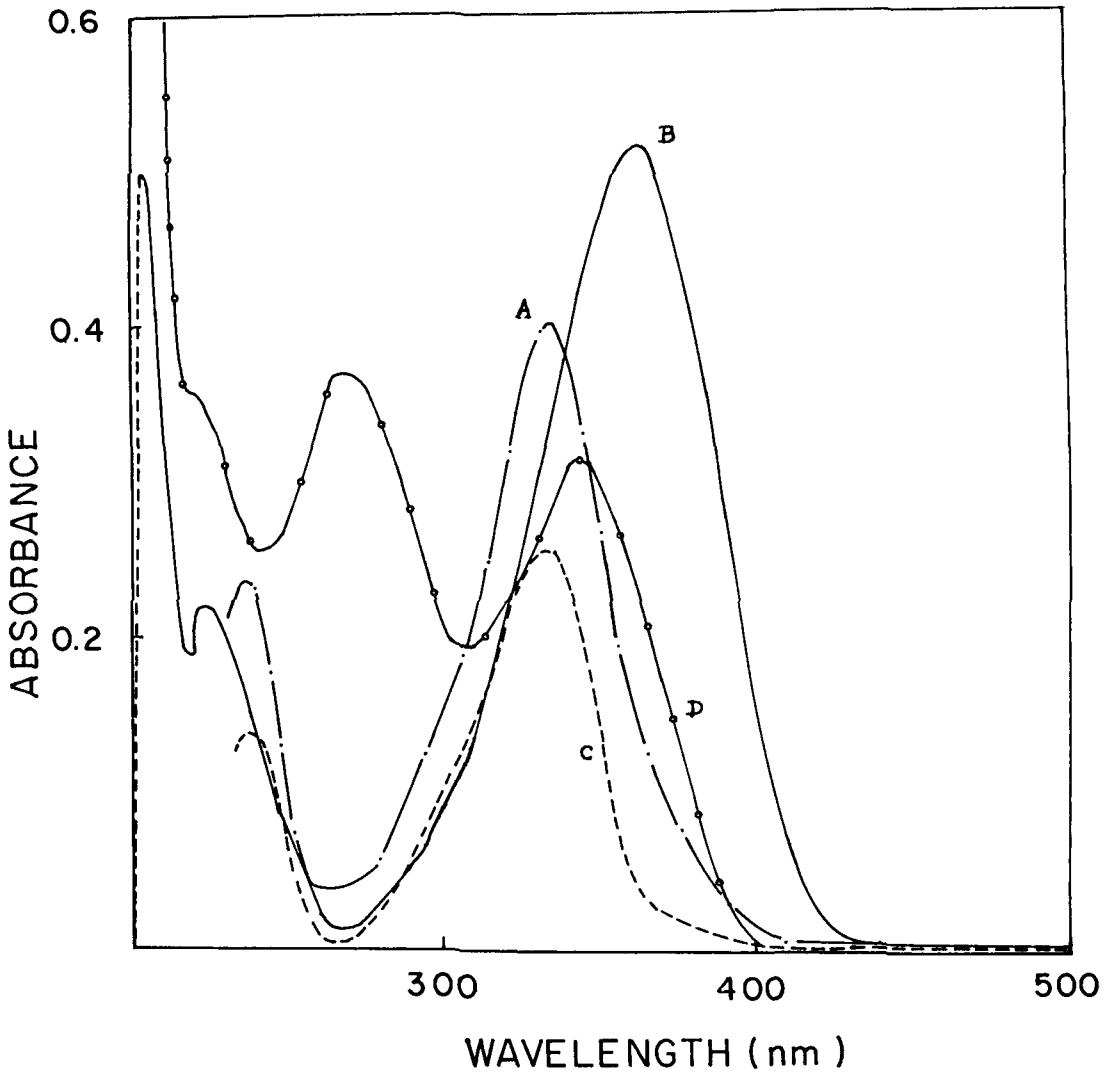

Fig.6.2 Electronic absorption spectra of aromatic Schiff bases

(A) DABPMA (B) BPNA (C) DABA (D) BOHA

conc. $\sim 10^{-4}$M

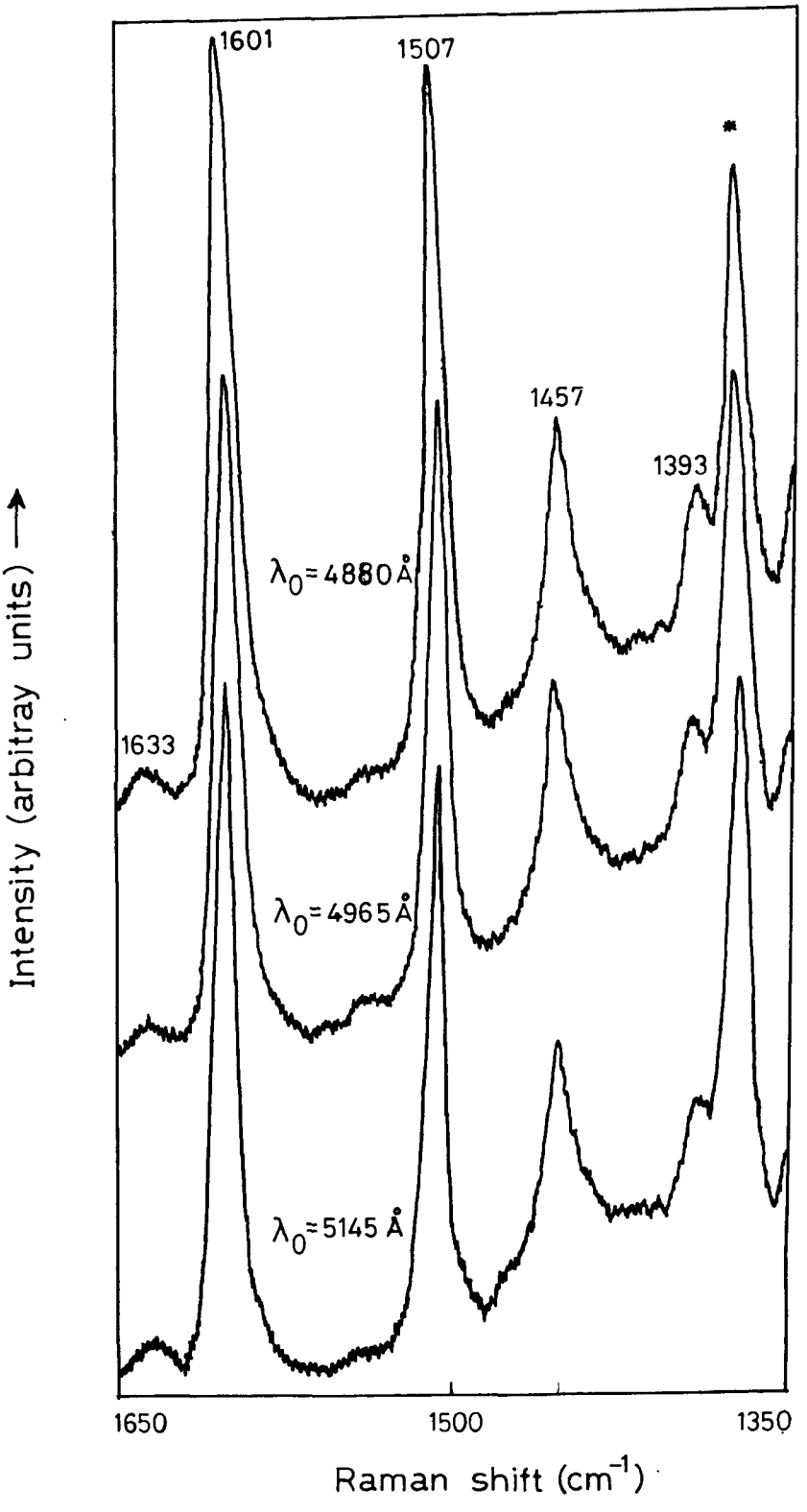

Fig.6.3(A) Pre-resonance Raman spectrum of BPNA in acetonitrite soln. conc. $\sim 10^{-4}$M

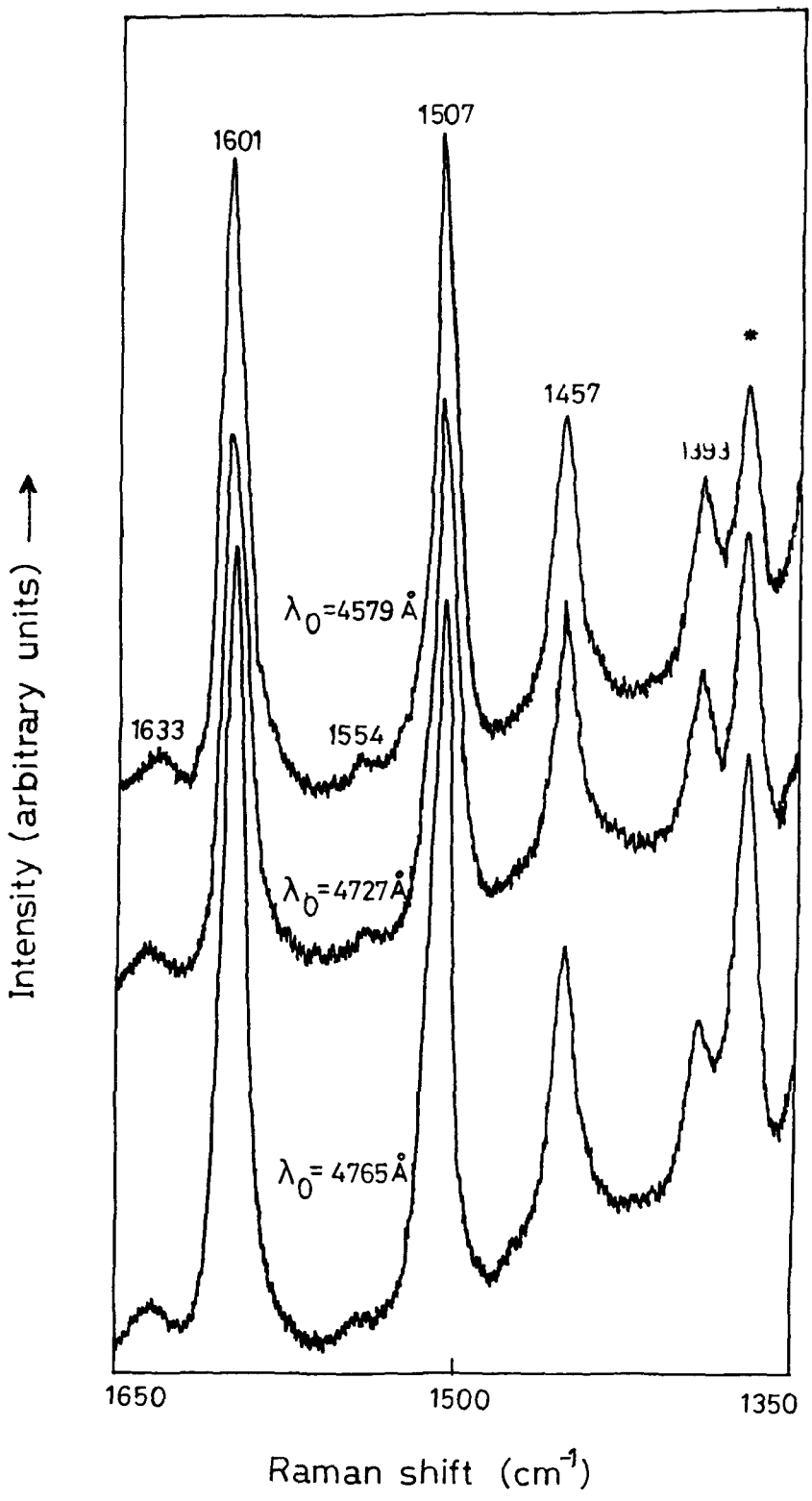

Fig.6.3(B) Pre-resonance Raman spectrum of BPNA in acetonitrite soln. conc.$\sim 10^{-4}$M

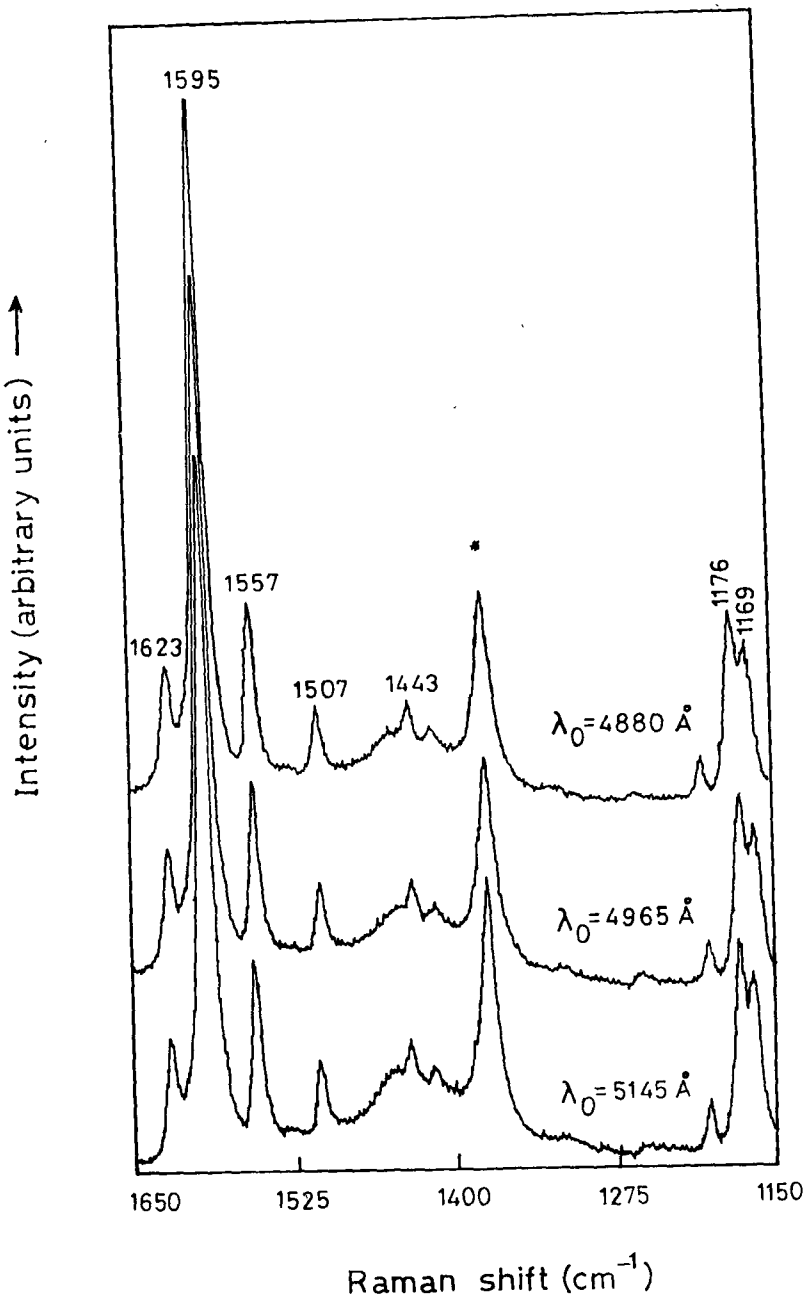

Fig.6.4(A) Pre-resonance Raman spectrum of DABPMA in acetonitrile soln. conc. $\sim 10^{-4}$M

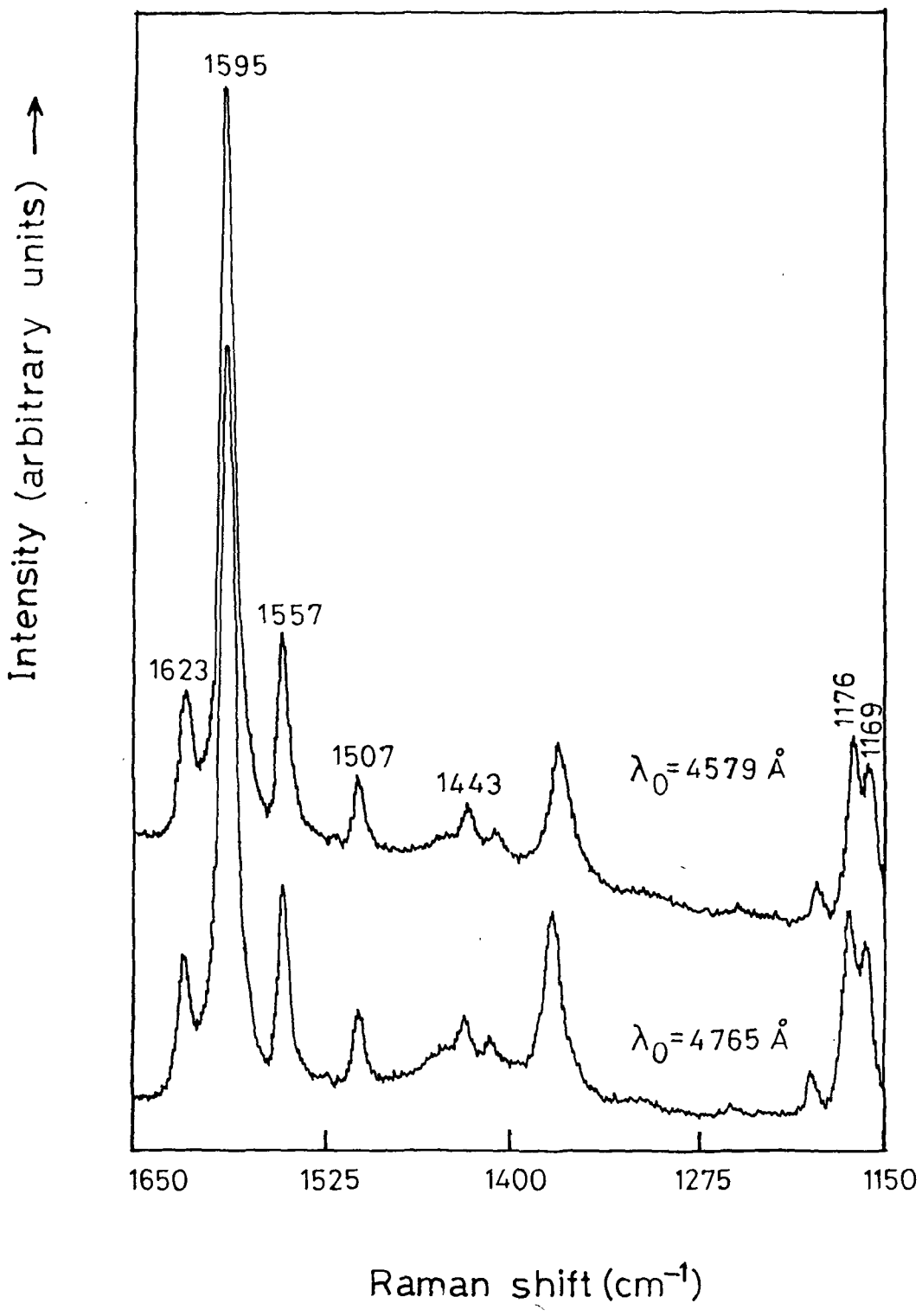

Fig.6.4(B) Pre-resonance Raman spectrum of DABPMA in acetonitrile soln. conc. $\sim$ 10^{-4}M

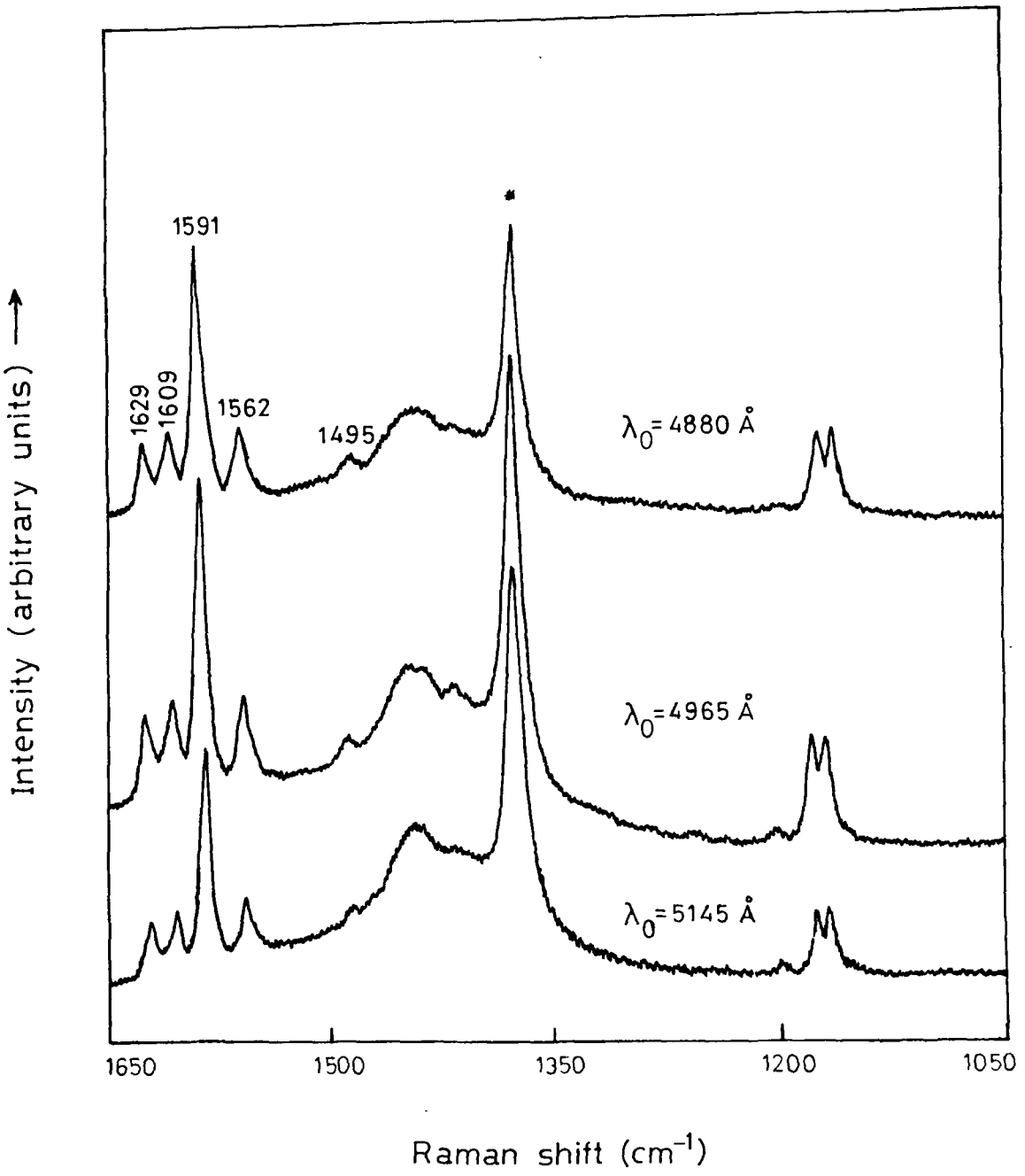

Fig.6.5(A) Pre-resonance Raman spectrum of DABA in acetonitrite soln. conc. $\sim$ 10^{-4}M

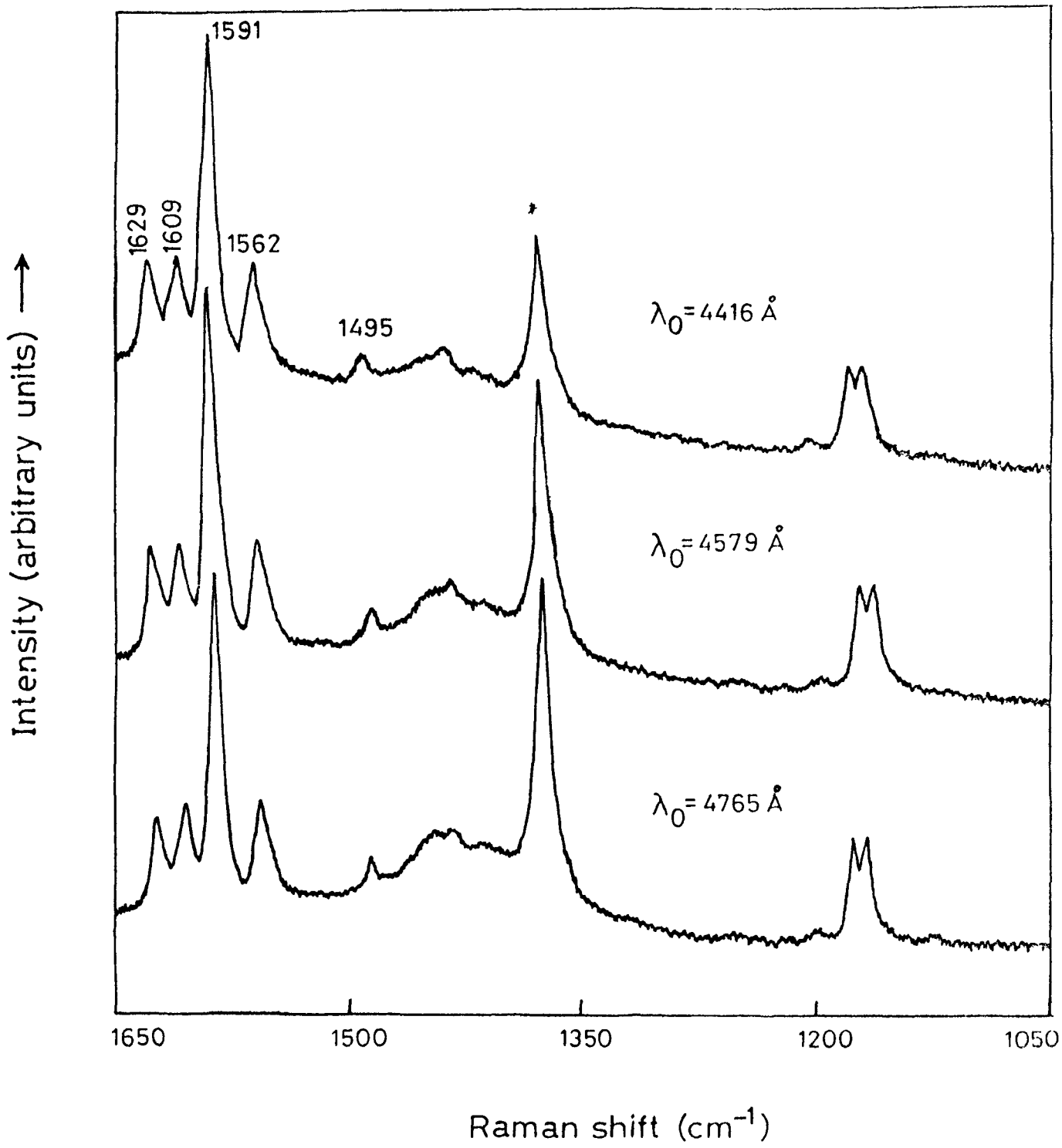

Fig.6.5(B) Pre-resonance Raman spectrum of DABA in acetonitrile soln. conc. $\sim 10^{-4}$M

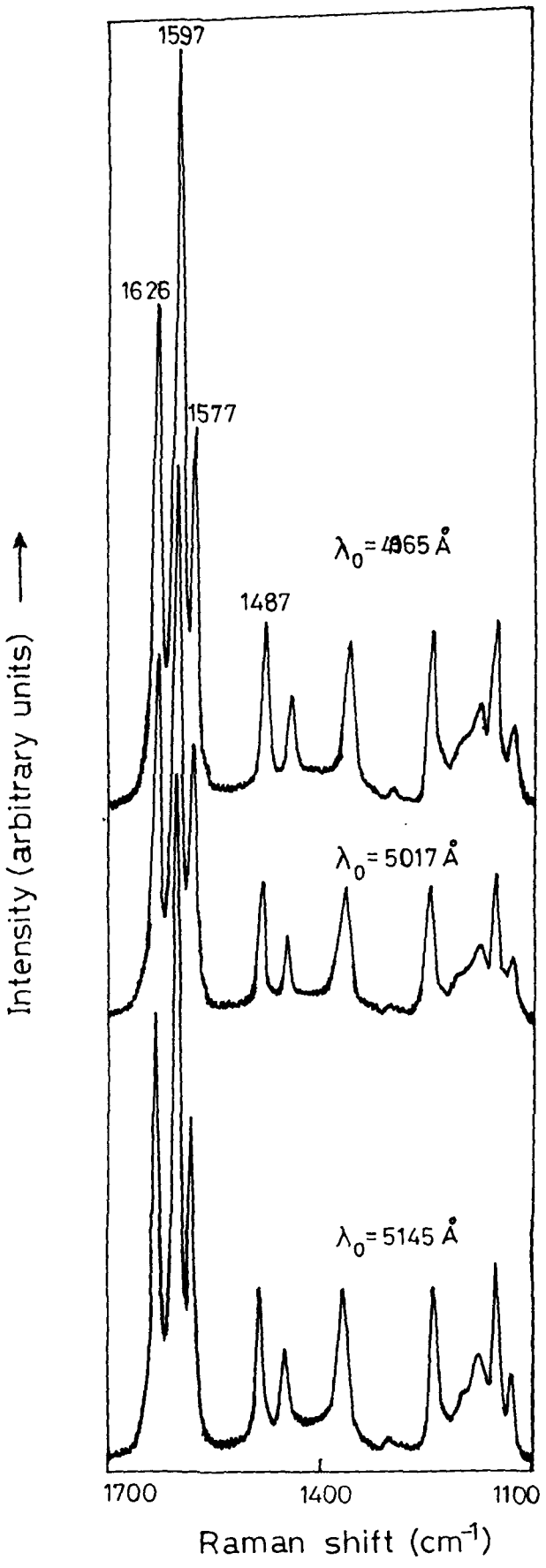

Fig.6.6(A) Pre-resonance Raman spectrum of BOHA in acetonitrile soln. conc. $\sim 10^{-4}$ M

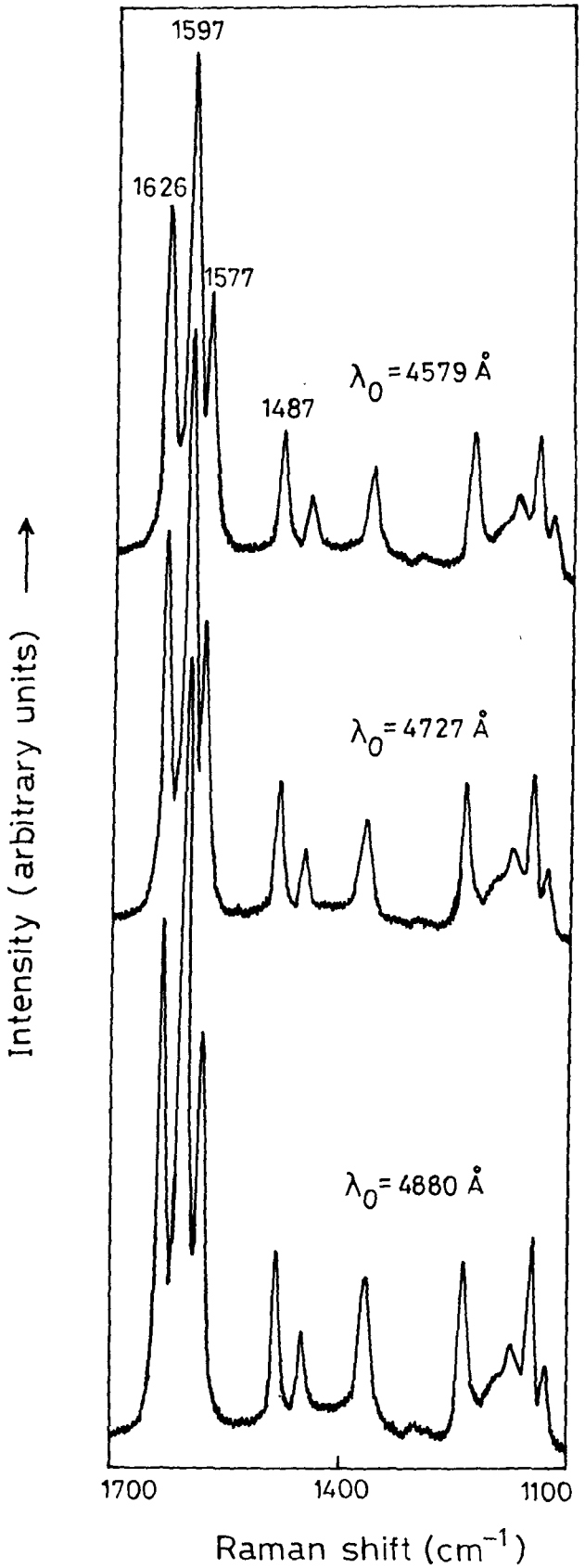

Fig.6.6(B) Pre-resonance Raman spectrum of BOHA in acetonitrile soln. conc. $\sim 10^{-4}$M

CHAPTER – VII

DIELECTRIC RELAXATION IN AROMATIC SCHIFF BASES DISPERSED IN IONIC MATRIX

ABSTRACT

The capacitance and dissipation factors of four aromatic Schiff bases dispersed in KBr matrix have been measured and interpreted in the frequency range 100 Hz to 100KHz. The results indicate that these systems exhibit dielectric relaxation below 5 KHz and the relaxation frequency depends on the chemical nature of the substituent groups. The dielectric dispersion in the observed frequency range is classified into two regions. The lower frequency region is dominated by the nomadic type of polarization arising due to the delocalization of the π-electrons. The dielectric dispersion in the higher frequency region is dominated mainly by the motion of the molecular fragments.

7.1 Introduction

The study of the dielectric and electronic properties of neutral molecules dispersed in a continuous medium is of immense significance in several fields of studies. Such studies are found to be of importance particularly in explaining the electronic properties and functions of biological systems and may help in the better understanding of the submolecular processes involved in cellular activity. Time-dependent polarization studies have been found to reveal significant features regarding dielectric relaxation and related phenomena in several biological samples.[1-3] Such studies have provided information for explaining steady-state conductivity and relaxation phenomena in polycrystalline biological samples. In order to get a deeper insight into the phenomena governing the steady-state electrical conductivity and dielectric relaxation processes in disordered solid systems, we considered it worthwhile to carry out a systematic investigation of the dielectric properties of some molecules of biological significance. We have studied the frequency-dependent dielectric behaviour of Schiff base molecules dispersed in ionic environment of the matrix of Potassium Bromide (KBr).

7.2 Sample Preparation and Dielectric Measurement

The purified powdered sample of KBr was dried in an oven at a constant temperature of 40°C for 24 hours. The four

Schiff bases PMBPNA, BPNA, DABPHA and BMHA [Fig. 7.1] were mixed separately with dry KBr in the ratio 1:10 (W/W) and were grinded to very fine powder. The uniformly mixed solid samples were then put into a cylindrical die where a high pressure of the magnitude 7 tons/cm^2 was applied using a hydraulic press. The pressure was released after about 3 minutes and the samples were collected in the form of pellets of radius 6.5 mm and approximately of 1 mm thickness. Similar pellets were also prepared for neat Schiff base samples. The pellets were preserved in a moisture-free dessicator.

The multifrequency LCR-meter, HP-4274A was used for the measurement of capacitance (C') and loss tangent (or dissipation factor) tanδ at ten discrete frequency value (100 Hz, 200 Hz, 400 Hz, 1 KHz, 2 KHz, 4 KHz, 10 KHz, 20 KHz, 40 KHz and 100 KHz). The measurements of capacitance were carried out in the series equivalent circuit mode of the instrument. The four terminal test fixture HP-16034B was used for all measurements. The measurements of capacitance and dissipation factors were carried out at least three times and showed good reproducibility. The maximum error limits in the measurement of capacitance and dissipation factor are $\pm$0.005 and $\pm$0.001 respectively.

7.3 Results and Discussion

The polarization requires finite times and as a result

energy losses do occur when the period of cycling approximates these time delays.

Considering the applied electric field E as

$$E = E_m \, Sin\omega t \qquad ....7.3.1$$

where E is the instantaneous value of the electric field at any instant of time, E_m is the amplitude and ω is the angular frequency of the alternating electric field. The charge density D, when there is no time delay, is given by

$$D = D_m \, Sin\omega t \qquad .... 7.3.2$$

and the situation can be depicted as shown in Fig. 7.2(A). With a lag in polarization with respect to the applied field, the charge density changes and may be expressed as follows[4]:

$$D = D_m \, Sin(\omega t - \delta) \qquad .... 7.3.3$$

where δ represents the loss angle. The corresponding hysterisis loop is shown in Fig. 7.2(B). In such a case, the maximum field and the maximum polarization are not coincident and a coercive field is required to return the polarization to zero.

The energy loss per cycle, ΔU, is represented by the

area of the hysterisis loop and is given as follows:

$$\Delta U = \pi E_m^2 \epsilon_o K \sin\delta \qquad \ldots\ldots 7.3.4$$

where K is the dielectric constant (relative permittivity). The power loss P_L is the rate of energy loss per unit volume and is given by[4]

$$P_L = \frac{\omega E^2 \epsilon_o}{2} (K \tan\delta) \qquad \ldots\ldots 7.3.5$$

where $\tan\delta$ is the dissipation factor or loss tangent and $K\tan\delta$ represents the loss factor. The dielectric constant may be written[4] in terms of the inphase component K' and the out-of-phase component K'' where

$$K = K' - iK''. \qquad \ldots\ldots 7.3.6$$

and $$\tan\delta = \frac{K''}{K'}$$

Both in high and low frequency limits the contribution due to the out-of-phase component K'' approaches negligible values. It is only near the resonant frequency i.e. when $\omega \sim \omega_o$ and $\omega\tau \rightarrow 1$, the out-of-phase component K'' and hence the dissipation factor $\tan\delta$ is at its maximum.[4] The maximum power losses, therefore take place near the

resonant frequency of the sample. The dielectric relaxation time in disordered solids where dipole-dipole interactions play role is given by[3]

$$\tau = \frac{3\epsilon_o(\epsilon_s - \epsilon_\infty)(2\epsilon_s + \epsilon_\infty)}{2\epsilon_s(\epsilon_\infty + 2)^2\sigma} \quad \ldots\ldots 7.3.7$$

where ϵ_s and ϵ_∞ denote the permittivities of the sample at low and high frequency of the applied electric field respectively and σ represents the macroscopic conductivity of the disordered solid.

The current density J for such samples[5,6] when subjected to an alternating electric field of angular frequency is given by

$$J = (\sigma + j\omega\epsilon_o\epsilon)E \quad \ldots\ldots 7.3.8$$

where E denotes the strength of the applied field. ϵ_o is the permittivity of free space. Using Eqn. (7.3.8), the complex macroscopic conductivity σ^* of the insulating dielectric medium can be written as:

$$\sigma^* = \sigma + j\omega\epsilon_o\epsilon \quad \ldots\ldots 7.3.9$$

Considering now, only the intrinsic quantities controlled by the dielectric medium, the complex permittivity ϵ^* can be defined as

$$\epsilon^* = \epsilon - \frac{j\sigma}{\omega\epsilon_o} \qquad \text{.... 7.3.10}$$

Eqns. (7.3.3) and (7.3.4) stresses the fact that the dielectric properties of the material are important at high frequencies whereas the conduction phenomena are dominant at low frequencies.

It has been found[7] that systems of neutral particles dispersed in electrolytes exhibit very large dielectric disperssions at frequencies of the order of 10 KHz and lower. Similar results have also been observed in several other systems in KCl solutions. For spherical particles of diameter of the order of 10^{-6} m, suspended in electrolytes, the relative permittivity of the system may exceed values greater than 10^4 at low frequencies (< 1 KHz). Such a large dielectric dispersion may be associated with the elecrical double layer surrounding the particles.[7]

The Schiff bases PMBPNA, BPNA, DABPHA and BMHA were dispersed in KBr matrix in solid phase at low concentration. The variation of capacitance (C') as a function of frequency was studied which represents dependence of the dielectric constant of the sample on frequency of the applied field '(Capacitance $C=\epsilon_o\epsilon A/d$ where ϵ is the dielectric constant, A is area and d is the thickness). The dielectric relaxations of these Schiff bases in KBr matrix exhibit difference in their behaviour. It is,

therefore, clear that the properties of the mixture are governed by the nature of the dopant materials.

The dielectric relaxation was not observed in the neat Schiff base molecules in the frequency range of 10^2 Hz - 10^5 Hz. However, when mixed with KBr at low concentration in solid phase, all the four Schiff bases show a decrease of the capacitance (C') as a function of the frequency of the electric field in the range 10^2 Hz - 10^5 Hz. The molecules BPNA, PMBPNA, and DABPHA show sharp fall of the capacitance whereas BMHA exhibits a broad pattern with the increasing frequency of the applied electric field.

The Schiff base molecule in such a mixture can be assumed to be dispersed in a random manner in the KBr matrix. The molecules under consideration are a sort of entity consisting of a fairly rigid part, the core structure and flexible parts consisting of the substituents. The entire molecule may be free to rotate about some axis which may not be along the most obvious line unless due regard is paid to the precise stereochemistry of the molecule. Moreover, molecular fragments may be rotating and even bending in relation to other sections of the molecule. Superimposed on these effects, we have the electronic interactions which may occur within the molecule and which may affect or be affected by the constrained motions. The molecular shape is also of importance in relation to other parameters and

factors in systems containing fragments capable of rotation. The ability of a molecule to reorient in a solid depends very much on its shape and on the strength of the interaction with its environment. Less symmetrical molecules change their directions relatively slowly from one stable orientation to another. Since the motions are accompanied by more rigid barriers in solid phase, the relaxation times are usually much larger in solids than in liquids.

The plots of capacitance (C') against logarithmic frequency for BPNA, PMBPNA and DABPHA in KBr matrix are shown in Figs. 7.3-7.5 which have more or less similar patterns showing sharp fall of capacitance with frequency. The other molecule BMHA, however, shows a broad feature [Fig. 7.6]. The relaxation frequencies of DABPHA and BMHA in KBr are observed in KHz range (<5 KHz). The other two molecules BPNA and PMBPNA, however, exhibit the relaxation phenomena at still lower frequency ($\sim$ 100 Hz). The maxima of tanδ in DABPHA, BMHA, BPNA and PMBPNA are around 1 KHz, 4 KHz, 0.2 KHz and 0.1 KHz respectively [Figs. 7.7-7.10].

While studying the behaviour of a lossy dielectric it proves expedient to replace the dielectric in question by a capacitance and an active resistance in parallel or in series (or by a more intricate combination of dielectrics and resistances). In case of the parallel equivalent circuit

consisting of resistance R_p and capacitance C_p, the dissipation factor tanδ is given by[6]

$$\tan\delta = \frac{1}{\omega C_p R_p} \qquad \text{.... 7.3.11}$$

where ω is the angular requency of the electric field. For the series equivalent circuit with resistance R_s and capacitance C_s, the dissipation factor is given as:

$$\tan\delta = \omega C_s R_s \qquad \text{.... 7.3.12}$$

The value of tanδ, however, does not depend on the selected equivalent diagram. The relations between C_p and C_s and also R_p and R_s when changing from a parallel model of a dielectric to a series one and vice versa are found by equating Eqns. 7.3.11 and 7.3.12 which yields

$$C_s = C_p(1 + \tan^2\delta)$$

$$R_s = \frac{R_p}{1 + (1/\tan^2\delta)} \qquad \text{7.3.13}$$

When the loss angle is small, one may write $C_s \approx C_p$. and $R_s \simeq R_p \tan^2\delta$.

If the loss angle is large, the capacitance (and therefore

permittivity if calculated from capacitance) becomes an indefinite quantity which depends on the selection of the model of a lossy dielectric and in such a case

$$C_s > C_p.$$

and $$R_s < R_p.$$

The dielectrics in which losses are due to electrical conduction only, the loss may be expressed as:

$$P = \frac{V^2}{R} \qquad \text{.... 7.3.14}$$

where V is the voltage in volts and R is the resistance of the conductor in ohms (the phenomenon such as skin effect and proximity effect are disregarded here). The dependence of tanδ in such cases is given by[6]

$$\tan\delta = \frac{1.8 \times 10^{10}}{\nu\,(\epsilon\rho)} \qquad \text{.... 7.3.15}$$

where ν is the frequency of the electric field, ϵ is the permittivity and ρ is the volume resistivity of the dispersed medium. For any number of components, the product of permittivity and volume resistivity is given by[6]

$$\epsilon_i \rho_i = \text{Constant} \qquad \ldots\ldots 7.3.16$$

Eqn. 7.3.15 Eqn. 7.3.16, essentially lead to the fact that for losses governed by the electrical conduction phenomena the value of tanδ is inversely proportional to frequency.

Figs. 7.11-7.14 show the variation of the dissipation factor (tanδ) as a function of reciprocal of the frequency ($\bar{\nu}^1$) of the electric field. It is evident from these plots that in the low frequency region the dissipation factor shows a linear variation with frequency whereas a non-linear behaviour of the same is observed in the higher frequency region. These regions may be called region I and region II. The extent of these regions, however, appears to depend on the chemical structures of the molecules and their interactions with the environment. The boundries of the region I to II in case of DABPHA and BMHA are observed at 1 KHz, 4 KHz respectively. A close examination of these Figures reveals that both nomadic type of polarization as well as relaxation due to intramolecular phenomena involving the molecular fragments may be of significance in determining the dielectric losses in these systems. It is probable that the nomadic type of polarization[7-11] provides the major contribution towards dielectric losses in region I. The relaxation processes involving molecular fragments and induced dipoles, on the other hand, seem to play role in the non-linear behaviour of region II. The linearity in region I [Figs. 7.11-7.14] indicates that the

lower frequency region is mainly influenced by the conduction phenomena. The electrical conduction is expected to be due to electronic conduction via delocalized electronic states. If the localized electronic states are involved in such a process, the electron transport takes place by a series of tunneling or hopping process. The time taken by the electron to traverse the path between two sites is much less than the time spent immobilized at those sites. The process of electron delocalization, on the other hand, involves an electron being excited into a band of energy levels extending over many atoms in the material. The electron in such a case is envisaged to travel in the form of a wave rather than a discrete classical particle.[7] The calculations for the energy band structures[5] of an infinite conjugated π-electron system of the form

.... -C=C-C=C-C=C- ....

yields two π-electron energy bands of the form

$$E_1(k) = \alpha + 2\beta\cos(ka/2)$$

and $$E_2(k) = \alpha - 2\beta\cos(ka/2)$$

where k and a denote the wavevector and the length of the lattice vector respectively and α and β denote the Coulomb and resonance integrals respectively. $E_1(k)$ and $E_2(k)$ represent the electron occupied band energy and the empty site band energy respectively as shown in Fig. 7.15. The conjugated π-electron chain, therefore, has metallic-like properties in the sense that the π-

electrons are able to occupy empty states enabling them to conduct along the chain. This fact is also in consistency with the chemist's concept of 'resonant' conjugated structures that result from circulating π-electron currents. The process of charge transport through π-electron delocalization in the conjugated systems of Schiff bases may extend to long distances along the molecular axis. In this process, of charge transport, the charge may traverse a distance equivalent to several molecular fragments. Such a phenomenon of intramolecular charge-transport may lead to the nomadic type of polarization.[7-11] When the frequency of the applied electric field exceeds a certain value depending upon molecular structure such that the time allowed is not sufficient for the charge to transport along the molecular axis, the nomadic polarization can not respond to the applied field. The point T represents this particular situation in Figs. 7.11-7.14. The point T, as such, marks the boundary of region I.

Intramolecular processes involving molecular fragments, leading to molecular deformation may be responsible for the dielectric losses and the dielectric dispersion observed in region II. The presence of a strong ionic environment is expected to play a significant role in modifying such processes. The K^+ and Br^- ions may be randomly distributed around the Schiff base molecules, therefore, there will be a strong change in the environment of the molecules. The applied alternating electric

field may, therefore, suffer a spatial non-uniformity in and around the Schiff base molecules. The neutral Schiff base molecules, can therefore be thought of as being polarized by the presence of the non-uniform external electric field. Because of the spatial non-uniformity of the electric field around the molecule, the local field changes, both in magnitude and direction as it spreads and crosses a particular site of the molecule. As a result, the non-uniform field produces unequal forces on the two effective charges in that particular site of the molecule which, in turn, may give rise to a net force acting on a fragment of the molecule and the molecular fragments, as such, may be pushed into the region of stronger field. These processes, therefore are likely to generate an electrostatic strain in sensitive molecular fragments. The motion of these molecular fragments with respect to the applied field may be of considerable significance in governing the dielectric losses in region II. The intramolecular phenomena leading to dielectric dispersion are expected to be markedly influenced by the conjugation effects due to the substituent groups. The substituent groups which can conjugate with the phenylene ring can enhance the anisotropy of the polarizability and thereby can influence the motion of molecular fragments. The effect of the substituent groups on the redistribution of π-electrons in aromatic molecules can be described in terms of the inductive and mesomeric properties of the substituent groups. Separation of these two effects, however, is not always possible nor meaningful

and, as such, these effects refer simply to the perturbation caused to the π-electrons as distinct from the σ-electrons. The observed dielectric dispersion in the four Schiff bases studied, seems to be influenced by the perturbation caused to the π-electron systems due to the substituent groups, The three samples BPNA, PMBPNA and DABPHA are observed to have a relatively sharp fall of capacitance as a function of frequency whereas the fourth one i.e. BMHA shows a broad frequency response. The molecules BPNA and PMBPNA contain nitro-group substituted in the para-position in the aniline ring. The nitro-group attached to the benzenoid ring is strongly electron-withdrawing and has a high tendency to polarize. The electron-donor methoxy group substituted in the para-position in PMBPNA can also bring about significant anisotropy of polarizability. The Schiff base DABPHA contains the highly electron-donor substituent - the dimethylamino group in the para-position and is expected to be conjugated to the benzene ring system. The other molecule - BMHA contains a hydroxyl group in the meta-position and is supposed to perturb the π-distribution to a lesser extent. The probability of hydroxyl forming a conjugated system with the benzene ring is the least in this molecule as compared to other molecules under study. Fig. 7.6 shows that the dielectric dispersion of BMHA is broader than that in other molecular systems. The dielectric dispersion of the molecules BPNA, PMBPNA, DABPHA and BMHA in KBr matrix in region II therefore seems to be governed mainly by the intramolecular phenomena, which may be also influenced by the

conjugation effects due to the substituent groups. The conjugative property and chemical nature of the substituents may, therefore, markedly modify the processes governing the dielectric dispersion in these molecular systems.

7.4 *Conclusion*

The four aromatic Schiff bases BPNA, DABPHA, BMHA and PMBPNA dispersed in KBr matrix are found to exhibit dielectric relaxation below 5 KHz. The relaxation frequencies in these systems depend upon the chemical nature of the substituent groups. The chemical nature of the substituent groups in the aniline ring plays important role in governing the relaxation frequency in these systems.

So far as the variation of the dissipation factor (tanδ) against the reciprocal of the frequency (ν^{-1}) of the applied electric field is concerned all the molecules show more or less similar pattern . It is therefore inferred that in region I the conduction phenomenon plays the major role where the delocalisation of the π-electrons of the aromatic systems is responsible for the conductive behaviour in the lower frequency range (region I). Therefore, nomadic type of electronic polarization in this range seems to be dominant.

The frequency range characterized by the nomadic type of polarization also depends upon the substituents in the aniline ring. In this type of polarization, motion of charges due to the applied external field is relatively extensive. It is due to the response of highly delocalized electrons moving on long molecular domains. The frequency-region charaterized by the nomadic polarization in the molecules DABPHA and BMHA is observed around 1 KHz and 4 KHz respectively whereas in BPNA and PMBPNA the same is observed around 0.2 KHz and 0.1 KHz respectively.

In higher frequency region (Region II in Fig. 7.11-7.14) where the nomadic polarization ceases to respond to the applied electric field, a number of physical phenomena may contribute towards the dielectric properties of these materials. The intramolecular processes involving molecular fragments and induced dipoles seem to have major contribution towards dielectric behaviour in region II.

References

1. P. Carnochan and R. Pethig *J. Chem. Soc. Faraday Trans. 1* 72, 2355 (1976).
2. S. Bone and R. Pethig *J. Chem. Soc. Faraday Trans. 1* 74, 720 (1978).
3. S. Bone, J. Eden, P.R.C. Gascoyne and R. Pethig *J. Chem. Soc. Faraday Trans. 1* 77, 1729 (1981). and references therein.
4. "*Material Science for Engineers*" L.H. Van Vlack p. 262 Addison-Wesley Reading Massachusetts (1982).
5. "*Dielectric and Electronic Properties of Biological Materials*" R. Pethig p. 161, 259 John-Wiley and Sons, Chichester (1979).
6. "*Physics of Dielectric Materials*" B. Tareev p. 144, Mir Publishers, Mascow (1979).
7. H.A. Pohl and J.K. Pollock in "*Modern Bioelectrochemistry*" Eds. F. Gutmann and H. Keyzer p. 347 Plenum Press, New York (1986).
8. R. Rosen and H.A. Pohl *J. Polym. Sci.* Part A4, 1135 (1966).
9. J.R. Wyhof and H.A. Pohl *J. Non Dryst. Solids* 11, 137 (1972).
10. H.A. Pohl *J. Biol. Phys.* 2, 113 (1974).
11. H.A. Pohl and M. Pollock *J. Chem. Phys.* 66, 4031 (1977).

Table VII - 1

Variation of capacitance (C') and dissipation factor (tanò) of BPNA in KBr matrix with frequency.

Frequency (Hz)	Capacitance C' (pF)	Dissipation Factor tanò
1×10^2	247.3	8.00
2×10^2	146.7	8.50
4×10^2	75.0	7.50
1×10^3	19.0	5.10
2×10^3	6.8	3.14
4×10^3	2.5	2.02
1×10^4	0.9	1.12
2×10^4	0.6	0.72
4×10^4	0.4	0.48
1×10^5	0.3	0.34

Table VII - 2

Variation of capacitance (C') and dissipation factor (tanò) of PMBPNA in KBr matrix with frequency.

Frequency (Hz)	Capacitance C' (pF)	Dissipation Factor tanò
1×10^2	45.0	3.8
2×10^2	20.3	3.2
4×10^2	8.2	2.1
1×10^3	3.1	1.3
2×10^3	2.1	1.1
4×10^3	1.5	1.1
1×10^4	0.9	1.1
2×10^4	0.5	0.9
4×10^4	0.3	0.6
1×10^5	0.2	0.4

Table VII - 3

Variation of capacitance (C') and dissipation factor (tanδ) of DABPHA in KBr matrix with frequency.

Frequency (Hz)	Capacitance C' (pF)	Dissipation Factor tanδ
1×10^2	1449.1	6.2
2×10^2	765.0	6.7
4×10^2	448.8	7.6
1×10^3	196.3	8.0
2×10^3	91.3	7.1
4×10^3	36.1	5.4
1×10^4	9.2	3.0
2×10^4	3.8	1.9
4×10^4	2.0	1.4
1×10^5	1.1	1.2

Table VII - 4

Variation of capacitance (C') and dissipation factor (tanδ) of BMHA in KBr matrix with frequency.

Frequency (Hz)	Capacitance C' (pF)	Dissipation Factor tanδ
1×10^2	2.30	0.27
2×10^2	2.10	0.24
4×10^2	1.97	0.33
1×10^3	1.68	0.48
2×10^3	1.37	0.58
4×10^3	1.07	0.61
1×10^4	0.74	0.55
2×10^4	0.57	0.47
4×10^4	0.45	0.36
1×10^5	0.37	0.22

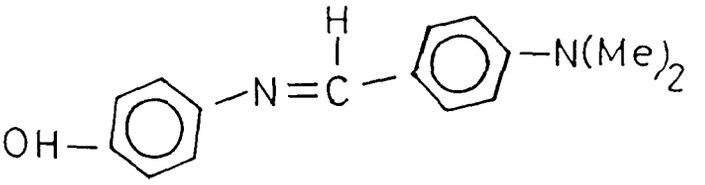

DABPHA

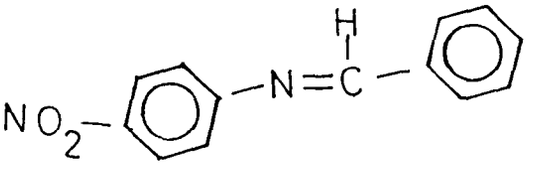

BPNA

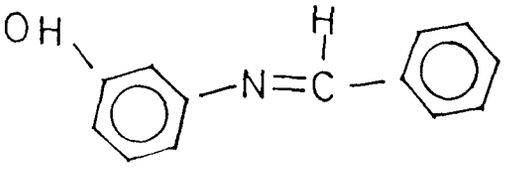

BMHA

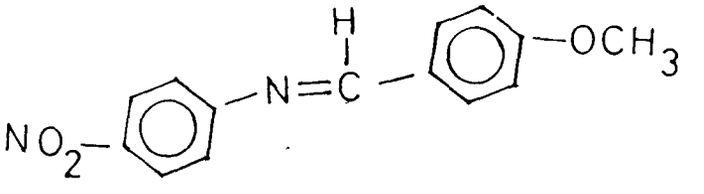

PMBPNA

Fig.7.1 Aromatic Schiff bases used in dielectric studies.

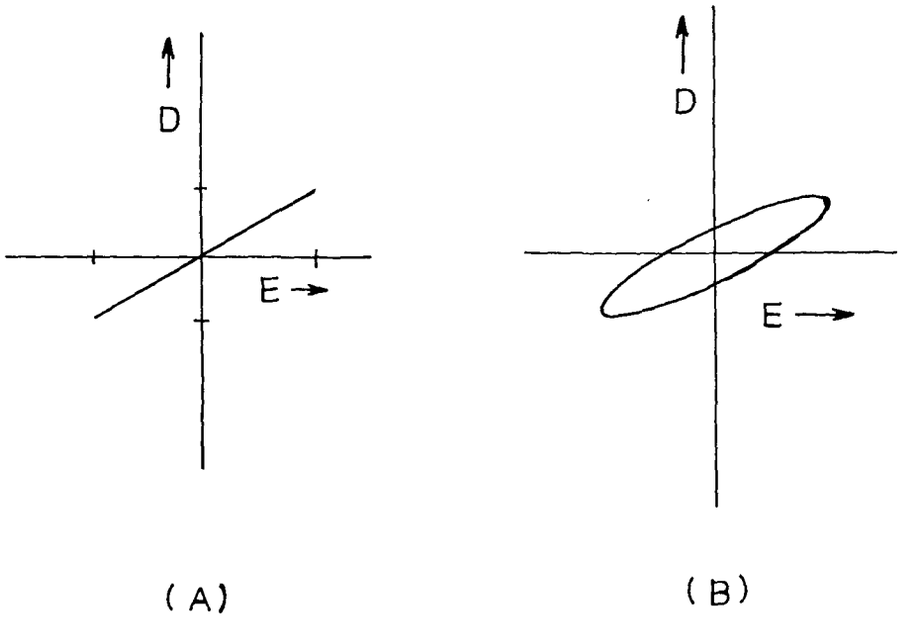

Fig.7.2 E-D cycle. E and D represent the electric field and the charge density respectively
(A) Loss-free (B) High-loss

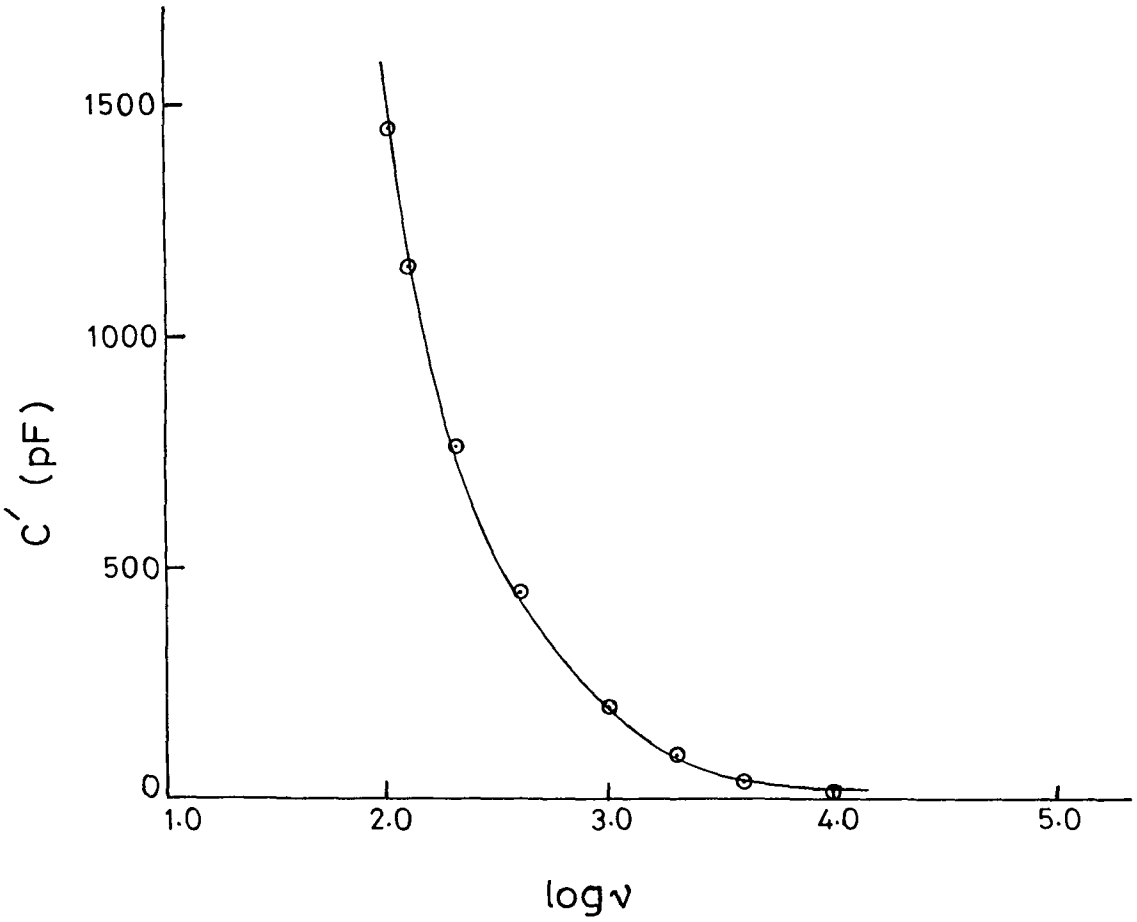

Fig.7.3 Variation of C′ as a function of log ν in DABPHA

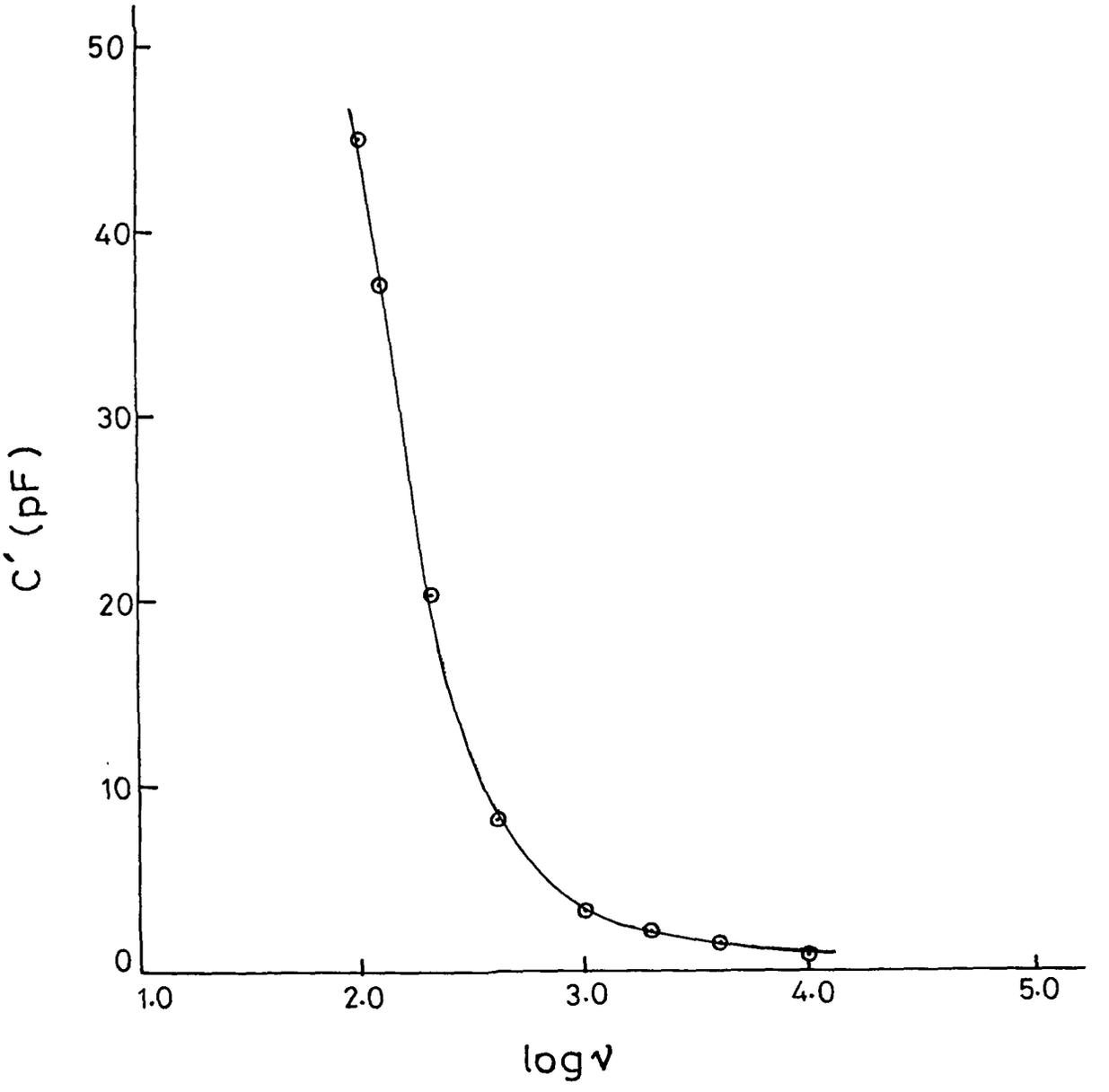

Fig.7.4 Variation of C' as a function of log ν in PMBPNA

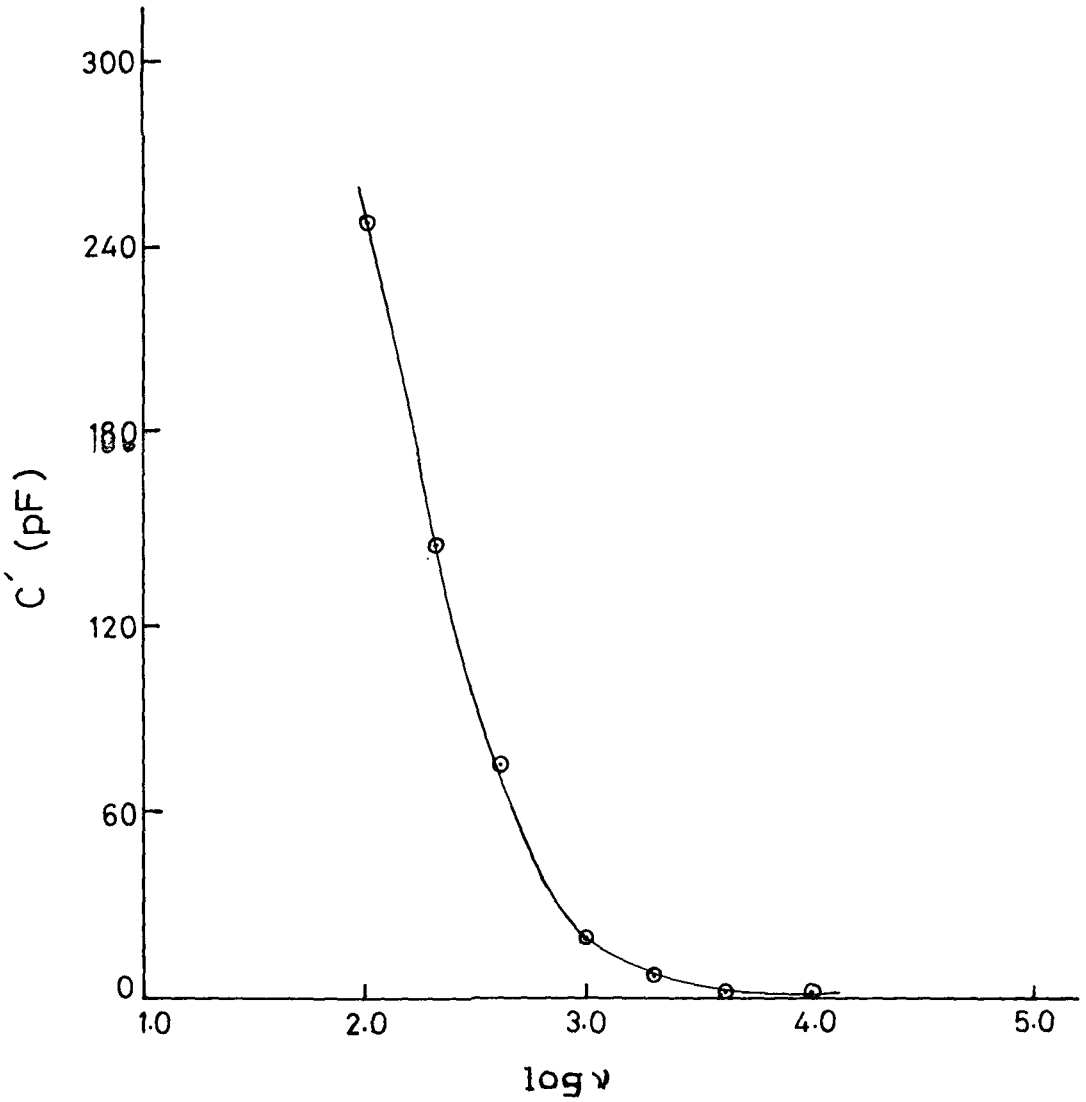

Fig.7.5 Variation of C′ as a function of log ν in BPNA

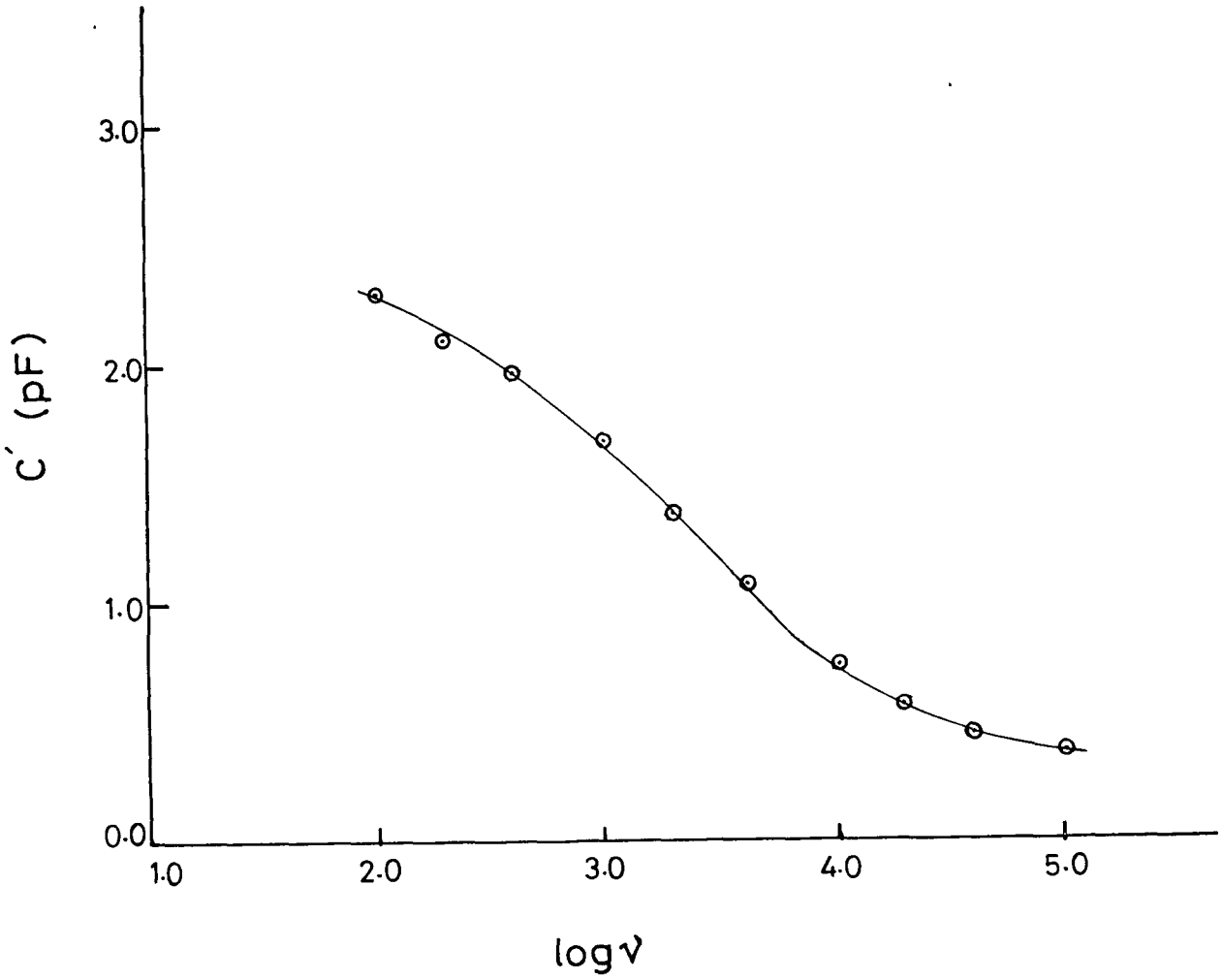

Fig.7.6 Variation of C´ as a function of log ν in BMHA

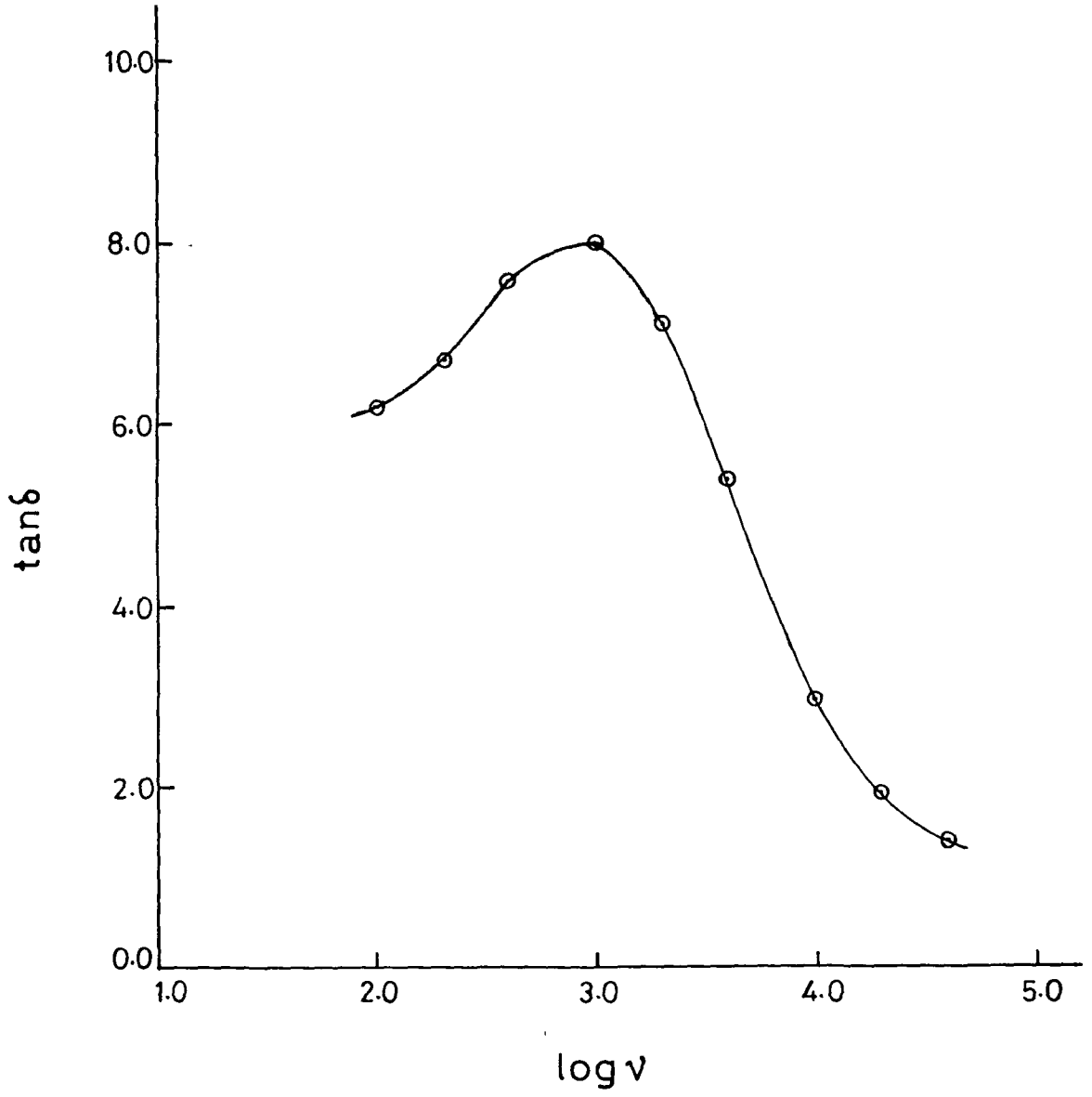

Fig.7.7 Variation of tan δ as a function of log ν in DABPHA

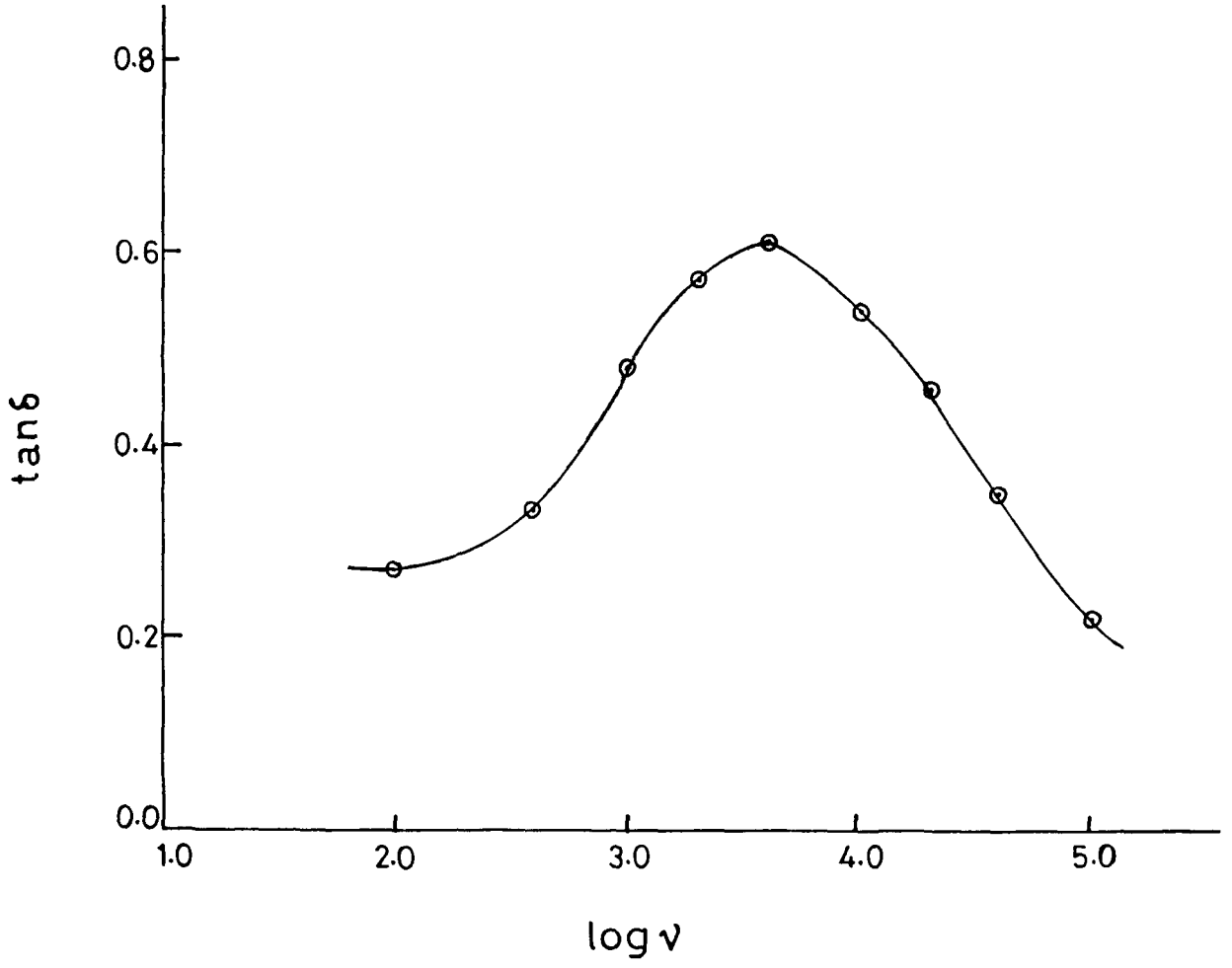

Fig.7.8 Variation of tan δ as a function of log ν in BMHA

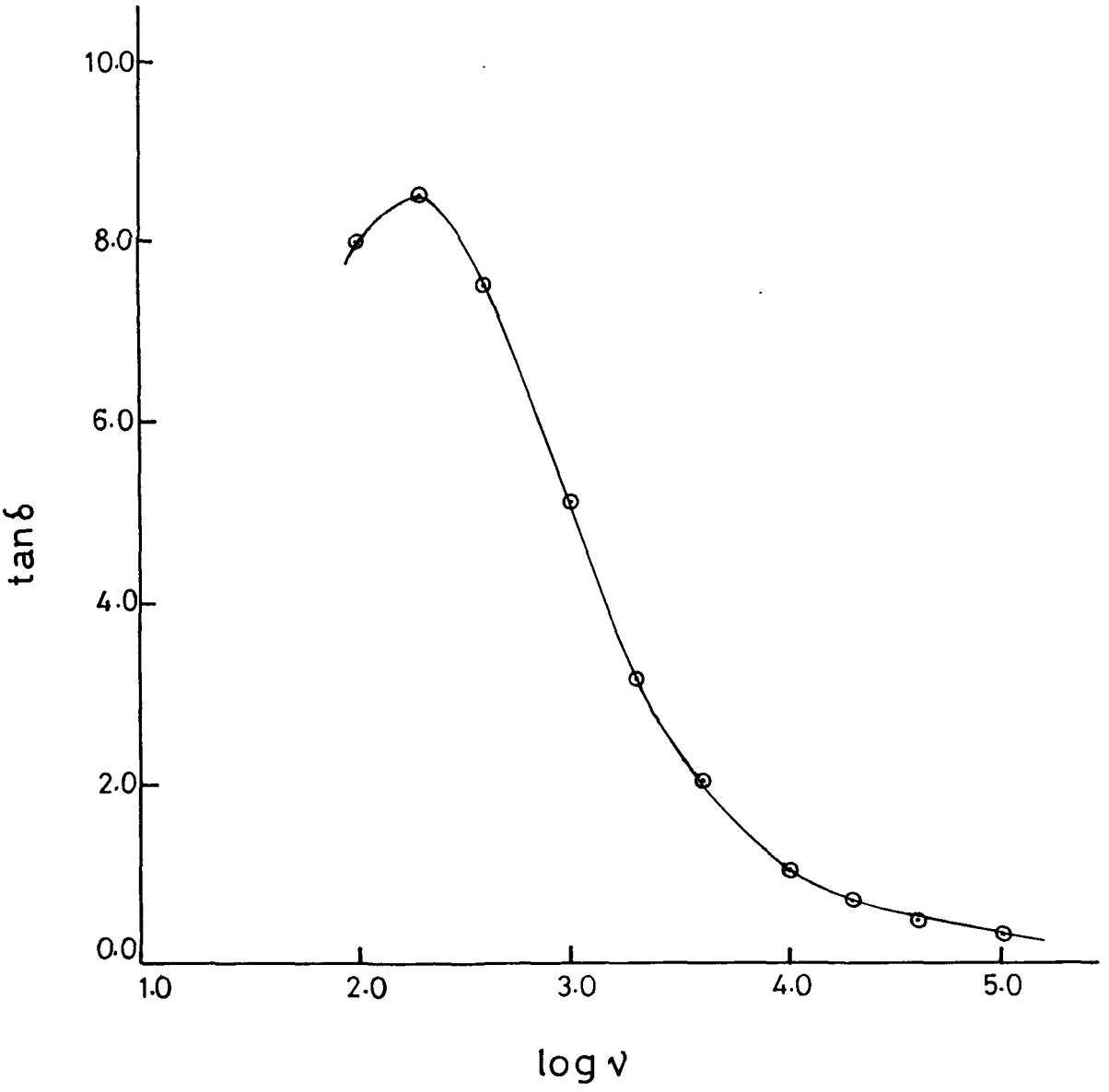

Fig.7.9 Variation of tan δ as a function of log ν in BPNA

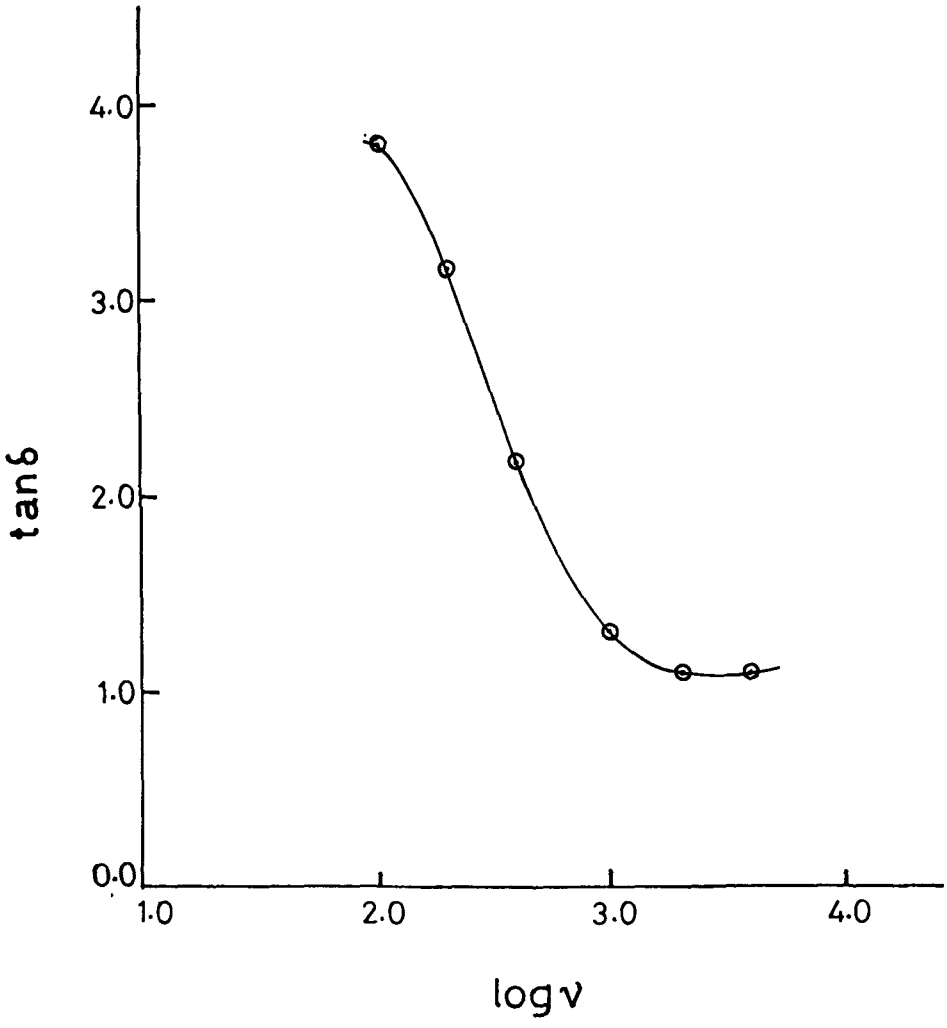

Fig.7.10 Variation of tan δ as a function of log ν in PMBPNA

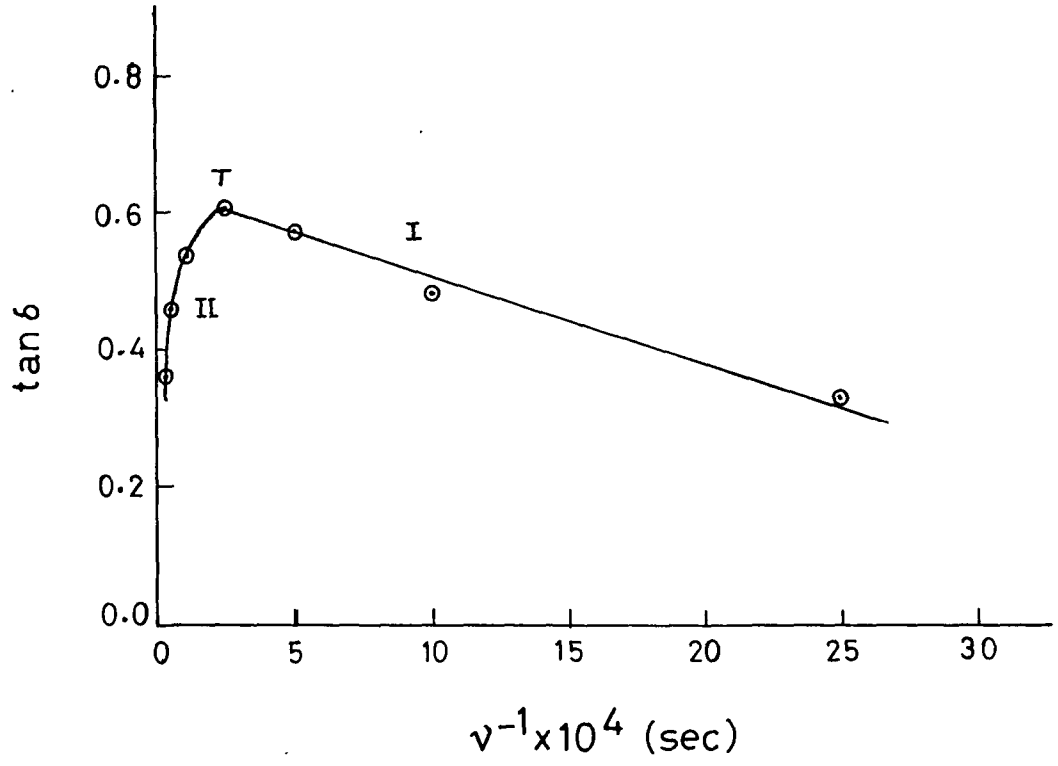

Fig.7.11 Variation of tan δ as a function of ν^{-1} in BMHA

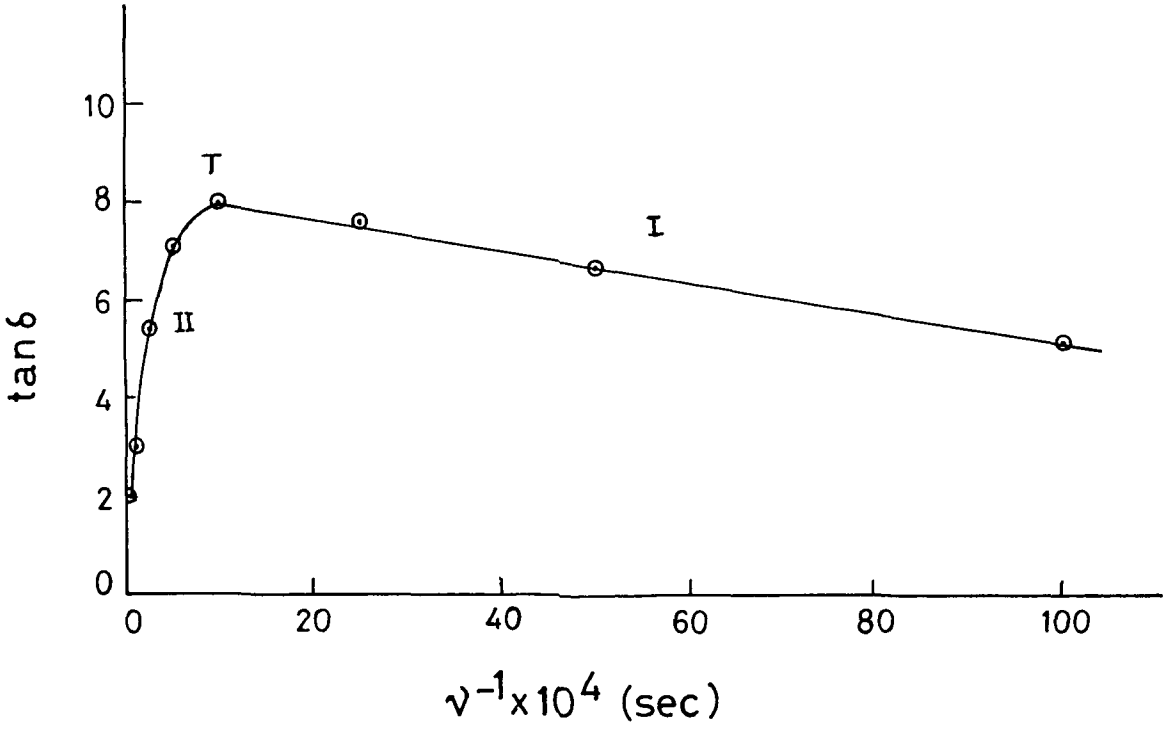

Fig.7.12 Variation of tan δ as a function of ν^{-1} in DABPHA

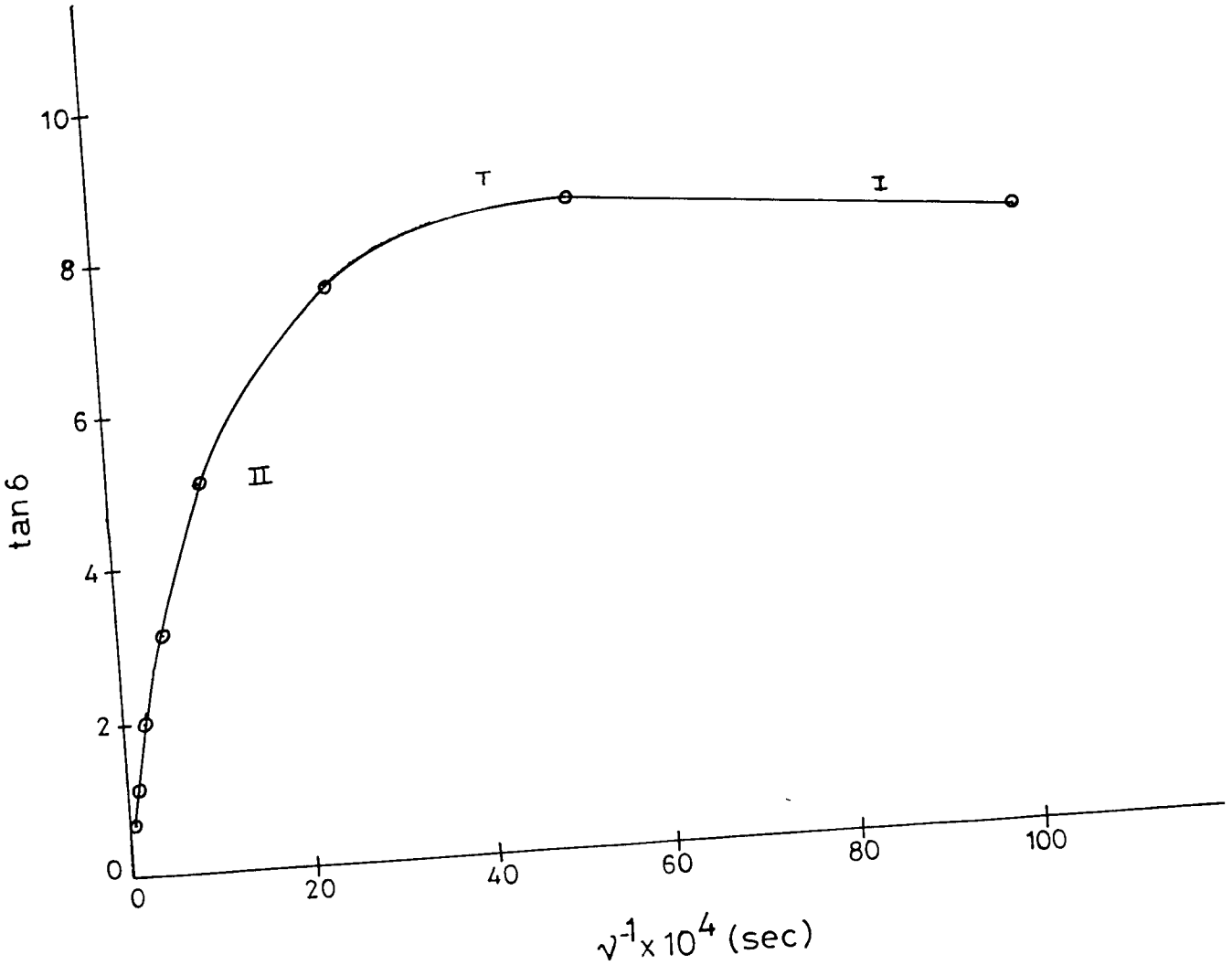

Fig.7.13 Variation of tan δ as a function of ν^{-1} in BPNA

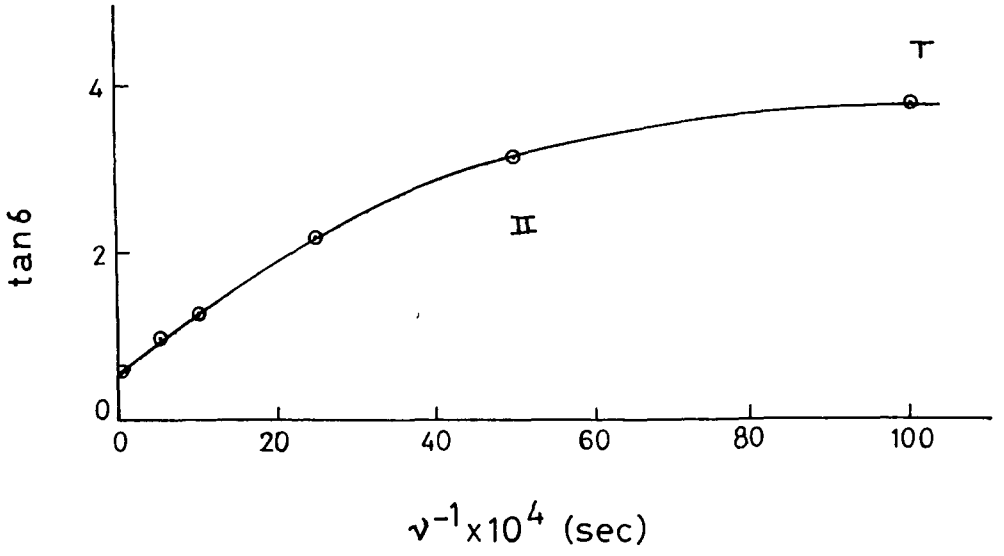

Fig.7.14 Variation of tan δ as a function of ν^{-1} in PMBPNA

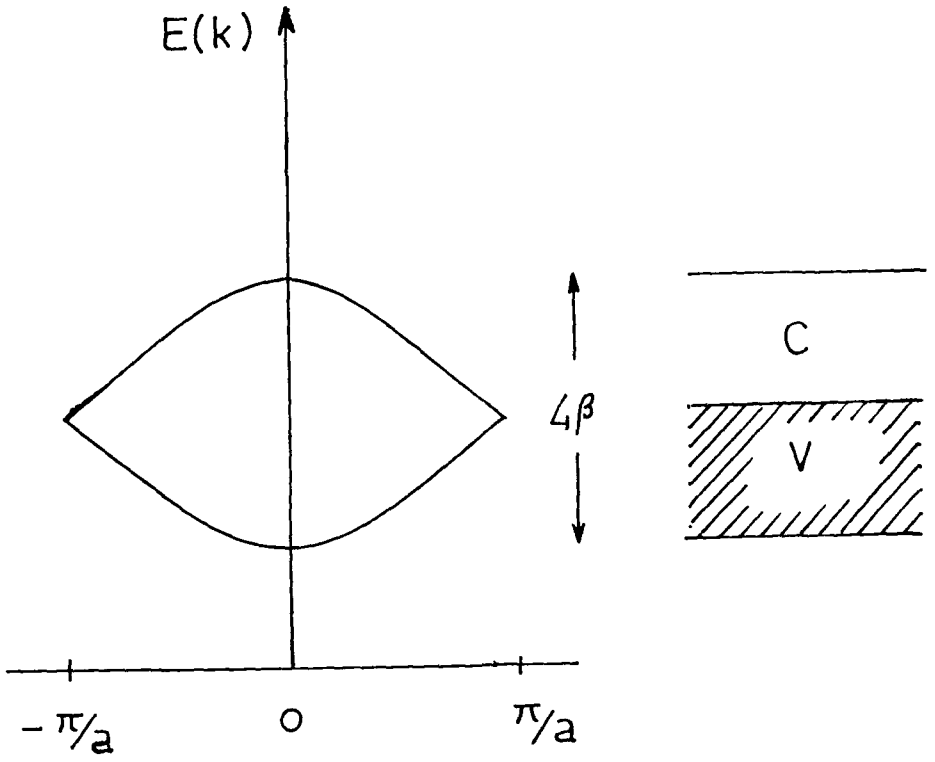

Fig.7.15 The Energy band schemes and electron occupancies for a linear π-electron conjugated carbon chain C denotes the conduction band and V denotes the valence band.

LIST OF PUBLICATIONS

1. Radhendu Das and Kamal Kumar *Spectrochim. Acta* 45A, No. 7 pp. 705-709 (1989).

2. Anusree Purkayastha, Radhendu Das and Kamal Kumar *Spectrochim. Acta* 46A, No. 11, pp. 1545-1548 (1990).

3. Anusree Purkayastha, Radhendu Das and Kamal Kumar *J. Raman Spectrosc.* 21, pp. 227-229 (1990).

4. Anusree Purkayastha, Radhendu Das and Kamal Kumar *Spectrochim. Acta* 47A, No. 5, pp. 525-528 (1991).